Deliverable 2.4.Data analysis and conclusions

Project acronym & number:	UNPLUGGED
Project Number	314 126
Project title:	Wireless charging for Electric Vehicles
Status:	Final
Authors:	José Sanz (CIRCE), Lourdes Garcia Duarte (ENDESA
Contributors:	Matthias Lammerman (FKA), Eleonora Sammartino (ENEL), Jens Fiedler (Continental), Stefano Spizzi (CRF), Roy Johansson (VTEC)
Reviewers:	
Due date of deliverable:	31.05.2015
Document identifier:	D.4 Data analysis and conclusions v260515
Revision:	V260515
Date:	26.05.2015

Dissemination Level

PU	Public	X
PP	Restricted to other programme participants (including the Commission Services)	
RE	Restricted to a group specified by the consortium (including the Commission Services)	
CO	Confidential, only for members of the consortium (including the Commission Services)	

Change History

Version	Notes	Date
0.1	Creation of the document	20.03.2015
V20052015	Integration all contributions	20.05.2015
V26052015	Review of the document	26.05.2015

Abbreviations

ADA	Advanced Distribution Automation	IPT	Inductive Power Transfer
BMS	Battery Management System	ISO	International Organization for Standardization
CAN	Controller Area Network	OCPP	Open Charge Point Protocol
CMS	Central Management System	PS	Power System
CPMS	Charging Protocol Management System	RFID	Radio Frequency Identification
DC	Direct Current	Rms	Root Mean Square
DFT	Discrete Fourier Transform	RTDS	Real Time Digital Simulator
EMI	Electromagnetic Interference	PWHD	Partial Weighted Harmonic distortion
ESS	Endesa Smartbox Subsystem	SE	Supply Equipment
EV	Electric Vehicle	SECC	Supply Equipment Communication Controller
EVCC	Electric Vehicle Charger Controller	SOA	Services Oriented Architecture
HD	High Definition	SOC	State of Charge
HMI	Human Machine Interface	THD	Total Harmonics Distortion
HV	High Voltage	VMU	Vehicle Management Unit

Table of Contents

List of tables

List of figures

1 Executive Summary

This is the last deliverable of the WP2 in which both inductive chargers: 3,7 kW and 50 kW are finalized and commissioned. Therefore, the document includes the final activities that have enabled successful completion of the objective of the project. In some cases the activities have not been reflected in the DOW, due to the fact that it was impossible to foresee them at the beginning, and much of the activities have been more complex than initially expected, implying in some cases an extra effort, but the commitment of the partners and good teamwork, have allowed to obtain 100% of the targets, ensuring the full success of the project.

First the 50 kW Demonstrator is explained, focusing on the modifications needed to assure the perfect operation of the system. It includes the HMI, the communication with the Control Center that allows remote control and the communication with the vehicle or the changes introduced in the control. In addition, the integration in the vehicle and the installation of the ground infrastructure is shown. After the tests with the van, the performance of the system is shown. Finally also the results of the field measurements are shown.

Second, the same description is done on the 3,7 kW Demonstrator, focusing on the control modifications and the modifications needed on the secondary rectifier to assure proper functioning. Vehicle integration is also explained and performance obtained is included, and finally, as in the 50 kW Demonstrator, the results of the field measurements are shown.

Then the final communication system installed in both demonstrators is presented, and the results of the test in both are explained with the recommendations for futures developments.

In Chapter five, the final positioning systems and the process for positioning are explained for both cases: using the camera and using the RFID sensors. Furthermore, the onboard HMI that helps the driver for positioning meanwhile a trajectory-planning algorithm is explained and the results are shown.

Chapter six shows the impact on the grid network for the inductive charging built up during the project. Starting from the results of the real test performed in the CIRCE lab, those have been given as input data for the simulation on a real Italian grid network and they have been considered in addition to the real consumption values recorded on one day in November 2013. The results compared with the international standards limits show how the examined inductive charging station does not influence the network quality and the THD values are fully compliant to the limits. These results can be pinpointed to the accurate design of the inductive charging station.

In the last chapter, three different electrical architectures to integrate inductive and conductive charge are explained, including fast and slow conductive chargers. Finally, the solution implemented by CRF in the IVECO Daily is presented.

2 50 kW IPT Demonstrator

2.1 Introduction

In this section the work done in the last phase of the project is explained, including those that are not included in the DOW but that were essential to accomplish with the final objective of designing, manufacturing and commissioning the 50 kW inductive Charger installed in CIRCE facilities.

Due to the Iveco Daily was not available till the third week of March 2015, it was necessary to adapt the CIRCE´s EV Emulator firstto continue with the test and later to work with the CRF Test Bench, that was received during the second week of December 2014. The behavior of the Test bench was quite similar to the behavior of the Iveco Daily.

The job done includes mainly:

- Design and programming of the communication protocol with the test bench and with the Iveco, including wired and wireless communication.
- Design and programming architecture and software of the HMI and the Control Center, including communications between them and with Power electronics module
- Design and programming registration and payment system
- Installing secondary side on the Van
- Installing primary side in the charger station, including cooling system
- Adaptation of the power electronics control to the specific characteristics of the final communication protocol and to the specific characteristic of the van
- Final test.

2.2 Test bench

The second week of December, CRF visited CIRCE installations to configure the communications of their test bench with the communication controller of the charger. The test bench was received the week before arrival. Figure 1 shows the test scenario mounted.

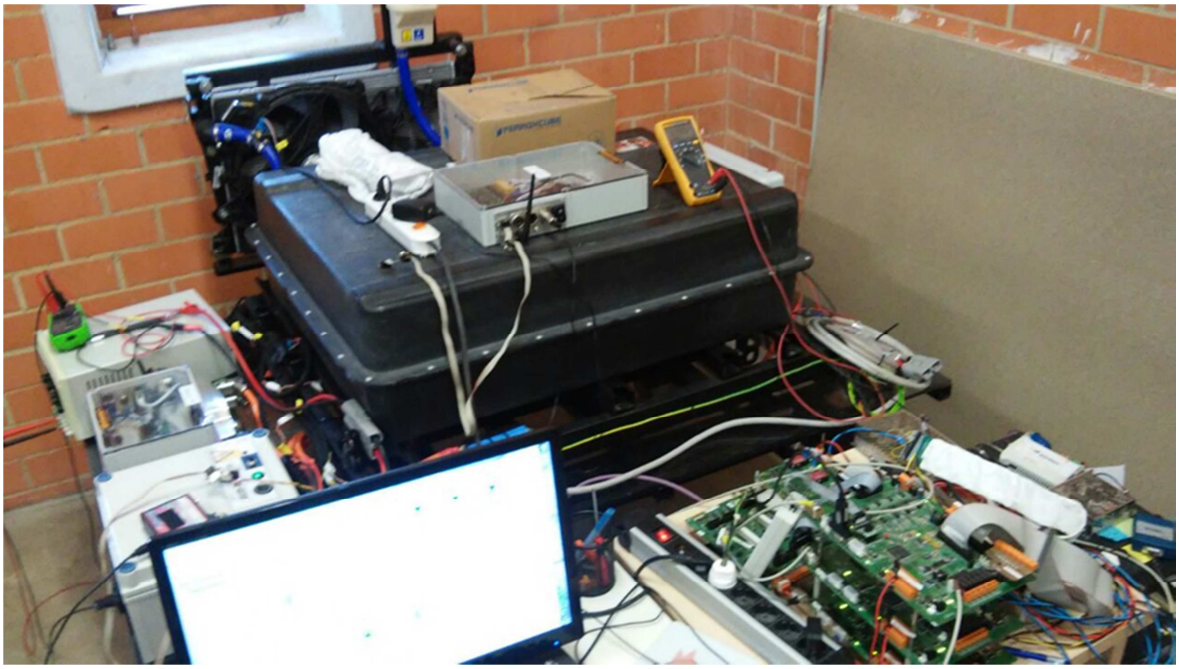

As described in Deliverable D2.1, a Test bench has been develop for initial tests, with following main objectives are:

- anticipating possible issues with respect to vehicle integration
- developing and debug communication between primary and secondary control unit
- tuning and test charging process
- performing initial EMC evaluation

Test bench represents a vehicle subsystem, for electrical equipment and for logic development for following reasons:

- high voltage battery systems is the same installed in vehicle
- EVCC is the same installed in vehicle and control logics have been developed to be transferred from test bench to vehicle
- Communication integration of wireless modules is the same defined for vehicle
- Power interface and connections are the same installed in vehicle architecture

A detailed description of Test bench with components, integration modules, logics and communication development can be found in D2.1.

The test sessions started trying to communicate the present devices, but the result was not satisfactory. The modules could not communicate with or without the Continental modules. To start solving problems, a wired communication between charger and battery was carried out to isolate the problems belonging to our own modules.

After making some changes on the Simulink model of CRF and in our programming, the vehicle and the charger could be able to perform a full charge with different ending scenarios. Then the Continental devices were included in the communication, but with this scenario there was impossible to establish a correct charge of the battery. In the next sections the whole process carried out from the beginning to the end will be explained thoroughly.

2.2.1 Communication Test

2.2.1.1 Test with wired communication

To achieve a correct communication between charger and vehicle several changes in the states machines and in the exchange of information had to be made. In this section we describe all the changes and improvements made with a further explanation.

The conditions described in the document “Unplugged Wireless Communication” to remain in each phase [COND0, COND1, COND2 and COND3] were added to the models in the cases there were some missing transitions.

Although the communication has been thought to behave as master and slave without resending of messages, a modification was included to resend a message of the vehicle after half second when the charger did not respond correctly or the response was lost. This allow the master to have some control in the communication flow and to be more robust because if we activate the timeout error and restart the communication every time a message has been lost or corrupted, there will be a lot of error of this type. In a real environment there are a lot of variables out of our control that could lead to an incorrect message. That problem could be solved just adding a resending of the master package.

A definition of appropriate stopping situations was carried out. For the case of a full charge or a manual stopping, the behavior will be the following: the current demanded by the vehicle will reduce with a slope of 10 Amp/sec. When the charger stops delivering energy, it deactivates the bits

of RCDStatus and PowerSwitchClosed and the vehicle could send the #21 message. The charger responds with the #22 message and the communication ends. When there is an error stopping, the vehicle sends directly the #21 message and the charger responds with the #22 and makes and emergency stop of the primary coil.

To include a protection board we have designed in the system, we defined the necessary communications to acknowledge the measures and reset the board when it's necessary. Our board will be connected with the vehicle side through three GPIOs, two for input measures of the overvoltage and the failure of supply, and one out to reset the board. The input signals will connect to analogue inputs with a threshold in the middle point (higher than middle point means overvoltage, lower means no overvoltage).

With those changes we afforded to make a complete charge and test the different finishing scenarios.

2.2.1.2 Test with Continental modules

After the successful communication between the charger and the vehicle, we included again the Wi-Fi devices in the system. The results were a bit better than the initials, but not satisfactory. After performing a lot of tests, it was unable to fulfill a complete communication in a continuous way.

The main problems we founded were the following:

The communication stopped during the process without apparent reason. This stop could happen in different steps of the communication, not the same. In some cases this problem was solved with the resending of the last message the vehicle had send, but this should not be necessary according to the definition of the protocol. Other times the modems stop communicating for a while and we could not reset the communication.

When the modems detect a timeout they should reset the communication, but when the timeout activates, just stop sending messages and never start over. The conditions established in the definition of the protocol we think are not checked because when one of those conditions is incorrect, it should resend the same message. The main problem is that if the Wi-Fi modules stop the communication if one of the conditions is not verified, it is not possible to go over even if the condition is verified after some delays (delays are possible both on vehicle side and on infrastructure side for operations and verifications executions).

2.2.2 Specific results of the simulations

Several logs of the simulations carried out were saved for being studied and to help solving the problems detected. Both CRF and CIRCE made our own logs to have the complete behavior of both sides. The files were in .csv format:

The files corresponding to the test without Continental modules are:

- Without_Conti_STOP_NORMAL: Manual Stop (without Conti modules) - early and last version
- Without_Conti_STOP_SOC: SOC Stop (without Conti modules) - early and last version
- Without_Conti_STOP_ERROR: Error simulation (without Conti modules) - early and last version

Early means first test before CONTI, last means after trying with CONTI.

The files corresponding to the test with Continental modules are:

- CONTI_Fault_Not_send_0x050: Conti not resend 0x050 Frame, COND0 is no true
- CONTI_Fault_Not_transmit_between_sides: Conti feedback is broken (0x171 & 0x0172 not recived but send by CRF)
- CONTI_Fault_Not_transmit_between_sides_0x01819: Now problem is in 0x018 & 0x019
- CONTI_Fault_Not_transmit_between_sides_0x01819(2): problem persist in all charges

2.2.2.1 Test with wired communication

For the wired simulations, the results recorded by CIRCE show that the communication was established correctly. For the state transitions CRF checks the reception of the response and the content, asking again the same message in case the conditions [COND0 COND1 COND2 COND3] were incorrect. The communication between devices never stops without sending package 0x0210 and waiting for the 0x0220 from our side.

In the files included, the correct stop sequence could be checked. The current reduce its value until 0 with a slope of 10 Amp/sec. The records correspond to the cases with normal stop and stop for battery complete charged.

In case of an internal error on the battery or an error in the secondary side, it could be observed the correct sending of packages 0x210 and 0x220.

2.2.2.2 Test with Continental modules

As it can see in the recorded logs, it was impossible to fulfill a complete charge without incidences. Most of the times the packages sent were not reflected on the other side of the communication, slowing down the correct working of the state machines of the charger and the battery.

Besides, the “CONTI_Fault_Not_send_0x050” shows the first steps of the communication, where CRF still not communicate. The package 0x050 was not resent although the package 0x060 was received with the COND0 incorrect. The protocol says that there must be a loop where the conditions described are incorrect. In that case the communication seems blocked.

Subsequently there are more blocks like this due to this fault of transmission during different states.

Also remarkable the amount of time needed to establish the wireless link and some other latencies produced in the state transitions when the sending rate of packages is high. To minimize this effect and try to avoid this failure, the amount of requests from the battery were reduced. It seems that this change improves slightly the failure rate but it was determined that the system was not capable of working with that amount of failures.

Finally it was decided to go back to the wired simulation to perform the final tests to check that we will be able to perform simulations without needing someone of CRF in site.

2.2.3 Test Bench CRF acquisitions

CRF performed acquisitions of CAN network/networks with a CanCase HW and a Canalyzer Pro SW. The results were the next.

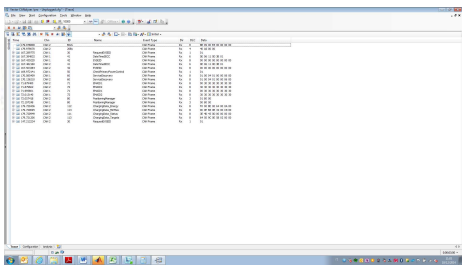

2.2.3.1 Tests with Conti Modules

Test with Conti Modules were performed with following configuration:

- Vehicle (Test Bench) side: CAN bus with VMU (Vehicle Management Unit), BMS and Conti SECC
- Infrastructure side: CAN bus with charger and Conti EVCC

On both networks a CanCase with Canalyzer SW was connected to acquire messages and verify communication steps. In some cases through Canalyzer some messages were forced on vehicle side to allow the communication continues.

Tests show that communication stops at different steps, without clear evidence of condition occurred that causes communication stops.

Acquisitions description:

- **20141212_Acq_Unplugged_BancoCIRCE6**: communication process ok until message 0x20, then problems:
    - Message 0x20 not correctly received on vehicle side --> Messages 0x18 and 0x19 not send from Vehicle Unit
    - Emulation with CanCase of correct 0x20 on vehicle side --> Messages 0x18 and 0x19 sent by Vehicle Unit --> only one cycle messages 0x18 and 0x19 forwarded on infrastructure side even if Vehicle Unit send other messages

- **20141212_Acq_Unplugged_BancoCIRCE7**: communication process ok until messages 0x121, 0x122, 0x123, then problems:
    - Messages 0x171 and 0x172 sent by Vehicle Unit, but not forwarded on infrastructure side
    - After some minutes, the message 0x30 is sent on both sides

- **20141212_Acq_Unplugged_BancoCIRCE8**: communication process ok until messages 0x111, 0x112, 0x113, 0x114, then problems
    - Messages 0x121, 0x122 and 0x123 not forwarded on vehicle side
    - After some minutes, the message 0x30 is sent on both sides.

- **20141212_Acq_Unplugged_BancoCIRCE9**: communication process ok until message 0x80
    - Messages 0x111, 0x112, 0x113 and 0x114 not forwarded on infrastructure side
    - After some minutes, the message 0x30 is sent on both sides.

It is necessary to understand with Conti the reasons that stops the communication at different steps to allow modifications in SW infrastructure on Vehicle side and on Infrastructure side.

A problem could be if the exact package sequence for each step is required without other CAN messages on the bus (for example 0x111, 0x112, 0x113, 0x114).

To increase communication robustness on Vehicle side logics for sending messages has been modified to allow repetition requests until conditions to proceed have been verified. This seems to make communication more robust.

Main problem encountered from the logics point of view is to understand reason that brings communication to stop. From Vehicle side or Charger side it is not possible to define if communication has been stopped because the other unit is not sending (EV or SE) or if it the Wi-Fi channel that is broken.

It could be useful to have some modifications that allow to gateway messages defined in the protocol present at Conti modules transceiver (at least the expected messages for each step, without evaluation on the conditions defined in the protocol).

Acquisitions are available in .blf format or can be converted other formats to be analyzed by other partners.

Attached some screenshots of Canalyzer acquisitions for the acquisitions described above.

Both channels are present: CAN1 is Infrastructure Side while CAN2 is Vehicle Side.

20141212_Acq_Unplugged_BancoCIRCE6

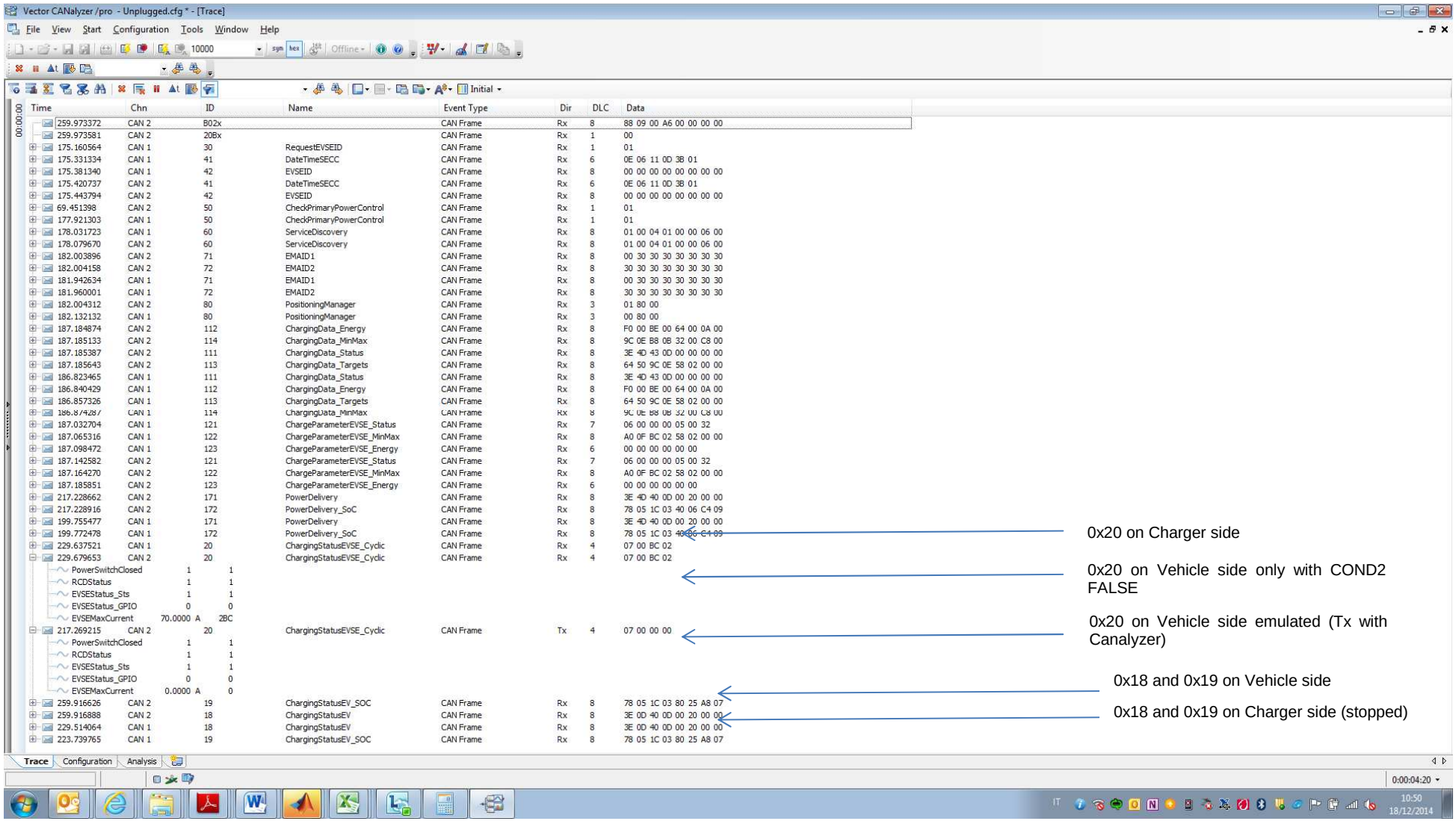

20141212_Acq_Unplugged_BancoCIRCE7

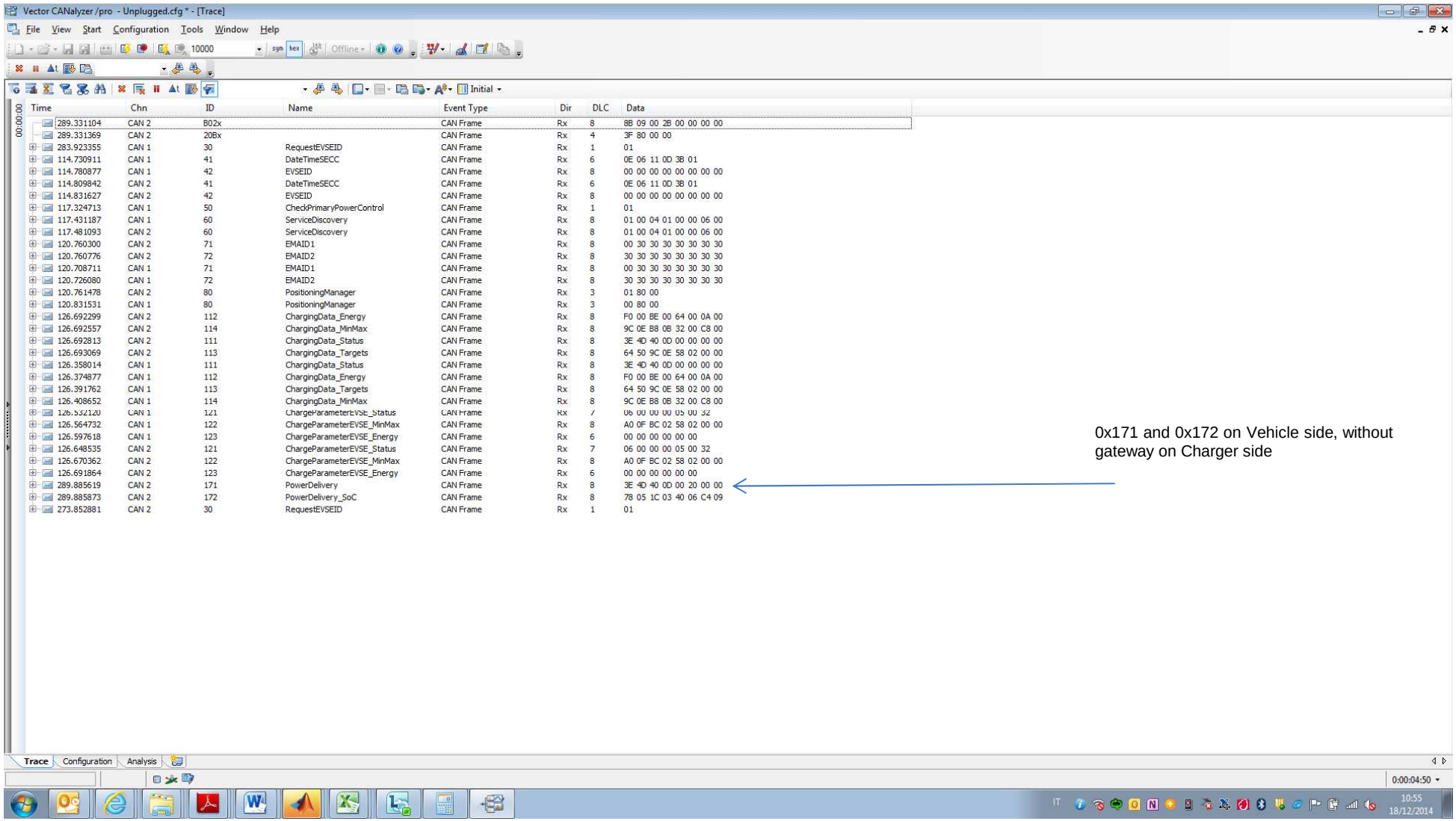

20141212_Acq_Unplugged_BancoCIRCE8

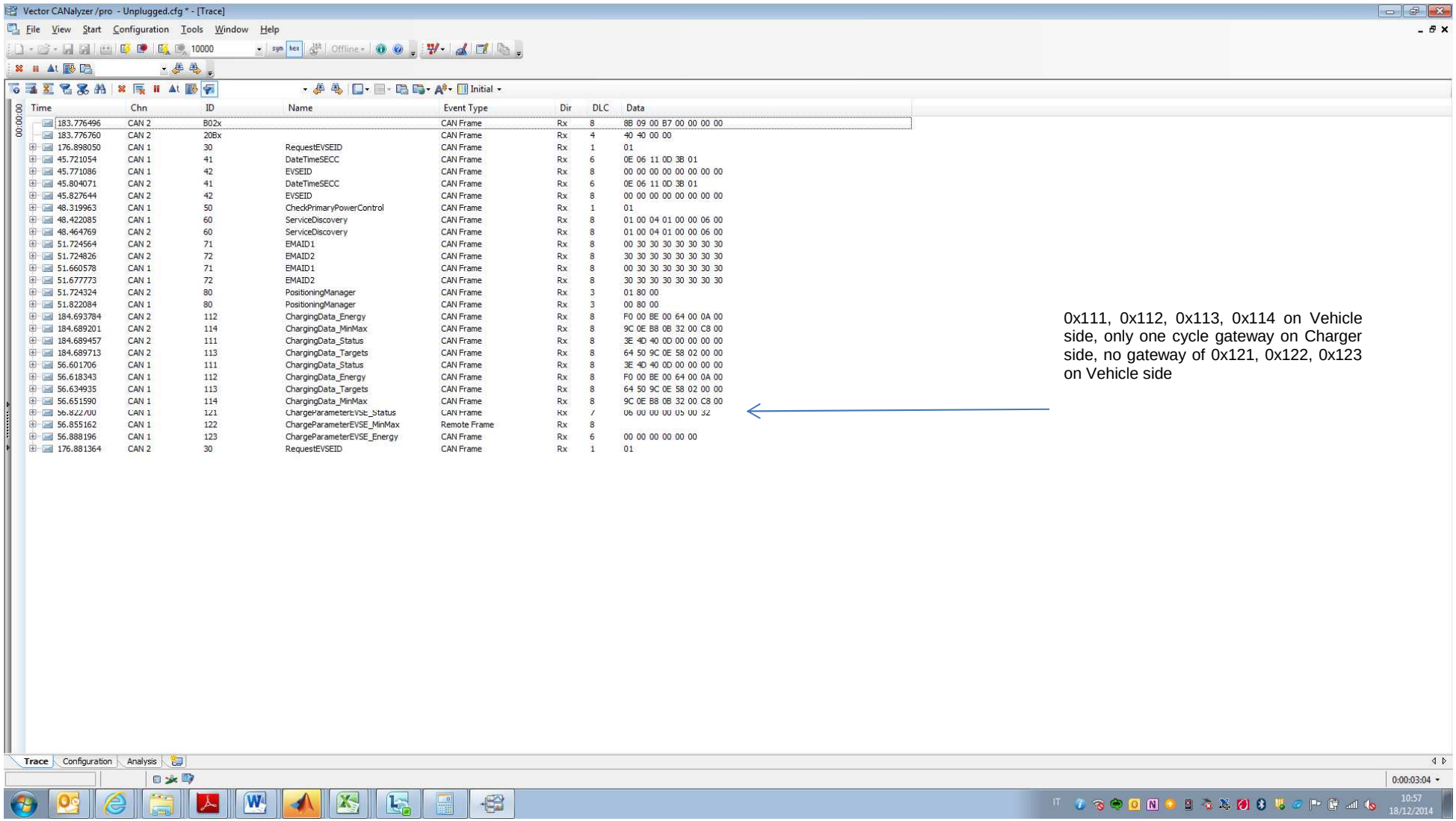

20141212_Acq_Unplugged_BancoCIRCE9

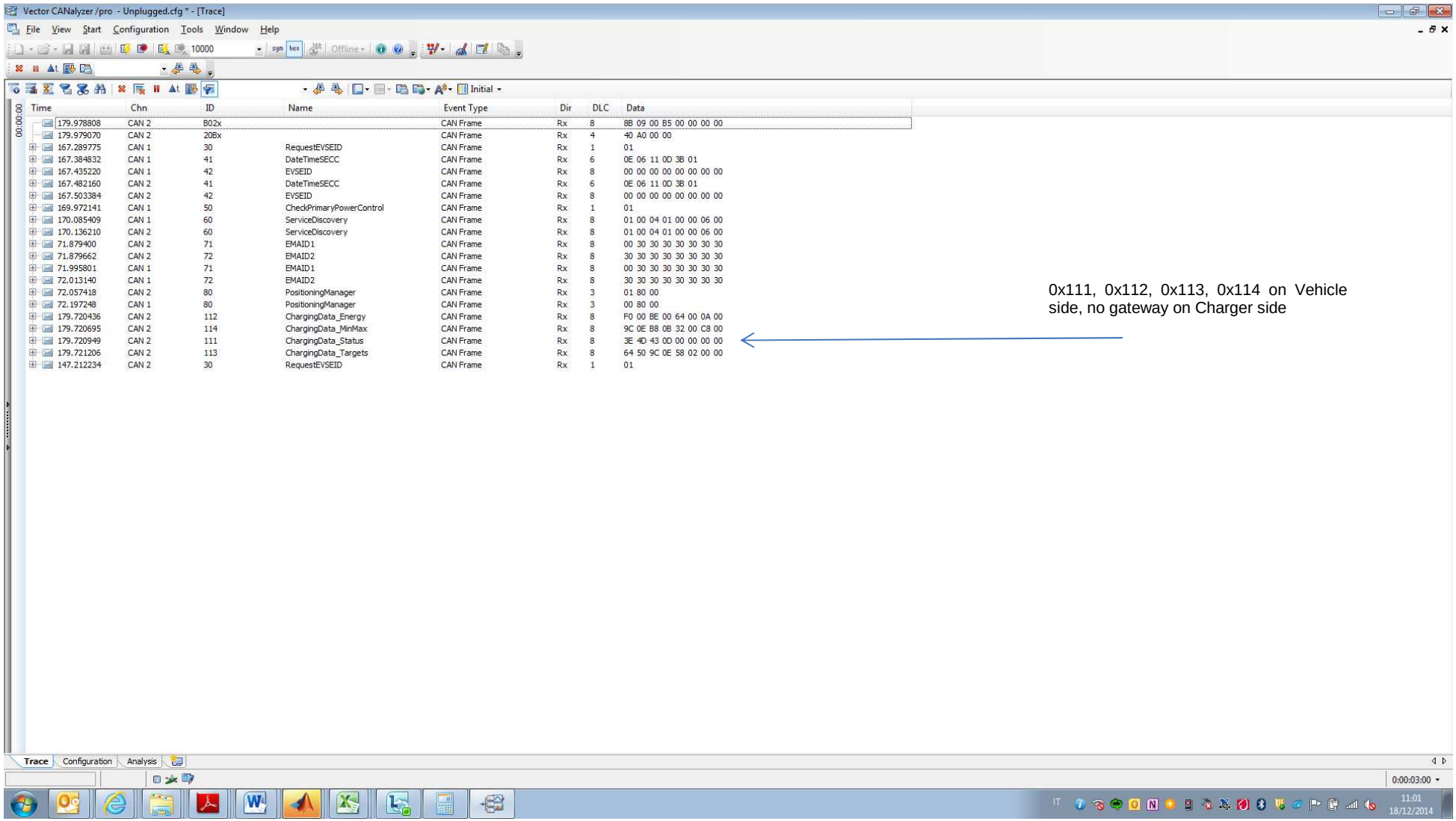

2.2.3.2 Tests without Conti Modules – direct CAN connection

Test without Conti Modules were performed with following configuration:

- CAN bus with Vehicle (Test Bench) side and Infrastructure side directly connected: on network units present were VMU (Vehicle Management Unit), BMS, charger.

On network a CanCase with Canalyzer SW was connected to acquire messages, verify communication steps and emulate messages in substitution of Conti modules (0x30 and 0x50 messages) to start the communication flow.

Tests show that communication was performed in the expected flow: identification and setup of the charging process, start charging, charging and stop of the charging.

Stop charging has been tested with three different procedures:

- with normal stop by user: target current ramp down 10 A/s until Charger communicates charge is stopped (RCDStatus=0 and PowerSwitchClosed=0)
- with normal stop by battery for charging completed: target current ramp down 10 A/s until Charger communicates charge is stopped (RCDStatus=0 and PowerSwitchClosed=0)
- with emergency stop by vehicle: 0x210 is sent directly to Charger without current reduction.

Acquisitions description:

- **20141212_Acq_Unplugged_BancoCIRCE15**: Manual Stop (without Conti modules) through a CAN flag emulates stop by user interface
- **20141212_Acq_Unplugged_BancoCIRCE18**: SOC Stop (without Conti modules) emulated on CAN forcing a low SOC threshold
- **20141212_Acq_Unplugged_BancoCIRCE19**: Error simulation (without Conti modules) of battery error

Acquisitions are available in .blf format or can be converted other formats to be analyzed by other partners.

Attached some screenshots of Canalyzer acquisitions for the acquisitions described above.

20141212_Acq_Unplugged_BancoCIRCE15 – Normal Stop by User

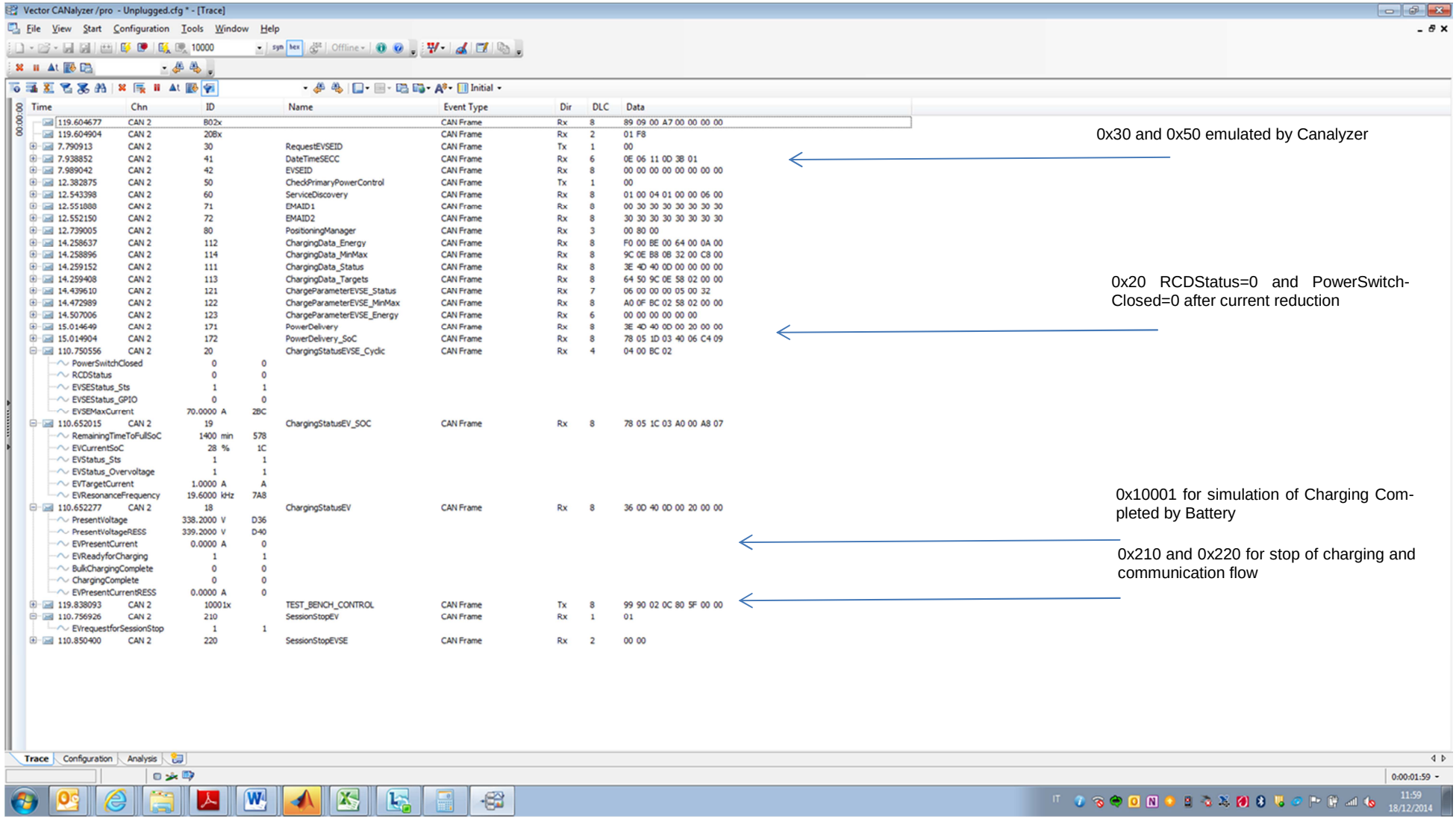

20141212_Acq_Unplugged_BancoCIRCE18 – Normal Stop by Battery (Charging completed)

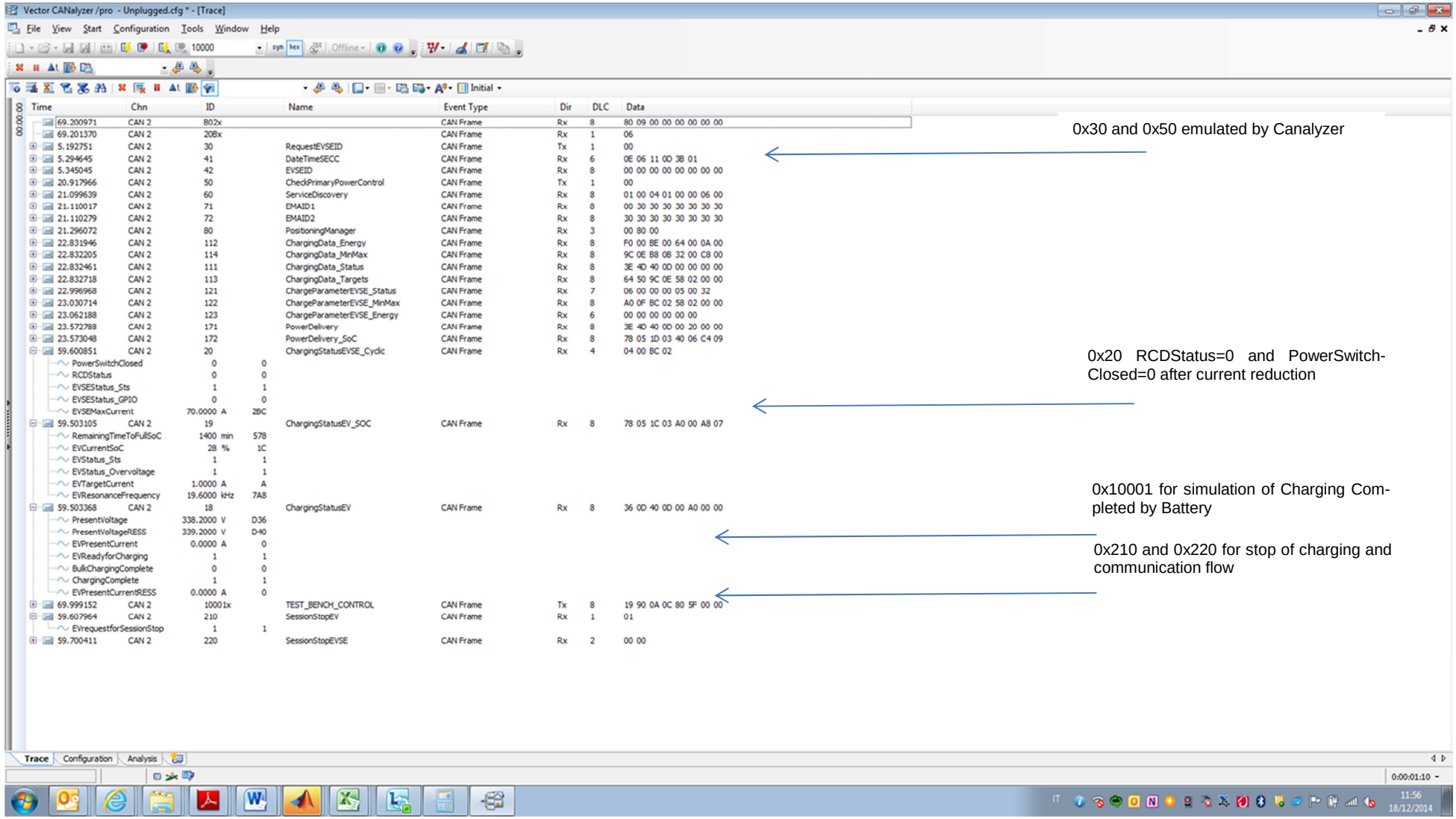

20141212_Acq_Unplugged_BancoCIRCE19 – Emergency Stop (battery contactors unexpected open)

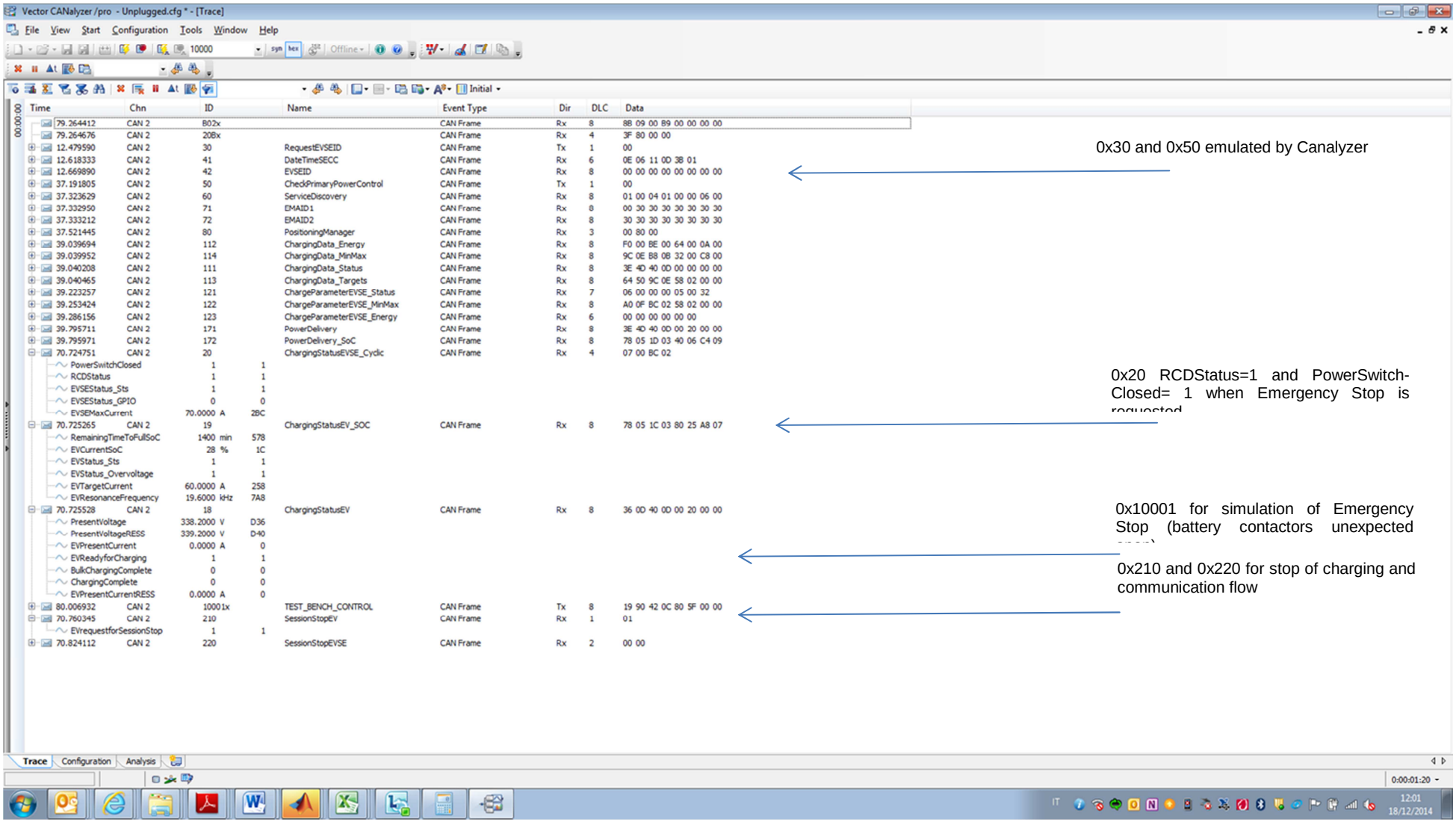

2.2.4 Conclusion

From tests in CIRCE lab with CIRCE equipment and CRF Test Bench following considerations derive:

- a setup for allowing CIRCE to perform additional test with real battery pack has been established with a configuration shared by CIRCE and CRF
- direct CAN communication between Vehicle Management Unit and Charger allows to complete all protocol steps, even if some further modifications and verifications are necessary (i.e. I/O on VMU for management of CIRCE error control board)
- communication over Wi-Fi with Conti modules need further verifications and SW tuning to be completed

2.2.5 Essays with two coils

The system was commissioned with both coils, to do this it was necessary to design and program two independent controls: voltage and frequency.

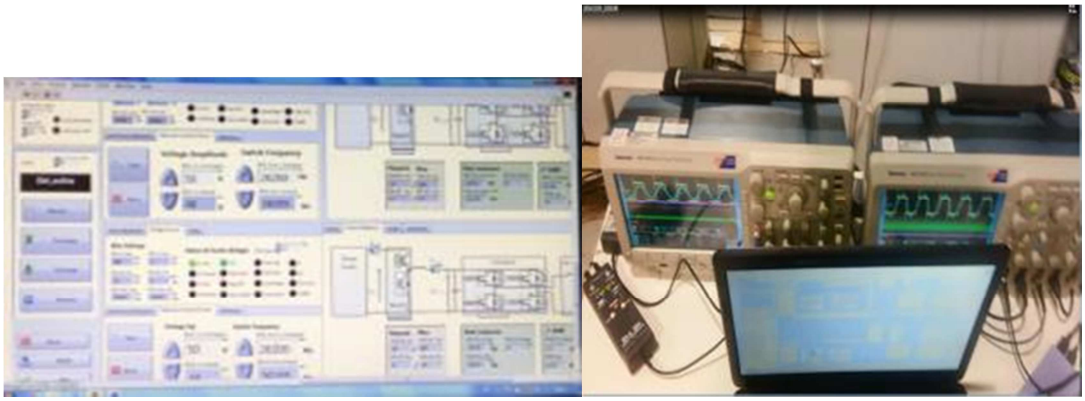

Figure 1 Controls Display

Without misalignment, the frequency of both coils was substantially the same: 26,4 kHz and 26,41 kHz.

Figure 2 current (blue) and voltage (yellow) in both primary coils

With this controls, both coils can work independently, it is possible to switch on only one coil, for example if 35 kW are needed it is possible to maintain one coil at full power and reduce the power to achieve the set point with the other, increasing the efficiency.

Other advantage is that it is not needed a great accuracy in the electric and magnetic characteristics of the coils and capacitors, increasing tolerance when manufacturing them.

The tests developed over the two modules show a good behavior and there are not significant differences between them, however the module 2 is able to transfer a little more power to the battery in the same conditions.

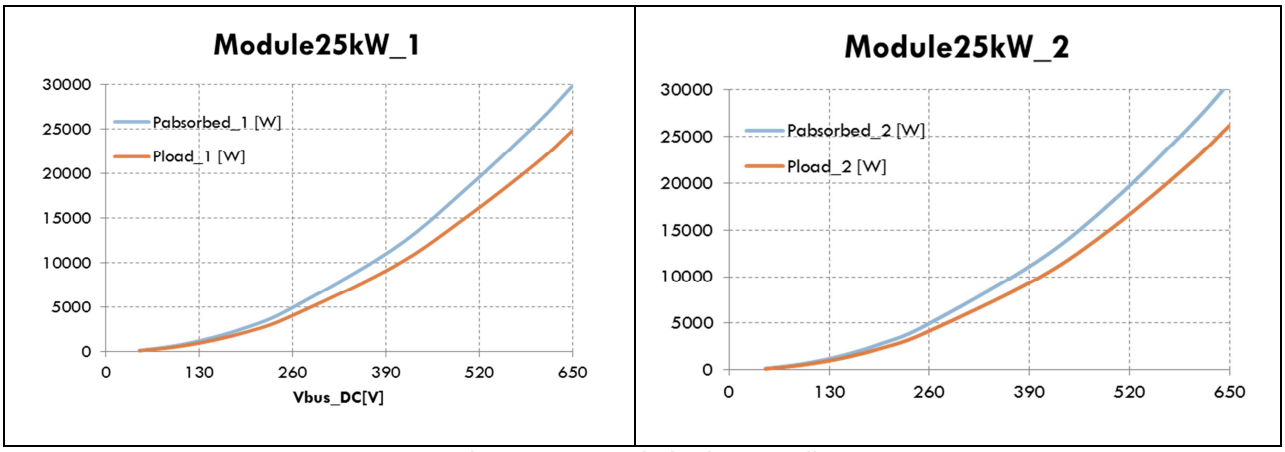

Figure 3 Power in both IPT coils

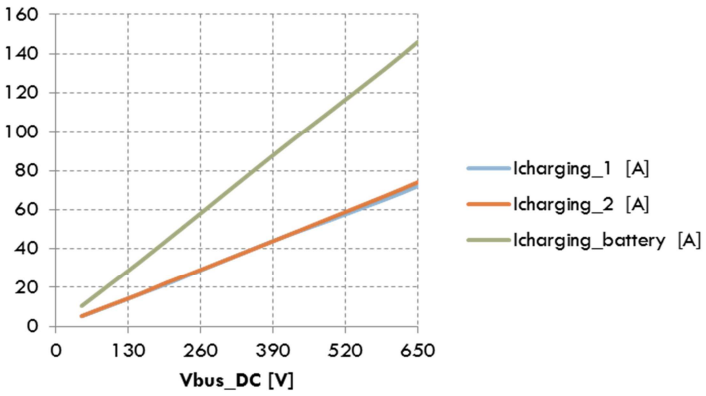

Figure 4 Total load current

The next table shows the difference between both coils:

Module_1	Vcc	V1	I1	VL	IL	Pabsorbed	PLoad	efficiency
Freq= 26400	47	42,3	3,67	23,8	5,2	155,241	123,76	79,7
	97	87,3	7,76	51	10,6	677,448	540,6	79,8
	150	135	11,9	78,5	16,4	1606,5	1287,4	80,1
	200	180,1	15,8	106	21,8	2845,58	2310,8	81,2
	250	225,1	20,1	134	27,7	4524,51	3711,8	82
	400	360,1	32	212	45	11523,2	9540	82,8
	500	450,2	40,3	270	55,5	18143,06	14985	82,6
	600	540,2	47,4	320	66,2	25605,48	21184	82,7
	650	585,2	51	345	72	29845,2	24840	83,2
Module_2	47	42,3	3,68	23,9	5,3	155,664	126,67	81,4

Freq= 26400	97	87,3	7,83	51,9	10,8	683,559	560,52	82
	150	135	11,9	80	16,5	1606,5	1320	82,2
	200	180,1	16	106	22,5	2881,6	2385	82,8
	250	225,1	20,2	136	28	4547,02	3808	83,7
	400	360,1	32,32	217,6	45	11638,432	9792	84,1
	500	450,2	40,4	272	56,5	18188,08	15368	84,5
	600	540,2	48,48	326,4	68	26188,896	22195,2	84,8
	650	585,2	52,52	353,6	74	30734,704	26166,4	85,1

Table 1 Efficiency of both coils

The efficiency is a little higher in module 2 probably due to differences in its construction.

The efficiency at maximum power is over 83 % in both modules.

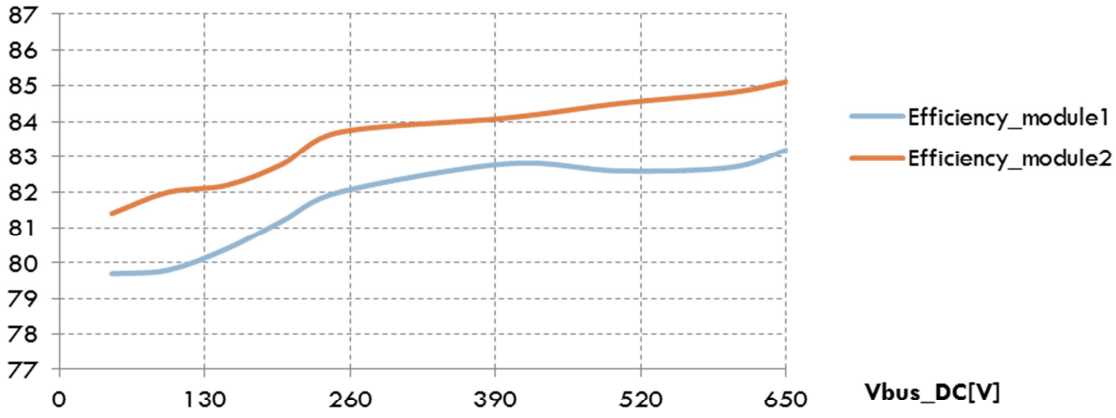

Figure 5 Efficiency of both coils

2.2.5.1 Misalignment test

Several test with different misalignment distances were performed, here are shown the results with a misalignment of 10 cm.

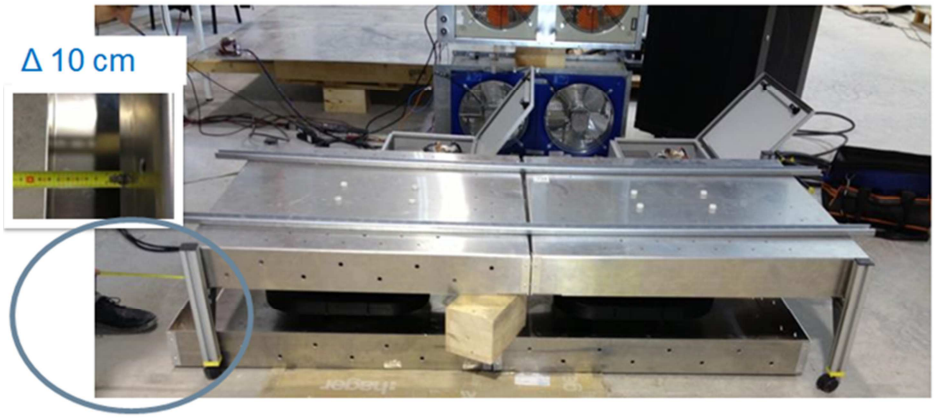

Figure 6 10 cm of misalignment

With 10 cm of misalignment, both frequencies have to be adapted obtaining: 26,2 kHz for the first coil and 26,15 for the second, as can be seen in the next figure.

Figure 7 Adjusting frequency to compensate misalignment.

Misalignment clearly affects to the efficiency of the system.

Aligned	Vcc	V1	I1	Argument [degrees]	VL	IL	P1	PL	efficiency
	47	42,3	3,68	0	23,9	5,3	155,6	126,67	81,4
	97	87,3	7,83	0	51,9	10,8	683,5	560,52	82
misalignment of 10 cm	47	42,3	3,9	-17	22,6	5,1	157,8	115,26	73
	97	87,3	7,5	-17	48	9,81	626,1	470,88	75,2

Table 2 Comparison aligned/misaligned

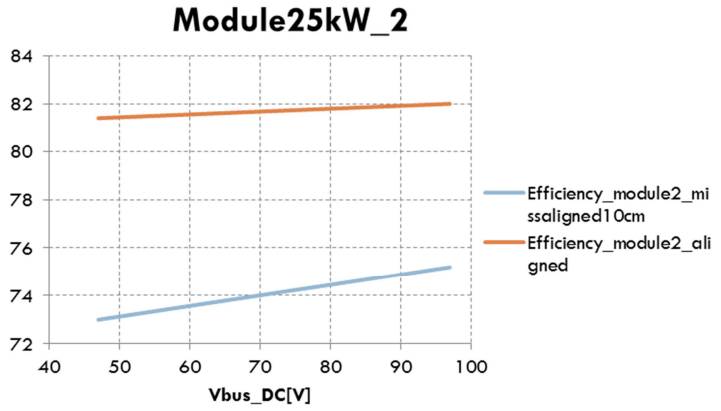

Figure 8 Comparison aligned/misaligned

2.3 Installation of the secondary side

The IVECO Daily was received in CIRCE the second week of March. The secondary side was installed between CIRCE and CRF as can be seen in the next figures.

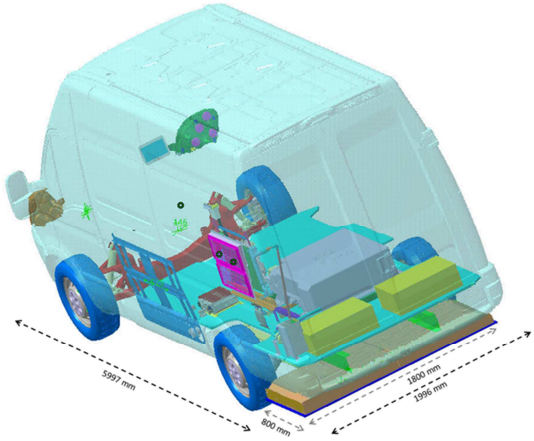

Figure 9 Schematic of the secondary side

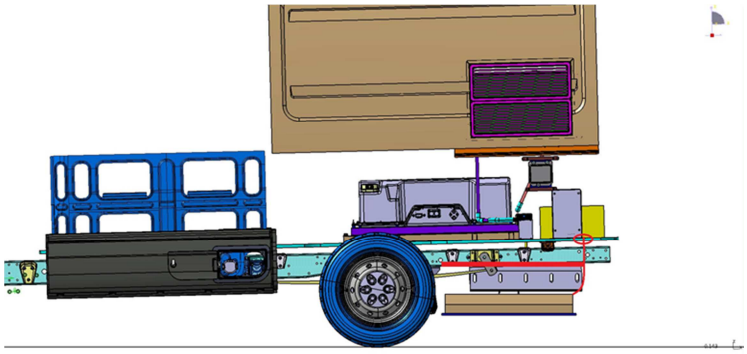

Figure 10 Detail of the secondary side

Brief installation activities of secondary coil and power electronics boxes has been described in deliverable D2.1.

Additional details and descriptions are given in this deliverable.

Main integration activities are:

- Electrical integration
- Mechanical integration.

For the electrical integration, both power and signals integration have been defined.

For the power integration, the choice has been to install the power electronics boxes inside the cargo compartment, next to the battery, with dedicated cables as short as possible between coils and power electronics.

The DC connection toward DC bus has been made easy through the realization of a HV distribution boxes, with a dedicated contactor, controlled by Vehicle Management Unit, to connect the Wireless Charge line to the DC bus for the recharge.

Figure 11: HV Distribution Box

For the signals integration, the main connection is the CAN integration between the Vehicle Management Unit and the Wireless Communication Modules.

Another foreseen functionality is the connection of the overvoltage control board and the Vehicle Management Unit.

For the mechanical integration, the aim was to make the process as much easier as possible, being compliant at the same time with some constraints:

- to allow regulation of vertical distance between primary and secondary coils
- to integrate an aluminum shield on the bottom part of the vehicle

For the first issue, the mechanical supports have been designed to be vertically adjustable; furthermore, being composed by two different parts for each side, it is possible to mount one part directly to the secondary coil, and then install the pre-assembled structure to the vehicle.

For the second issue, the integrated aluminum shield has been divided in two parts: one is directly integrated in the bottom part of the vehicle, while the other one is just above the coil, guaranteeing the better shield for the vehicle iron parts.

A special structure was included in the van in order to fasten secondary coils and EMI shielding, allowing modifying the airgap between primary and secondary side, that can be seen in the next figure.

Figure 12 Restraint system secondary coil

The EMI shielding and the coils were fixed using special nylon screws.

Figure 13 Installing secondary coils and EMI shielding

Figure 14 Secondary coils and EMI shielding installed in the Iveco Daily

Figure 15 Adjusting the height of the secondary coils

Figure 16 Installing secondary side power electronics on the Iveco Daily

2.4 Installation of the primary side

The installation of the primary side included:

- Cooling system installation
- Coils, resonant capacitor and EMI shielding installation
- Power electronics cabinet installation

The cooling system consists in an oil circuit that cools the primary coil.

Figure 17 Oil cooling system

Figure 18 Installing the oil cooling system

The oil flows through a pipelines system and is introduced into a sealed aluminum boxes that also act as EMI shielding where the coils are installed.

Figure 19 EMI shielding and cooling pipelines

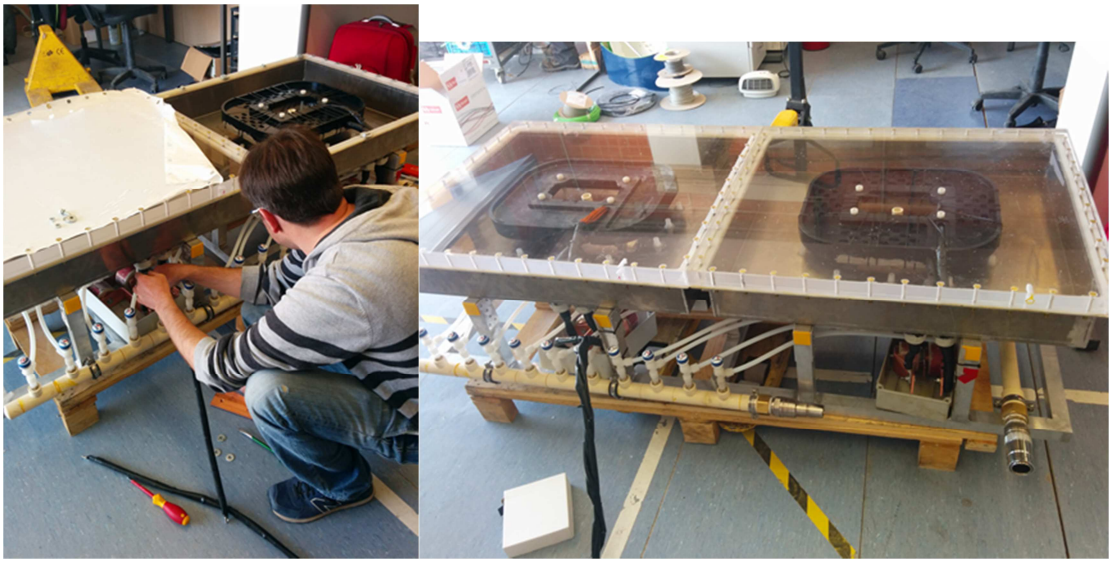

Figure 20 Installing coils and resonant capacitors in the lab

Figure 21 Installing Primary coils in the Charging station

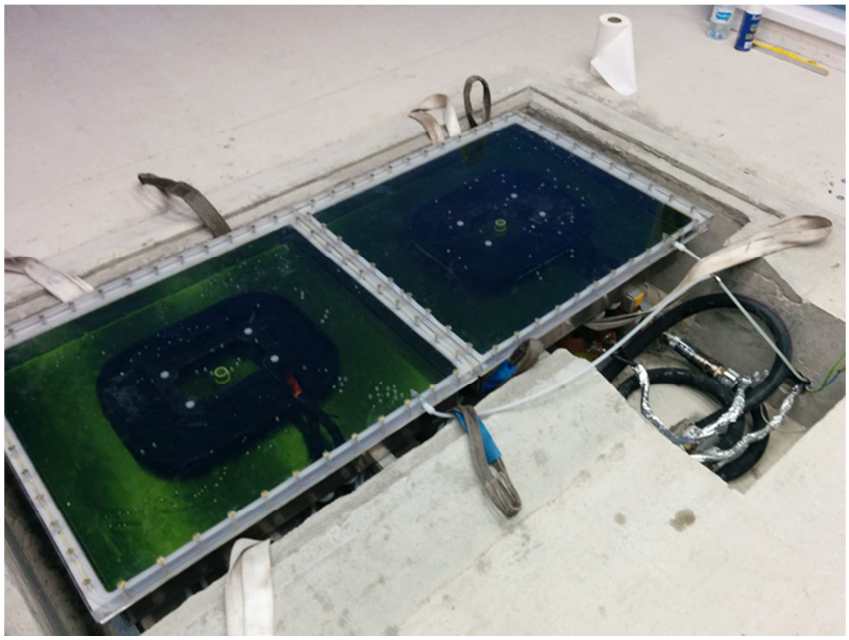

Figure 22 Primary side with oil refrigeration installed

Figure 23Detail of the resonant capacitor

Figure 24 Installing Power electronics in the charging station

Figure 25 Power electronic cabinet Installed including the HMI

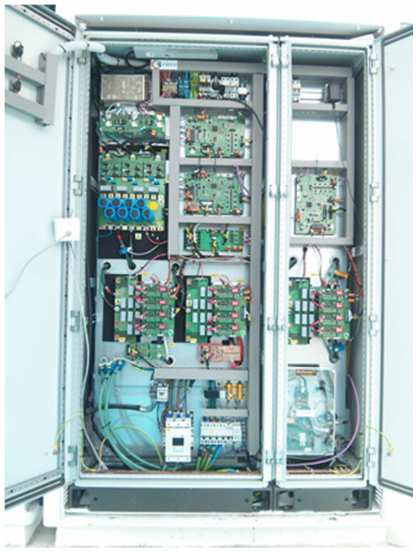

Figure 26 Power electronics cabinet installed with Conti communication module integrated

Figure 27 Positioning of the van

2.5 Software architecture of communications in charger side

2.5.1 Definition of the architecture.

To achieve the correct charge of the vehicle in the demonstrator, apart from a good control of the power delivered and ensuring the security of the power system, it is necessary to develop a communications architecture that allows sharing information between charger and vehicle.

From the charger side, the architecture was divided in two parts, the communication protocol between charger and vehicle and the communication system inside the charger that connects all the systems and devices.

2.5.1.1 Communication protocol

Nowadays does not exist a standard protocol for inductive charge, so a new protocol had to be defined to solve this problem. Inspired in the ISO 15118 protocol, known as COMBO protocol, the new protocol was designed to exchange information about the charging parameters and to follow a predefined sequence of messages that allows controlling the status of the charge.

The protocol was initially defined by Continental, but as the project advanced both charger and vehicle developers started to help improving and defining changes on it. In the charger a specific system was developed to communicate with Continental modules via CAN communication. Some timeouts were added to avoid problems with the power control; the identifier of the user was defined to follow the e-Mobility ID format (eMA-ID) and the communication process was modified in some points to allow the correct integration of the protocol with the rest of the units. The result was a work in parallel with the development of other units that form the charger to achieve a general behavior without contradictions between modules.

2.5.1.2 Communication system of the charger

From the outside, there is a frontend that communicates with the WiFi devices using a data structure defined between all the partners involved. However, inside the charger the extraction of these data is not so easy. There are several subsystems, each with their specific behavior, using different communication protocols, some of them developed before the definition of the communication protocol. In Figure 28 can be observed the complexity of the system and the amount of modules developed.

This scenario force us to develop interfaces between each system to translate information from one communication protocol to another and a management system that monitors the rest of the systems, receives the information and distributes it to the system that require it and carries out the security necessary in case of errors during the charge. In the next section this development will be explained in detail.

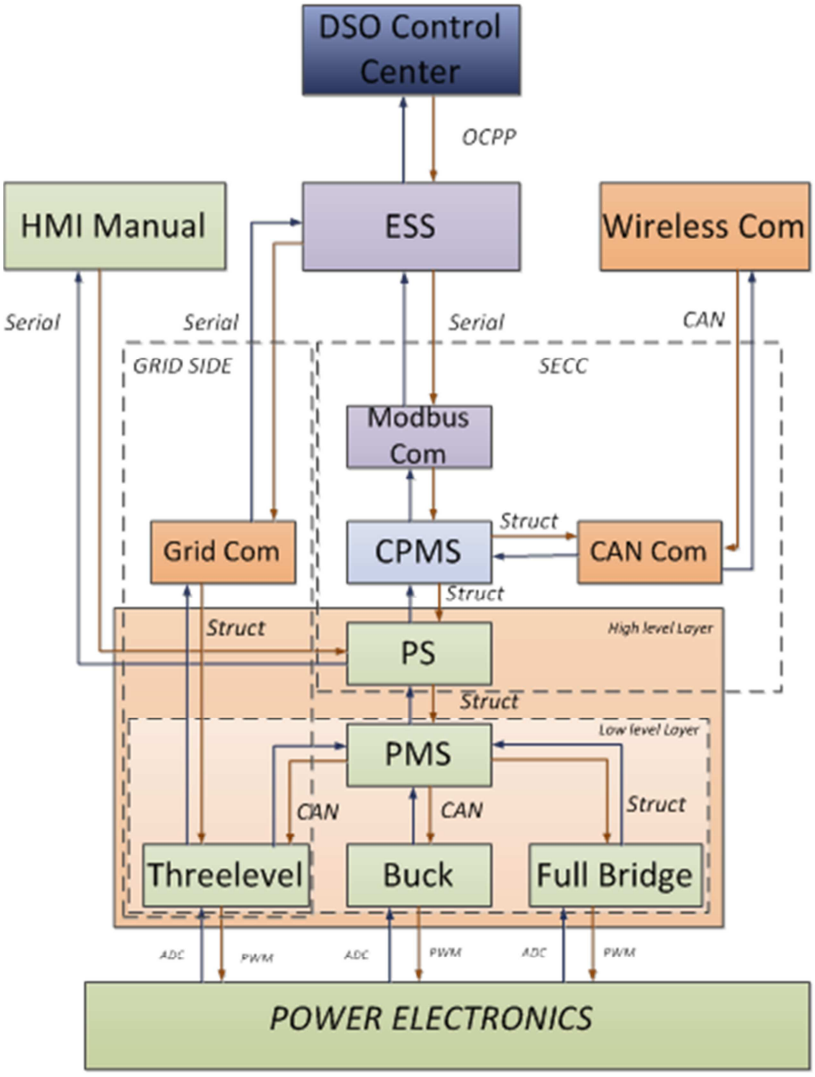

Figure 28 Modules from the charger side

2.5.2 Charger system modules

In the previous section the module distribution of the charging system and the general development of the communications have been showed, now the packages developed to perform the communication between modules are being described.

Figure 29 shows the different communication modules inside the charge, and the interfaces that connect each to the others. The modules that have major functions in the system are the Endesa Smartbox System (ESS), the Power System (PS), the Control Center and the Charging Protocol Management System (CPMS). The rest of the modules where developed to communicate between systems. Instead of developing a big communications model that includes all the systems and change the communication established by each of them, we decided to include interfacing modules designed to exchange information just between two systems. Those new packages just need to know the interfaces and the protocol of communication of each system (CAN, Modbus…) to connect both units.

Modularization requires a bigger developing phase, but in the long term have advantages over a centralized solution. The problem is divided into subsystems, meaning that each solution for each communication is easier to understand and deal with than a general overview. Even more, if a module or a communication is substituted by another one, for example, communication between ESS and CPMS is changed from CAN to TCP/IP, the substitution of the interfacing module will be enough to ensure the well-functioning of the system.

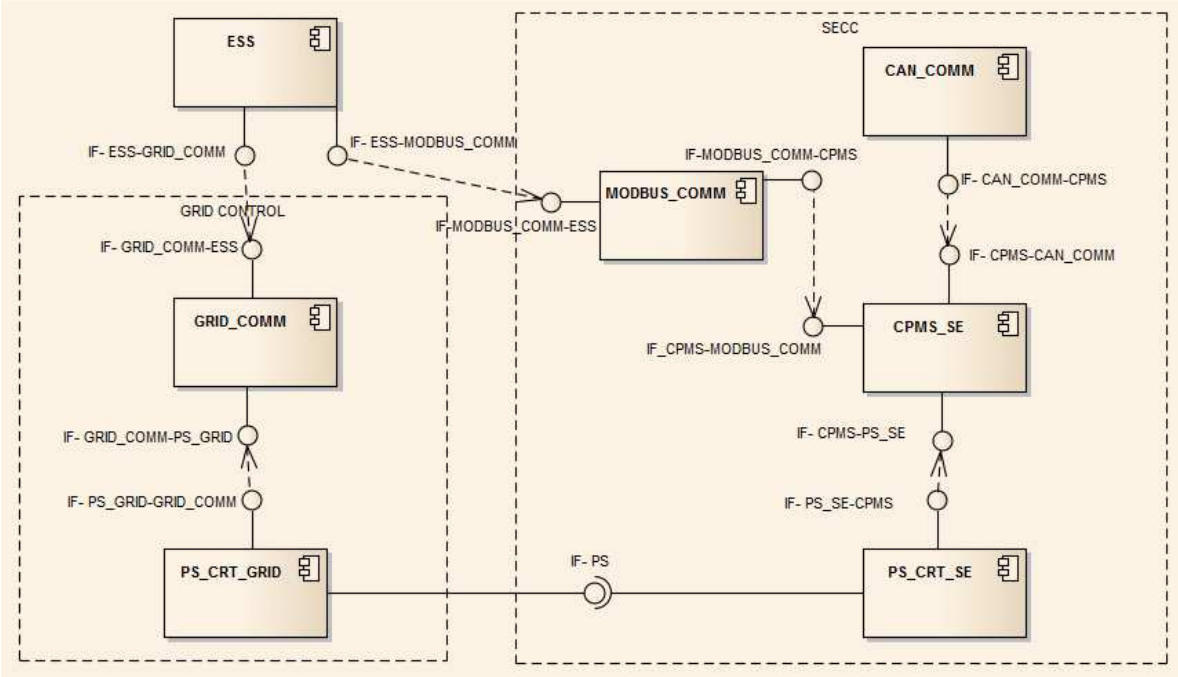

Figure 29 Package division of charging side

To go in depth in the development, we are going to divide the modules between two branches: the grid side and the Supply Equipment Communication Controller (SECC) side.

2.5.2.1 Grid side

The grid side involves the power modules that generate the signal used to energize the primary coil. It controls the threelevel electronic board and obtains active energy from the grid to charge the vehicle. It compensates the disturbance on the grid too by obtaining or delivering reactive energy.

The information of this system is stored in the database of the ESS to be consulted in the future in case it will be needed. To communicate with the ESS the GRID_COMM module was developed. It exchanges information between the interface of the ESS and the one from the power control unit. It translates the information of the serial link with the ESS in an understandable structure in the power side. The ESS can control de amount of energy required to the grid via this communication too.

2.5.2.2 SECC side

The SECC side is more extensive than the grid side. First, it includes the power control system. This module performs a control algorithm of the power delivered. Using the actual and the target values of the voltage and current of the vehicle, it calculates the necessary voltage and frequency in the primary coil needed to provide the required energy in the secondary side. In addition, it controls and supervises all the power electronic modules, and in case of an error during the charge, carries out a safe shutdown of the equipment to avoid unwanted situations.

The other main module present in this part is the Charging Protocol Management System. This module was developed along with the interfacing modules. It was designed as the “brain” of the whole process. The CPMS receives all the information from the ESS, the power control units, the grid control unit and the vehicle side. In the cases of the modules inside the SECC the communication is performed using data structures as interfaces, to communicate with other boards an intermediate module is needed. Modbus module is used to communicate with the ESS and a CAN module was programmed to communicate with the Continental modules.

CPMS holds the state machine that implements the communication protocol defined for the inductive charge, performing the upper control of the charging process and redirecting the data between packages. In case one of the modules is in error status, it transmits the error to every module in every level of communication to finish the charge with security.

The CAN module controls the master-slave behavior of the protocol. The vehicle always starts the communication, and is the charger the one who has to answer the requests received. Therefore, this module needs a state machine and some intelligence to send the correct answers to the vehicle.

To summarize the development carried out, nine totally new modules were defined and implemented, increasing the difficulty of integrating all the system. The amount of data exchanged every moment, more than 1 KB, has been a real challenge too. We faced timing problems that required a temporary study to ensure the compliance of the timeouts established in the communication protocol. Finally, the interconnections of all the systems force us to expend effort in developing software for several different protocols (OCPP, Modbus, CAN, Serial…) and big data structures.

2.5.3 Implementation and integration of the communication system

All the software necessary for controlling the power electronic boards was programmed in DSPs. We use specific software from Texas Instruments for the DSPs that is based on C. To add the new communication features we decided to use the processors we already had instead of adding new ones. The use of new processors should had been easier because the DSPs already had a lot of tasks and the timing was an important aspect to take into account, but including new hardware would had taken designing and manufacturing time, and we don't have a lot of free space too in the charger and there is no need to integrate new boards in the system. We thought was easier to have the hard work in the software part than in the hardware one.

After the developing of the software, the integration steps with the overall system started working with the existing modules of the charger, HMI and power control, and with the communications of the vehicle side. As we perform a modularized solution, we could be able to make both integrations in parallel without affecting the rest of the modules.

2.5.3.1 Integration with the HMI and power control

The first step was to check the behavior together with the power control. Both systems were deployed in the same processors, so the main problem was the software compatibility. The verifications consisted in ensure the state machines were compatible and didn't have contradictions on the status flow; the right exchange of information between packages; the correct management of the SECC by the CPMS and the adequate control in case of error.

After that, we include in the test bench the HMI. In this case the software of the HMI was designed for other projects with Endesa, and the idea was to integrate the new inductive charger in the charging system of Endesa. This existing architecture forced us to adapt the software to it and made the integration more difficult. After checking the correct communication via Modbus, we tested if the user was able to activate and deactivate the charge using the HMI.

2.5.3.2 Integration with Continental modules and vehicle side

The testing with the secondary side was performed in several steps. It was a bit more difficult because of different software programs used and the difficulties of making changes and discovers what is wrong when something was not working as it should have. The first tests were made using the software developed by FKA. They developed a model of the vehicle side using Matlab and Simulink modules. We had to connect our software to Matlab and spend some time trying to understand the functioning of the model. Also we worked with the model of CRF that included changes specifically for the vehicle.

After the initial approach using simulation software, we move on to test with the real equipment, first with a test bench provided by CRF and finally with the real vehicle. This step was hard at the beginning due to the differences in some points of the protocol, but with the collaboration of all the parts involved we achieve to fulfill the specifications. This integration lasted until the final presentation because in the last tests with the vehicle some changes in the authentication and the communication were made to prevent unsafety situations. At the end the result was successful, achieving a full communication using different ways of authentication depending on the privileges of the user and two ways of starting the charge, manually and automatically.

2.6 Design and implementation of the HMI

It has been developed a management system and external communications for two reasons. First, it allows the user of the electric vehicle to control the management or the charge and second, the status of the charger can be monitored and controlled remotely.

It has been tried to carry out the different developments under the premise of using always free and reliable software. For that purpose, in the implementation of the system has been used the programming language ADA under the GNAT compiler, because it is an object orientated concurrent language, designed for environments with necessities of security and reliability.

2.6.1 Operating System.

All the developments were executed under Debian (Linux) operative system, covering all the necessities as well as tools as technologies necessary for implementing the charging management system of the vehicle, the communication with the control center and the management of the payment system.

2.6.2 User Interface (HMI).

We defined the sequence of screens, using, for the developing of a graphic interface, the guidelines pointed by the usability study provided by Andrea Meneghin from the Industrial Engineering department of the University of Florence.

Before the implementation a study was made to establish the different possible behaviors and use cases. With the results obtained a flow diagram, showed in Figure 30, was presented with the different windows and transitions between them that should be showed in the HMI during the charging process in each use case.

Apart from the software already mentioned, to perform these windows it was used the GTK open source graphic libraries.

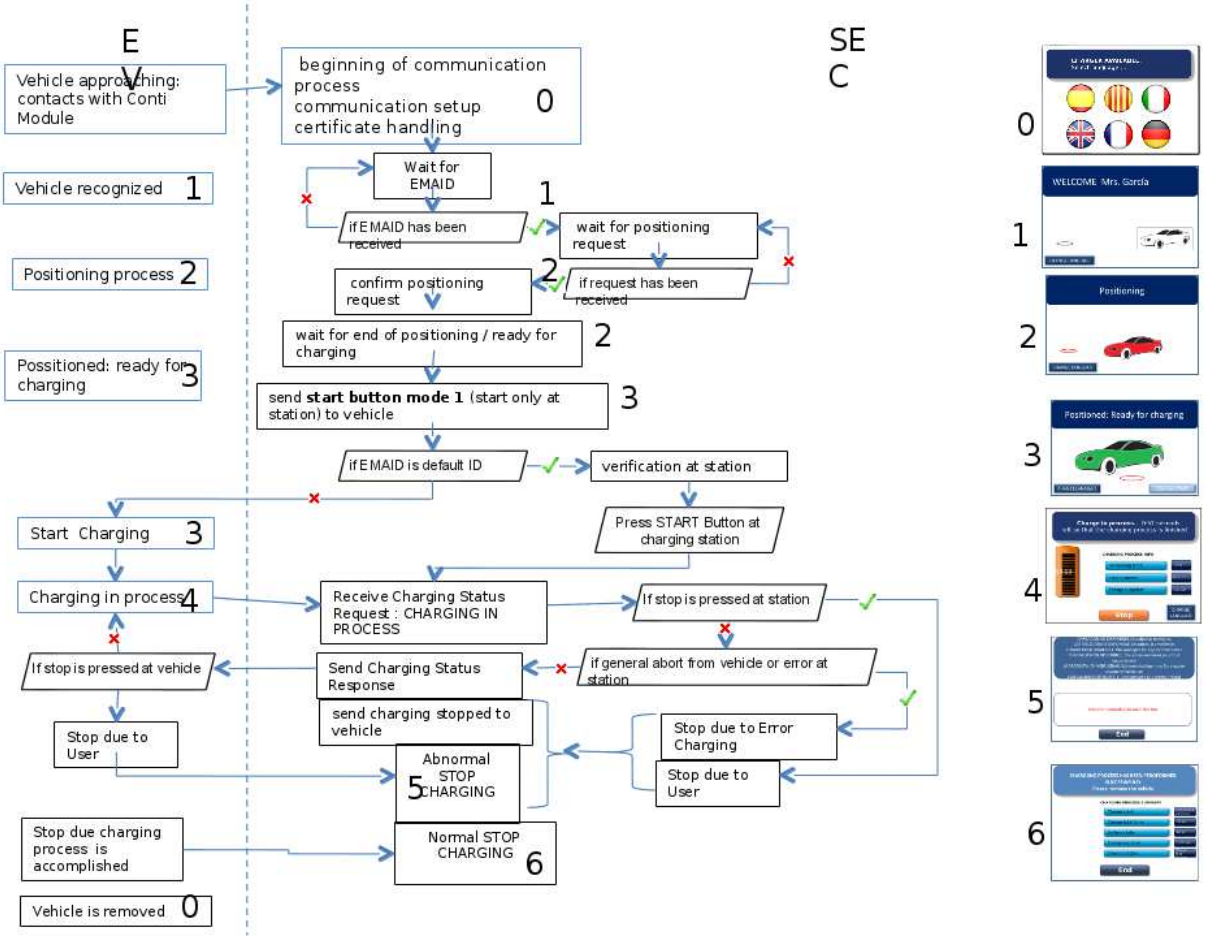

Figure 30 Screen flow during the charge for each use case

2.6.3 Internal Communications ESS-CPMSs (inductive and network).

Another study of the system was made, taking into account aspects like scalability, modularization of the different subsystems, and the grid. Keeping that in mind a class hierarchy that satisfy our necessities was defined and implemented.

Following the frame of the Fasto GF project, other project of conductive charge with Endesa, the new class hierarchy, presented in Figure 31, that include the CPMS for the inductive charge and the grid, was aggregated to the existing. For the new features a new memory map was added to perform the communication with the CPMSs, using Modbus protocol. With this new map the manager could access the information relative to the CPMS parameters, as well as monitoring and control of the CPMS status and situation and management of the errors.

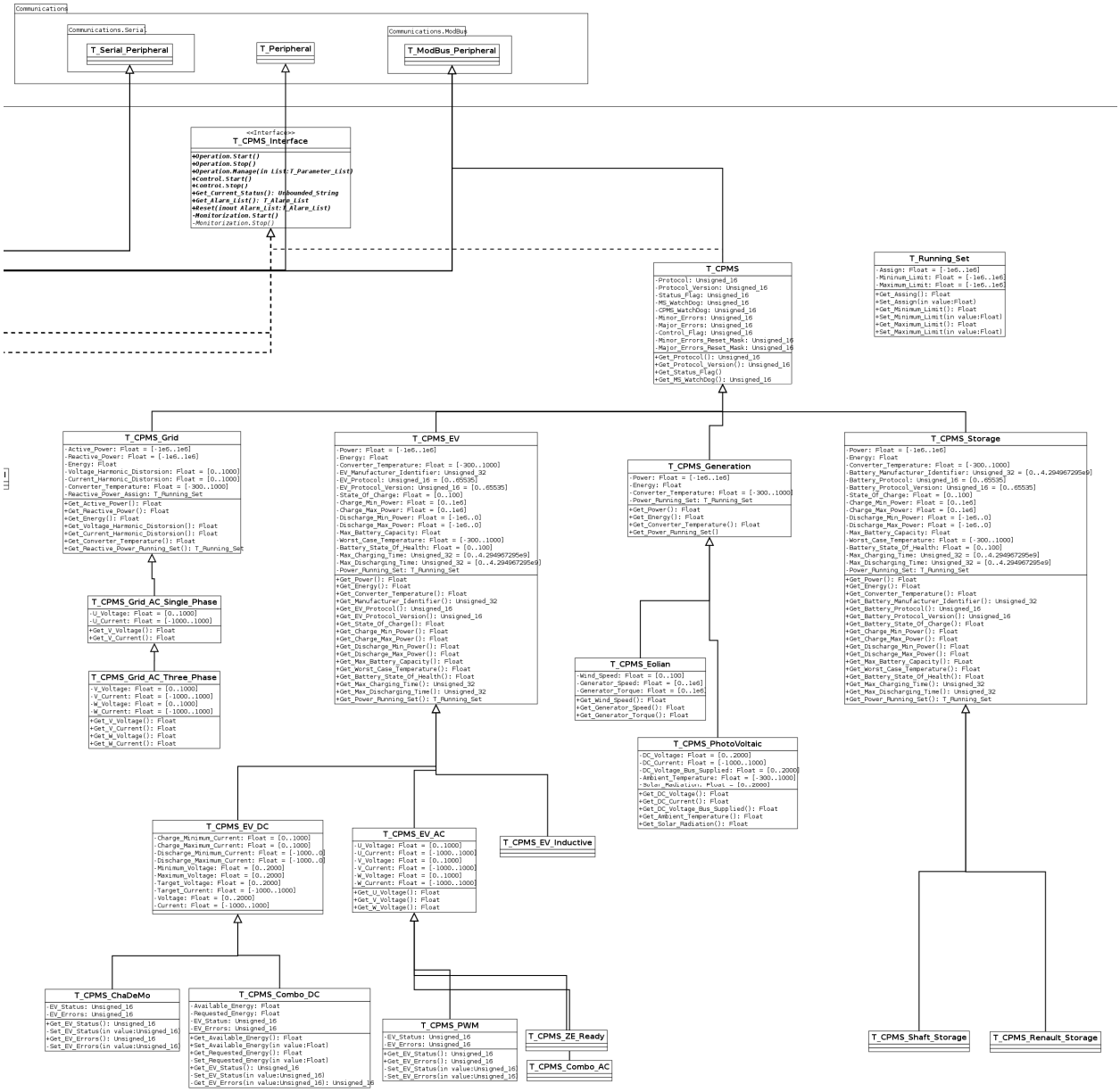

Figure 31 Class hierarchy for the new CPMSs

2.6.4 External Communications ESS-CMS (OCPP 1.5).

To the transference of information between ESS and the control center (CMS) it was used the standard protocol OCPP 1.5. Some additional features were added to cover the necessities not considered in the original OCPP 1.5.

This communication follows a Services Orientated Architecture (SOA). Both client and server parts has been developed, where the communication could be initiated from both sides.

OCPP 1.5 functionalities initiated externally, than means the ESS implement the server side, are the following:

- Cancel Reservation
- Change Availability
- Change Configuration
- Clear Cache
- Data Transfer
- Get Configuration
- Get Diagnostics
- Get Local List Version
- Remote Start Transaction
- Remote Stop Transaction
- Reserve Now
- Reset
- Send Local List
- Unlock Connector
- Update Firmware

OCPP 1.5 functionalities initiated by the ESS, that is the client side of the functionality, are the following:

- Authorize
- Boot Notification
- Data Transfer
- Diagnostics Status Notification
- Firmware Status Notification
- Heartbeat
- Start Transaction
- Status Notification
- Stop Transaction

2.6.5 Registration and database.

A new relational database was created specifically for this project. This database has been implemented using Postgresql 9.1 tools. The information stored corresponds to:

- Charging curves from the batteries and monitoring of the grid.
- System events (errors, change of status of the CPMS, etc.)
- User management.

2.6.6 Payment and user validation system.

One new class hierarchy was defined for performing the payment system control, allowing the possibility of adding any possible way of payment.

More specifically, for this project has been implemented the payment using RFID cards for managing the validation of the user and the credit of the card. With the unique ID of each card, the provider could know who wants to charge and if has permission or not. If the user is invalid, the charge is stopped at the beginning. If it has permissions, the charge carries out and the credit of the card spent is removed.

2.6.7 Adaptation of CMS to the new architecture.

For adapting the CMS to the new architecture, it has suffered several deep modifications from the previous version to be able to manage the new web services.

- Actualization of web services from tomcat7 to tomcat8.
- Addition of AXIS module to allow a web services architecture.
- Addition of Hibernate module for the communication of the application with the database. In the previous version it was used jsp with our own libraries in J2EE.
- Addition of Spring Framework module for generation of web services. In the previous version this was carried out using jsp.
- A database was developed with Posgresql to hold the new architecture, in the previous version it was used using MySQL
- Implementation of the OCPP 1.5 functionalities. These are the same implemented in the ESS, but the opposite side of the communication. That means if the ESS holds the client side, the CMS implements the server side, and vice versa.

2.6.8 Tests

There was two phases of tests in the process. In the initial phase the management system was tested with the test bench provided by CRF. In the tests it was verified that the data from the vehicle were received properly, the screens flow was correct compared with the status of the CPMS and the charge could be managed suitably.

In the final phase, the tests were made using the vehicle provided by CRF. Some modifications had to be made to adapt to the final changes in the communication and in the Control Center, but finally the process obtained was satisfying for our purposes and the charge could be managed properly.

2.7 Control and automation

Although the specific controls for each subsystem that composes the 50 kW charger have been implemented in previous development, eventually it has been necessary to integrate all of them, along with the communication systems, in order for the device to act as a whole.

An important part of this abstraction level which, obviously, it has not been possible to thoroughly test until all the elements were available, is the global automation of the system, without human intervention. However, aiming to guarantee that the task could be carried out with operational safety using only the received elements, it has been necessary to perform some changes in the development, which were not initially considered.

2.7.1 Changes in the development

Basically the modifications which have had to be performed have been due to slight not conformities of other subsystems with the set out specifications, and to the need for improvement of the tolerance of the global system when facing possible faults in the operation of some of its subsystems.

2.7.1.1 New tolerant control method with latency communication system

Some maximum response times in the communication system were specified at early stages in the project, to assure the operation of the power control system. However, the conventional WiFi technology used in the implementation, although having an acceptable latency most of the time, could surpass largely the maximum specified time in transient events.

For that reason, the power control algorithm initially proposed had the risk of becoming unstable in case of a possible micro-interruption of the wireless communication, and this was unacceptable from an operational safety point of view, and could make necessary to restart the charging process if some of the subsystems became not operational. As an example, if the maximum current admitted by the battery was exceeded, due to a transient communication cut, the BMS could decide to open the protection breakers and to generate an error condition, which would force the system to restart the charge protocol from the beginning.

To avoid this possibility, work has been done to create a new control method based both on the measurement received from the vehicle and on various state variables which can be obtained from the primary side.

The direct charge current and battery voltage measurements sent by the vehicle are irreplaceable information for the charger, since they are the ones unaffected by losses, misalignment or parametric drift. However, if an accidental communication interruption occurs, it is possible to maintain system stability trying to control the state variables which are measurable from the primary, since the controlled variables will not suffer significant variations during this short period. Obviously, some error in the control of the power supplied to the battery can arise but, as it has been experimentally corroborated, the control level is enough to avoid interruptions in the charge process due to a transient communication error.

Besides, it has to be considered that if the communication error is permanent, the charge process will be interrupted when the timeouts are exceeded, quite more generous, that imposes the communication protocol.

2.7.1.2 New method for vehicle presence detection

Another risk which can appear in the charge process is the activation of the power system while the vehicle is not positioned over the emitting coil. Although the ICPT system is misalignment tolerant, it was necessary to activate a protection in case of an error in the vehicle positioning system leading to the vehicle not being in the desired position, leaving the primary coil without either load or shielding.

The risk for the equipment was limited by its own inner protections for the electronic stages bur, in any case, those act once a magnetic field much larger than the admissible one has been emitted.

To avoid this situation, a load identification procedure was developed. Once the behaviour of the real ICPT system had been characterised, including losses and non-linearities, it was proposed and algorithm that iteratively emitted various low power magnetic field bursts to detect the effect of the resonance of a secondary winding tuned to the primary coil. This process lasted about 50 ms and it was performed at the lowest possible operational bus voltage, generating a very low magnetic field emission.

Once a valid load has been detected in the secondary, the charge process is started with power and phase control to supply the power demanded by the battery. If, on the contrary, a valid load is not found within a few cycles (10 cycles were set for the prototype) the charge process is aborted, generating an error condition.

2.7.1.3 Vehicle bus overvoltage protection

An eventuality which had not been considered in the first stages of the development of the Project was the possibility of the vehicle BMS unexpectedly disconnecting the safety breakers while the charge was underway. Taking into account that the energy stored in the passive components of the ICPT system implies some inertia in the power sent to the load, the maximum voltage at the DC bus could be exceeded, since there was no path for this energy to flow.

To avoid possible damage in the equipment, two IGCT in common emitter bilateral switch configuration were included, providing the possibility of short-circuiting the secondary coli of the ICPT, before the secondary rectifying bridge. By doing this, an immediate interruption of the power sent to the vehicle DC bus is achieved. Besides, this protection profits from one of the advantages of the SPS topology, since it tolerates secondary short-circuit without a dangerous primary current increase. What can be observed from the control side is a sudden primary current phase shift, which is interpreted as a fault situation and the operation of the charger is immediately interrupted, causing a safe cascade disconnection of all the subsystems.

2.7.2 Operating results

This part of the document shows the results obtained in the automation and the implemented power control algorithm. More specifically, it shows the operation of the vehicle detection algorithm and the power control, keeping the optimal phase shift to maximize the efficiency.

2.7.2.1 Detection algorithm and tuning with the vehicle

As aforementioned, it is desirable that the power control confirms the presence of a valid load in the ICPT before applying full power. By doing this, operational safety is achieved in the event of an error of the positioning system.

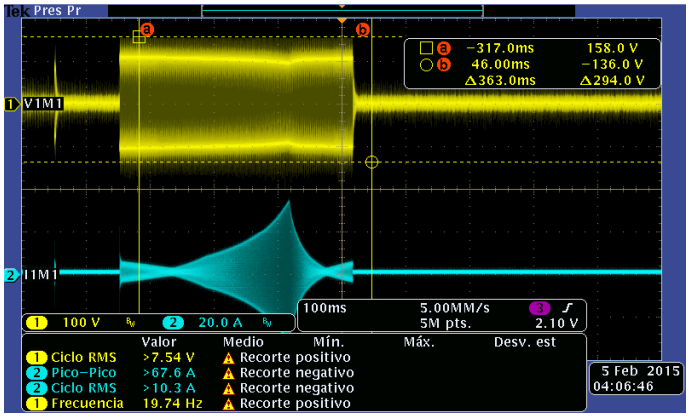

Figure 32 Detection of secondary load without load

Figure 32 shows one of the sweeps that the system performs to detect the secondary. The yellow graph shows the voltage supplied by the high frequency inverter, keeping a voltage almost constant in amplitude but with a variation of the modulated frequency.

The subsequent current absorbed by the ICPT (blue) varies with frequency. The sweep is preformed from the highest frequencies, considered intrinsically safer, to the lowest ones. The peak corresponds to the resonance of the unloaded ICPT, which would have fatal consequences for the equipment if this peak was not detected by the control system. The response of the algorithm is a fast increase in frequency to protect the equipment avoiding an unwanted heating of the inverter.

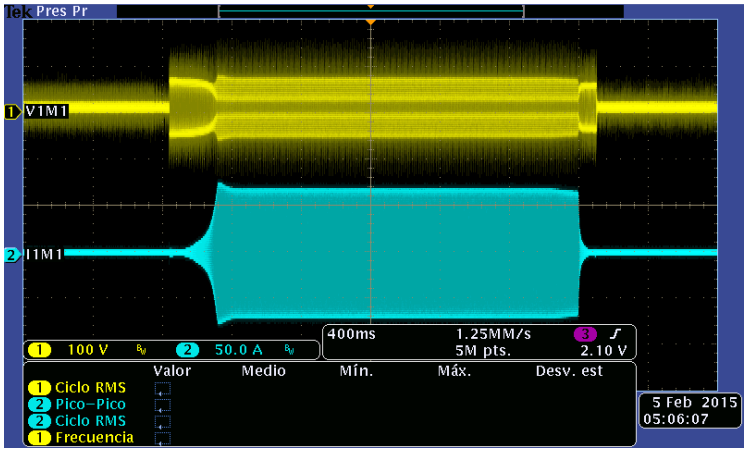

Figure 33 Detection of secondary load with load

Figure 33, shows the case when a valid load is present. In this case, the algorithm switches to power and phase control mode, which will be maintained until the end of the charge.

2.7.2.2 Power control and phase control

In power control mode, the algorithm focuses on keeping the desired power supplied to the battery, and the optimal phase shift to minimize power losses in the inverter.

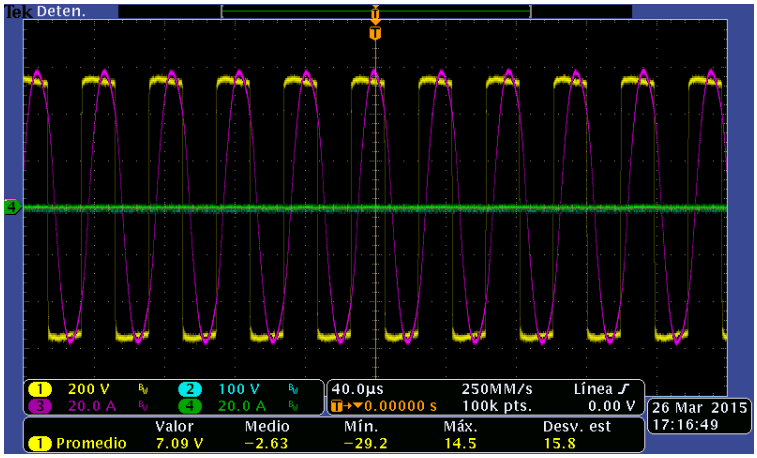

Figure 34 Power control and phase control

Figure 34 shows voltage (yellow) and current (magenta) waveforms during the charge process with a correct phase control. It can be observed that the phase shift is not zero, but it is kept at a point where losses in the inverter are as low as possible. A slight current delay favours the commutation of the switches since it ensures a brief conduction of the anti-parallel diode of each IGBT prior to the change to the ON state. In this situation the voltage across the transistor is already zero (strictly speaking the small current across the conducing diode) which avoids a fast voltage transient. This type of switching, called ZVS implies a significant reduction of the losses in the transistor and the reverse diode, and the electro-magnetic emissions due to the switching (the ringing phenomenon associated to hard switching does not appear).

Notwithstanding, during this mode of operation the charge keeps being controlled in the way explained in the previous section. By doing this, if a significant modification in the operation point occurs, for instance if the vehicle has moved for any reason, resonance has been lost or the secondary has been short-circuit, the algorithm will initiate the process of fast frequency increase in order to protect the equipment, and it will return to the search for a valid load, in case the error is due to transitory causes, and the system can recover.

2.8 Commissioning and final results

Weather during the days of commissioning was very bad, rainy, cold and windy, this made very difficult to work due to the Power electronics is a delicate 50 kW system and had to take certain security measures for both: people and equipment.

It was necessary to use a tent to cover people and power electronics, as can be seen in the next figures

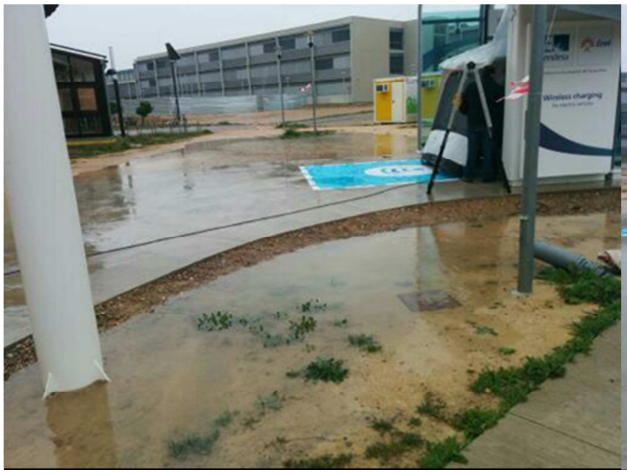



ed

But finally, the work was done and the rain allowed taking nice photos of the charging station

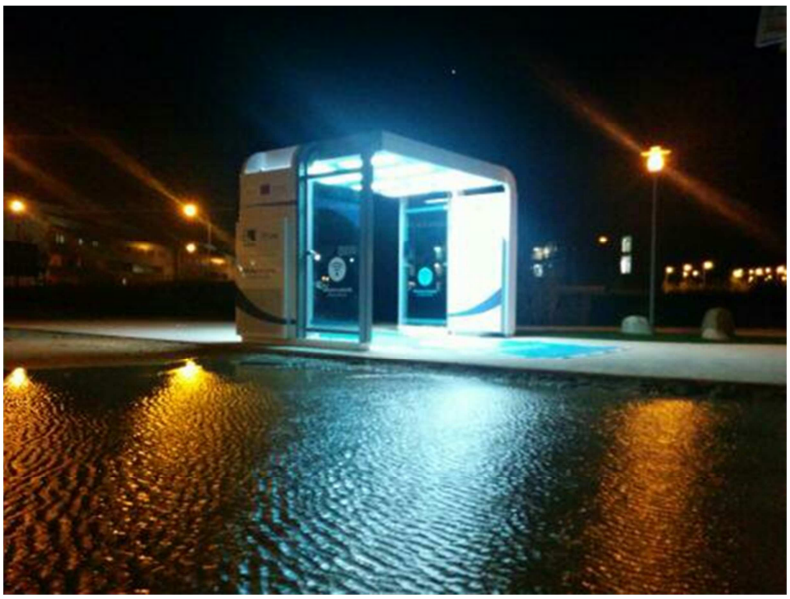

Figure 35 Charging station at CIRCE facilities

Figure 36 Charging station at CIRCE facilities

2.8.1 Test of the charging process

The power delivered to the van is defined by the Van itself according with several parameters such as SOC and battery temperature.

Four test were done: two of them measuring absorbed power from the grid side and the power delivered to the battery pack, and two measuring the power at the output of the HF bridge and the power delivered to the battery. It can be obtained the total efficiency, the efficiency of the power electronics and the efficiency of the IP (including secondary power electronics).

As the power was limited by the van and it never was bigger than 17 kW, the grid side converter worked always at less than 34% of the nominal power, while HF worked at 68% of the nominal power, the same than the IPT. This is why we have done an estimation of the efficiency at full power.

2.8.1.1 Test 1: from the grid to the battery

Results obtained are:

Grid Power:	21142 W
Battery Power:	15914 W
Grid-Battery efficiency:	75.27 %
Losses:	5228 W

Next figure shows voltage an current in the grid side, as there was only two voltage an current sensors, the third phase (red in the figures) is obtained adding the other two phases, this is why it shows a different shape.

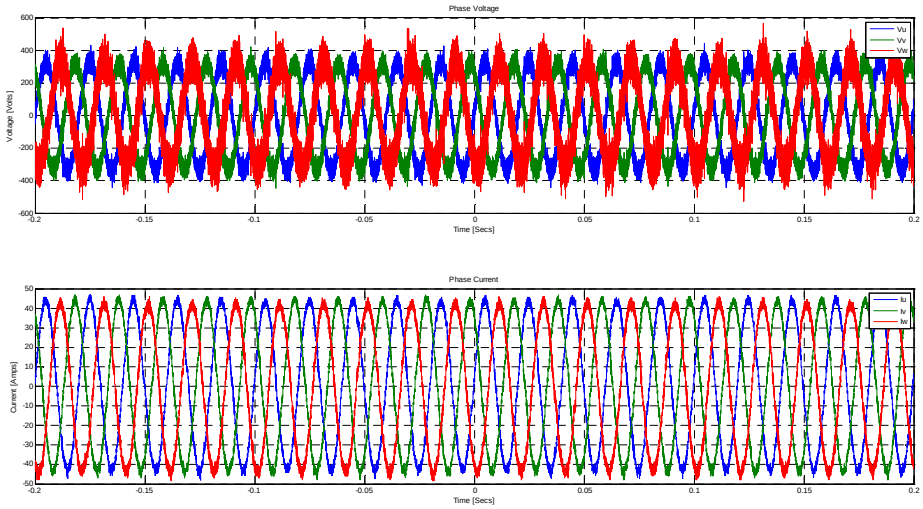

Figure 37 Test 1: voltage and current at the grid side

Next figure shows voltage and current at the battery

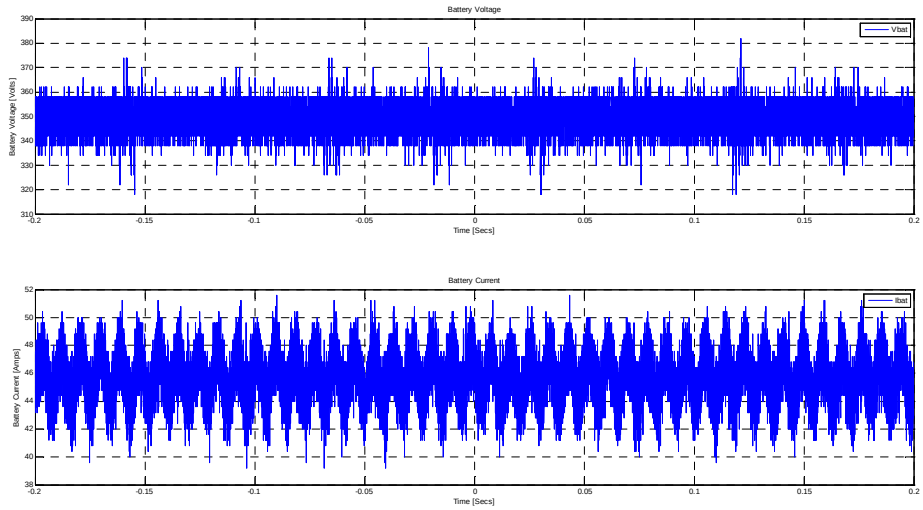

Figure 38 Test 1: voltage and current at the battery

2.8.1.2 Test 2: from the grid to the battery

Results obtained are:

Grid Power:	21149 W
Battery Power:	16028 W
Grid-Battery efficiency:	75.79 %
Losses:	5121 W

Next figure shows voltage an current in the grid side, as there was only two voltage an current sensors, the third phase (red in the figures) is obtained adding the other two phases, this is why it shows a different shape.

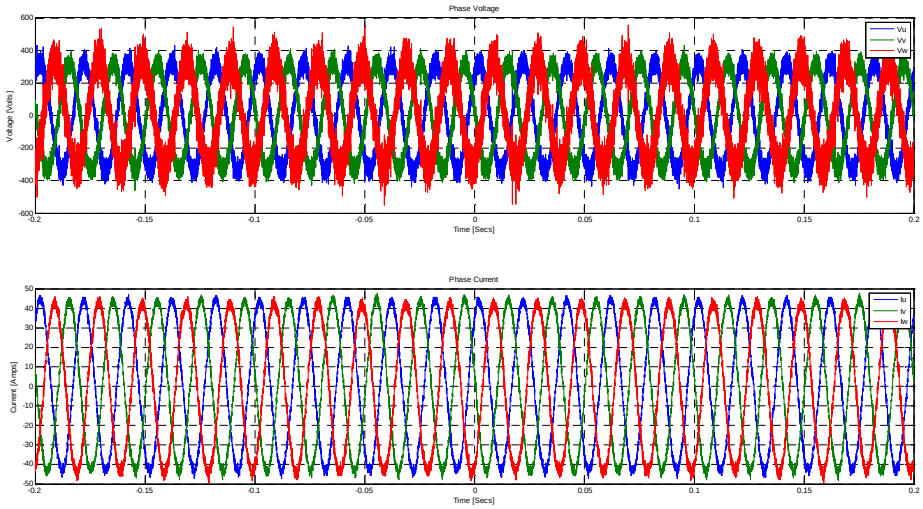

Figure 39 Test 2: voltage and current at the grid side

Next figure shows voltage and current at the battery

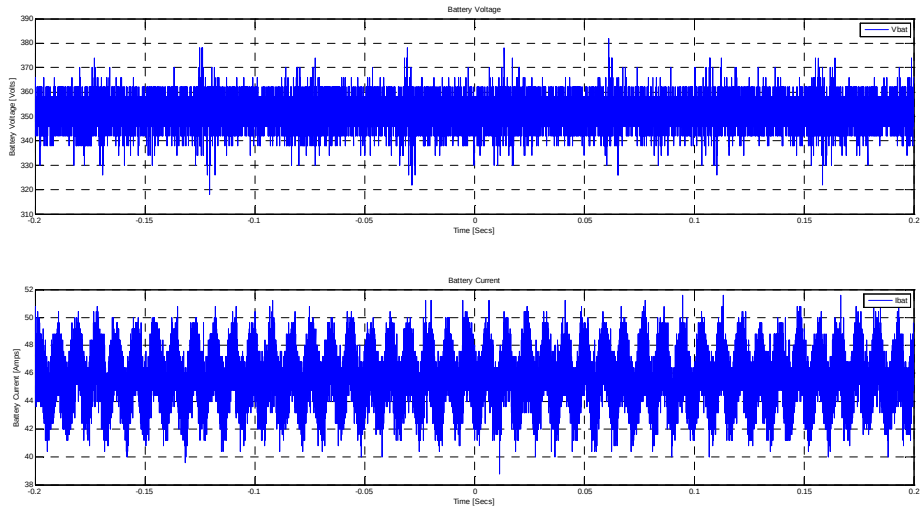

Figure 40 Test 2: voltage and current at the battery

2.8.1.3 Test 3: from HF inverter to the battery

Results obtained are:

HF Power:	20016 W
Battery Power:	16422 W
Grid-Battery efficiency:	82.04 %
Losses:	3594 W

Next figure shows voltage and current at the output of the HF bridge.

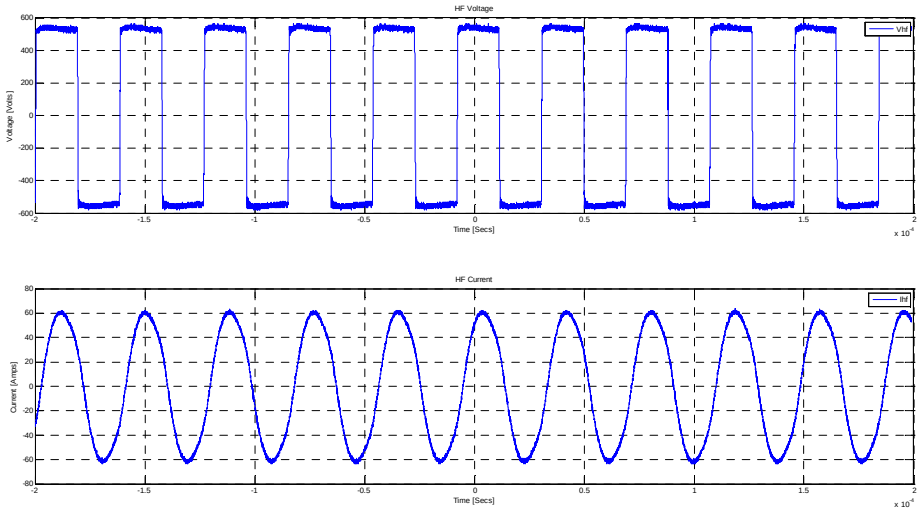

Figure 41 Test 3: voltage and current at the output of the HF bridge

Next figure shows voltage and current at the battery

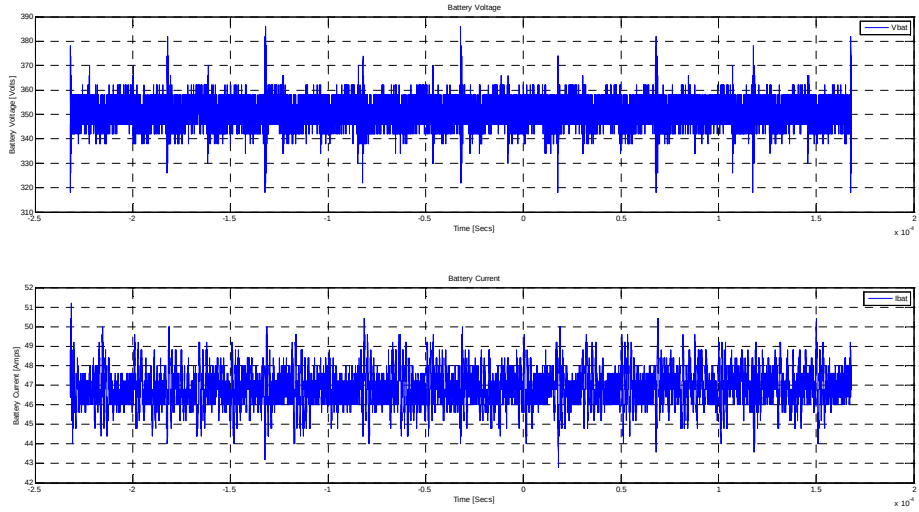

Figure 42 Test 3: voltage and current at the battery

2.8.1.4 Test 4: from HF inverter to the battery

Results obtained are:

HF Power:	18560 W
Battery Power:	15562 W
Grid-Battery efficiency:	83.84 %
Losses:	2998 W

Next figure shows voltage and current at the output of the HF bridge.

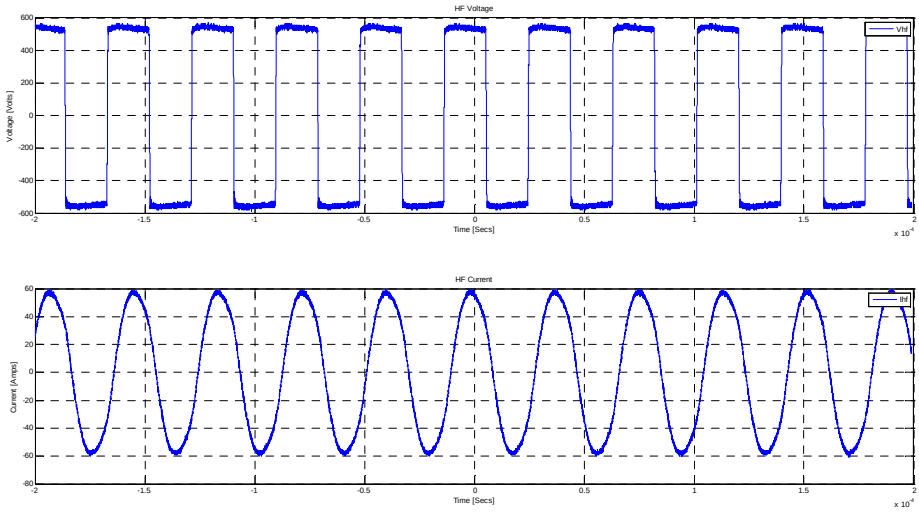

Figure 43 Test 4: voltage and current at the output of the HF bridge

Next figure shows voltage and current at the battery

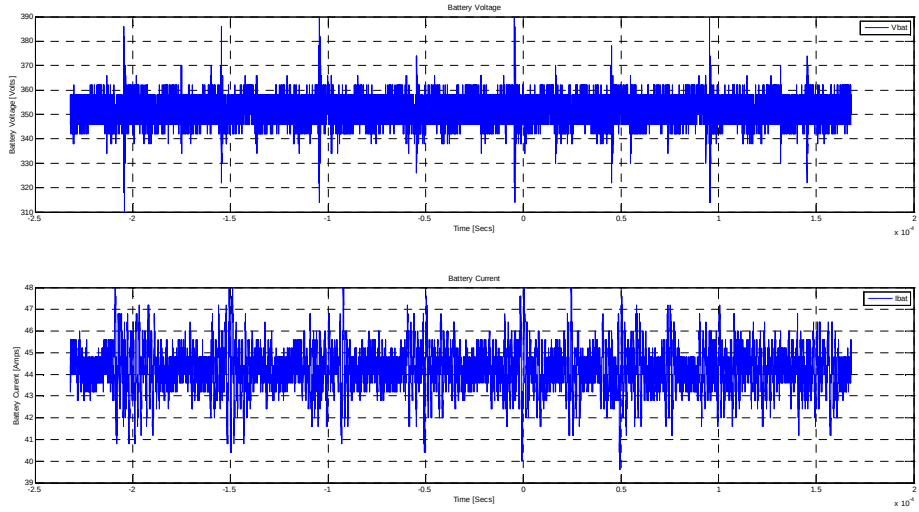

Figure 44 Test 4: voltage and current at the battery

2.8.1.5 Conclusions

Averaging the results of performance between the four test and considering as mean output power from the four test. can be obtained:

Mean Batt power:	15982 W
Mean HF power:	19267 W
Mean Grid power:	21160 W
IPT losses:	3286 W
IPT efficiency:	82,95 %
PE losses:	1892 W
PE efficiency:	91,06 %

Total efficiency:	75,53 %

Table 3 Mean values from the test

Losses at the IPT system are quite big due to:

- The coils still are handmade prototypes.
- The connection between resonant capacitors and coils is completely made by hand with high restriction of space, giving high temperatures when working due to bad electrical contact.
- The installation of the primary coils in the EMI shielding should be improve putting both terminal cables together using only one hole, instead of two independent and separated holes, reducing the electromagnetic field induced in the aluminum plate and then reducing the losses.

Then improving the manufacturing of the coils, their connection with the capacitors and the installation of the coils, the losses in the IPT could be reduced, obtaining better results than in the final installation, and even better efficiency than obtained in the lab.

On the other hand the losses in the IPT system are basically constant, because in the chosen topology the primary current in the resonant circuit L-C is constant regardless of the power.

Regarding power electronic efficiency, it includes passive elements: filter in the grid side, and a coil at the output of the buck inverter. As said at the beginning of the item, the grid side converter works always at less than 34% of the nominal power, while HF worked at 68% of the nominal power, the same than the IPT. Nevertheless, losses are practically constant in passive elements because they are due mainly to the ripple of the current, and the ripple reduces as the power increases. On the other hand losses in the power electronics components increase with the current. At this point in order to obtain some figures giving 50 kW to the battery, it has been considered: IPT losses are the doubled due to there are two coils working: 6572 W; losses at the passive elements of the filter side are constant, while the losses due to the buck coil is doubled, and finally, losses at the electronics components are doubled, giving 3513 W. With this, total losses are estimated at 9725 W. The next table shows the estimated values considered at 50 kW.

Batt power:	50.000 W
HF power:	56572 W
Grid power:	59725 W
IPT losses:	6572 W
IPT efficiency:	88,38 %
PE losses:	3153 W
PE efficiency:	94,7 %
Total efficiency:	83,71 %

Table 4 Estimated values at 50 kW

2.9 Field measurement procedure and results

2.9.1 Protocol

Our goal was to measure the magnetic induction **B** magnitude inside the vehicle when the charging system is running. We performed measurements at the driver seat, at various locations: feet, head and chest in order to find the maximal value of the field. We also performed measurements in the van's trunk.

In addition, we performed measurement close to the coils in order to assess the maximal value of the field in the vicinity of the coils.

It is to note that only one coil was powered : the Iveco is designed to be charged at 20KW.

2.9.1.1 Sensor used

We used an Aaronia Spectran high frequency (HF) magnetic sensors, the NF-5035 3 axis magnetometer. The later can measure B fields between the [1 kHz -10 MHz].

This high frequency sensor can perform measurement of the field created by the induction coil (20 KW, f~25 KHz).

2.9.1.2 Standard used

We compared the measurements with the ICNIRP guidelines [1]. The recommended levels are summarized in tables Table 5 and Table 6.

Frequency range	E-field strength ($V\ m^{-1}$)	H-field strength ($A\ m^{-1}$)	B-field (μT)	Equivalent plane wave power density S_{eq} ($W\ m^{-2}$)
up to 1 Hz	—	3.2×10^4	4×10^4	—
1–8 Hz	10,000	$3.2 \times 10^4/f^2$	$4 \times 10^4/f^2$	—
8–25 Hz	10,000	$4{,}000/f$	$5{,}000/f$	—
0.025–0.8 kHz	$250/f$	$4/f$	$5/f$	—
0.8–3 kHz	$250/f$	5	6.25	—
3–150 kHz	87	5	6.25	—
0.15–1 MHz	87	$0.73/f$	$0.92/f$	—
1–10 MHz	$87/f^{1/2}$	$0.73/f$	$0.92/f$	—
10–400 MHz	28	0.073	0.092	2
400–2,000 MHz	$1.375f^{1/2}$	$0.0037f^{1/2}$	$0.0046f^{1/2}$	$f/200$
2–300 GHz	61	0.16	0.20	10

Table 6

For each measurement, we plotted the data acquired along with the ICNIRP maximum acceptable value.

Frequency range	E-field strength ($V\ m^{-1}$)	H-field strength ($A\ m^{-1}$)	B-field (μT)	Equivalent plane wave power density S_{eq} ($W\ m^{-2}$)
up to 1 Hz	—	1.63×10^5	2×10^5	—
1–8 Hz	20,000	$1.63 \times 10^5/f^2$	$2 \times 10^5/f^2$	—
8–25 Hz	20,000	$2 \times 10^4/f$	$2.5 \times 10^4/f$	—
0.025–0.82 kHz	$500/f$	$20/f$	$25/f$	—
0.82–65 kHz	610	24.4	30.7	—
0.065–1 MHz	610	$1.6/f$	$2.0/f$	—
1–10 MHz	$610/f$	$1.6/f$	$2.0/f$	—
10–400 MHz	61	0.16	0.2	10
400–2,000 MHz	$3f^{1/2}$	$0.008f^{1/2}$	$0.01f^{1/2}$	$f/40$
2–300 GHz	137	0.36	0.45	50

Table 5. Reference levels for occupational exposure to time-varying electric and magnetic fields

Frequency range	E-field strength (V m^{-1})	H-field strength (A m^{-1})	B-field (μT)	Equivalent plane wave power density S_{eq} (W m^{-2})
up to 1 Hz	—	3.2×10^4	4×10^4	—
1–8 Hz	10,000	$3.2 \times 10^4/f^2$	$4 \times 10^4/f^2$	—
8–25 Hz	10,000	$4{,}000/f$	$5{,}000/f$	—
0.025–0.8 kHz	$250/f$	$4/f$	$5/f$	—
0.8–3 kHz	$250/f$	5	6.25	—
3–150 kHz	87	5	6.25	—
0.15–1 MHz	87	$0.73/f$	$0.92/f$	—
1–10 MHz	$87/f^{1/2}$	$0.73/f$	$0.92/f$	—
10–400 MHz	28	0.073	0.092	2
400–2,000 MHz	$1.375f^{1/2}$	$0.0037f^{1/2}$	$0.0046f^{1/2}$	$f/200$
2–300 GHz	61	0.16	0.20	10

Table 6. Reference levels for general public exposure to time-varying electric and magnetic fields

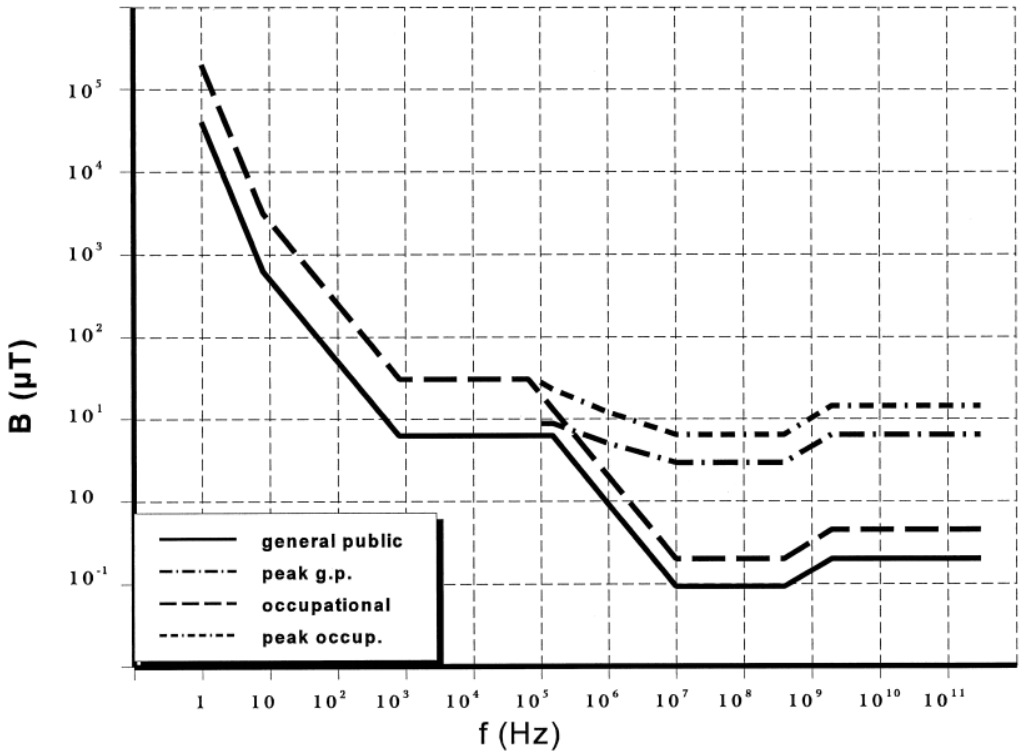

Figure 45. Reference levels for exposure to time varying magnetic fields.

2.9.1.3 Position of the sensor for measurements

The sensor was positioned at several places in the Iveco: head, seat and feet for both the driver and the passenger seats. We checked that these locations were representative from the value of the magnetic field inside the car. Indeed, we displaced the sensor inside the car, and we could not find a location showing particular magnetic field value peaks.

2.9.1.4 Description of the configurations investigated

We performed several measurements, with parameters as follow:

- location of the sensor (several locations around the driver's seat)

- door opened or closed (to assess the shield effect)

It is to note that the inductive charging cannot be turned on if the car power is turned on. This is to avoid the case when the driver would move the car while it is charging.

2.9.1.5 Precautions to follow by the user with the Aaronia Spectran sensor

We noticed 2 sources of errors in the measurements

1. An USB extension cable generates a peak @540 kHz. It must be avoided.

2. The user must be careful when using the Aaronia sensor the right attenuator value has to be chosen manually particularly with very strong signals to avoid overloading the external SMA input.

2.9.2 Results

2.9.2.1 The shielding effect cancels the field inside the car

The results of the measurements show that the measured magnetic induction inside the car is far under the maximal acceptable threshold defined by the ICNIRP (31 µT). Indeed, the maximal value measured inside the car is 10 nT @ 25KHz.

This can be explained by i) the distance between the driver' seat and the charging coil (roughly 4 meters), and ii) the shield effect of the car body.

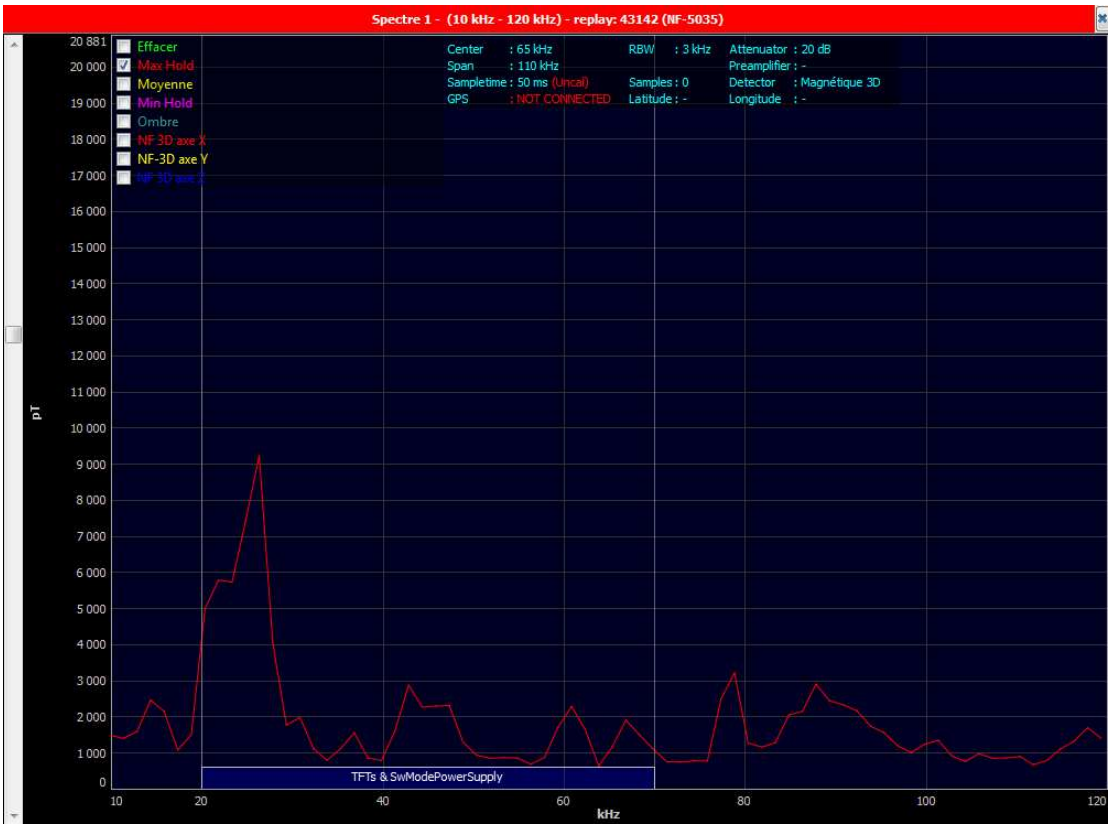

Figure 46: the highest value measured at the driver' seat is 9 nT.

2.9.2.2 Measurements around the primary coil

We performed measurements in the vicinity of the primary coil, in order to measure the maximum value of the field measurable close to the coil. The estimated distance between the sensor and the coil was in that case about 20 cm, so this situation is not representative of a usage scenario, for which the user is far away from the primary coil.

The higher value we measured is 9.3 µT, which is under the limit of the ICNIRP occupational limit (30.7 µT).

Figure 47: the highest value measurable is 9.3 µT, very close (20 cm) to the primary coil. This value is still lower than the ICNIRP value.

2.9.3 Conclusion

We have performed several measurements inside the Iveco vehicle.

The highest value we obtained was a peak of 9.3 µT, only measurable in the vicinity of the primary coil. All the measurements done are compatible with the ICNIRP limits.

Consequently, the inductive system does not lead to any magnetic induction value in contradiction with the ICNIRP recommendation.

3 3.7 kW ICPT Demonstrator

During the trials, the system was tested for efficiency. Numerous components are involved in the inductive energy transmission. The system can be divided into two basic groups namely the primary side and the secondary side. The primary side consists of the inverter, the capacitor and the transmitting coil. The inverter prepares the energy provided by the mains network for the oscillating circuit. The capacitor and the transmitting coil form the oscillating circuit for the inductive transmission. On the secondary side the magnetic field is taken up by the coil which in turn resonates with the capacitor. A rectifier then converts the energy so that it can be stored in the battery. Current flows through all these components involved in the process. Since the components are not ideal, they are prone to losses i.e. every component loses a small part of the energy in the form of for e.g. heat. To estimate these losses, measurements were conducted. Since it is not possible to measure all the components during operation, their losses were determined by calculation. For this purpose, the series resistances were determined using an LCR meter. To control the system, currents on the primary and secondary side were measured. Using the currents and the parasitic resistances, the losses in each component can be determined. The following table shows the LCR measurements for each component. The components were measured at a frequency of 150 kHz. It can be seen for the table that the series resistances are higher on the primary side than on the secondary side. It can thus be concluded that there are fewer heat losses on the secondary side as compared to the primary side.

Measured components	
PrimaryC	
nF	Ohm
15	0,17
10	0,66
10	0,66
10	0,66
15	0,175
	2,325
	1,5
PrimaryL	
uH	Ohm
478	1,96
SecondaryL	
uH	Ohm
200	0,14
SecondaryC	
nF	mOhm
25,1	31
13,6	227
25,1	25
	0,283

Table 7 LCR-Measurement results

The transmission parameters are listed in the following table (Figure 48). The primary power of 2453 W can be seen which can be calculated from the primary current and voltage. Similarly, the output power is 2012 W. Thus, the power loss is 441 W.

Characteristic power values			
Uprim[V]	Iprim[A]	Ppri[W]	Ploss[W]
310,6	7,9	2453,74	441,34
Usec[V]	Isec[A]	Psec[W]	eff [%]
223,6	9	2012,4	0,820135793

Figure 48: Transmission parameters

With the help of these values, the 441W power loss can be distributed as below. It can be seen that most of the heat losses occur in the inverter, primary coil and the primary capacitor. On the secondary side, only 64 W of the transmitted power is lost.

Measured components			**Calculated losses**
			Ploss[W]
PrimaryC			93.6
PrimaryL			122.3236
SecondaryL			11.34
SecondaryC			22.923
Rectifier			10.8
Inverter?	Determined by other values		169.5384

Figure 49: Power losses of each component

The losses can be expressed with respect to the complete system in the table Figure 50. It can be seen that almost 14% of the losses occur on the primary side.

Measured components			**Calculated losses**
			Ploss
PrimaryC			3.82%
PrimaryL			4.99%
SecondaryL			0.46%
SecondaryC			0.93%
Rectifier			0.44%
Inverter?	Determined by other values		6.91%

Figure 50: Power losses of each component corresponding to the input power

If the same procedure is followed, individual components can also be measured for e.g. with respect to coil displacement. The following graph (Figure 51) of showing the losses in the coils as a function of the displacement was generated by this method. The proportion of the losses as a function of the displacement is shown here. The losses in the coil are shown here as part of the total losses.

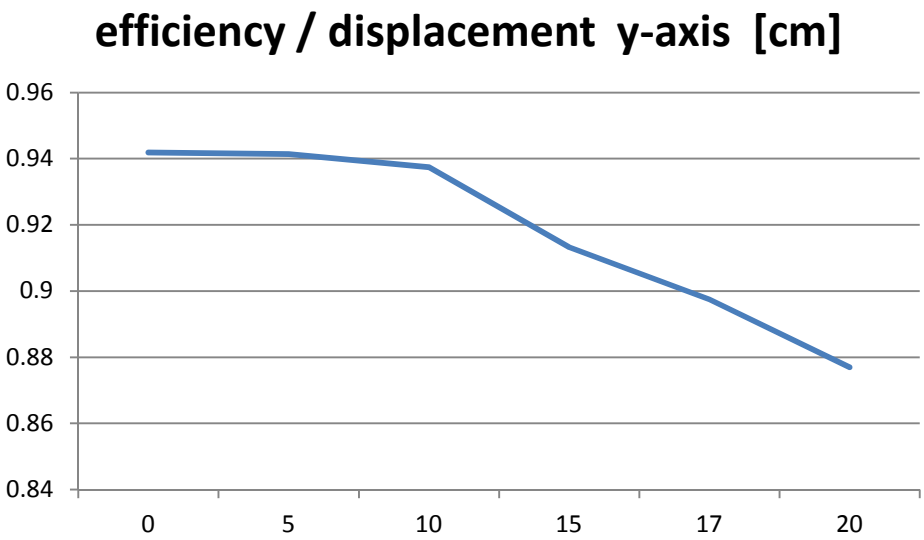

Figure 51: efficiency of the coils due to misalignment

3.1 Frequency sweep to determine resonance

As part of the first prototype tests, the start-up behavior of the system could be further optimized. With this we mean the process of starting up the power electronics and reaching maximum power capability. The start-up behavior can be split into three phases. Two phases serve to determine the output frequency. With the aid of this output frequency it is possible to deliver maximum output in the third phase.

In the first phase, the system frequency is ramped up from 140 kHz to 150 kHz in 500 Hz steps. The applied voltage is held constant at 40 V. At each step, the power at the system input is measured. The frequency is determined at which this power will be maximum. 2 kHz above the resulting frequency another frequency sweep is done. This next sweep is conducted with a finer resolution by decreasing the step size. During this process the maximum output point is estimated and frequency and power are measured for the same. The frequency is the starting point for the power transmission. The power at the system input has to exceed a specific limit. If the coils are displaced this minimum power limit is not reached and the system can detect the underlying positioning error. Figure 52 shows the current over a frequency range. It can be seen that the current increases as the frequency approaches the resonance frequency. It can also be seen that the current drops once the resonance point has been crossed.

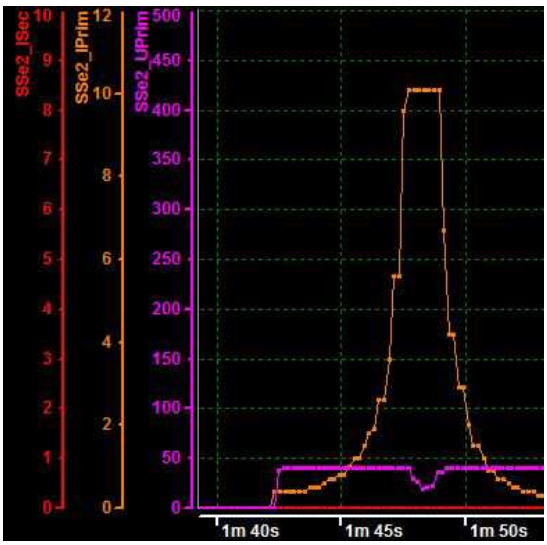

Figure 52: Frequency approach

Once the two phases to determine the frequency are done, the power output can be ramped up. Figure 53 shows the current on the primary and secondary side. The intermediate voltage of the inverter is shown in violet. The image shows the three start-up phases. The frequency detection can be roughly

seen till 9 min 40 sec. The rising and falling of the primary current can be seen clearly. At 9 min 42 sec it can be seen that the frequency is set at 2 kHz above the roughly determined resonance frequency and the second phase follows. This happens at the same intermediate voltage. Just before 9 min 50 sec, the intermediate voltage is increased after checking the input voltage. The intermediate voltage is increased in steps. The frequency is adjusted after every step. The frequency adjustment is done till a justifiable level of power loss is reached. Following this, an additional step is taken. Thus the start-up phase can have varying durations based on the position, requested power and other parameters. The process was chosen for the prototype stage to develop a robust and safe system. If parameters stay constant during series production, the start-up phase can be further optimized. The poses the question for e.g. of it is sufficient to limit the frequency range to 143 - 148 kHz instead of 140 - 150 kHz.

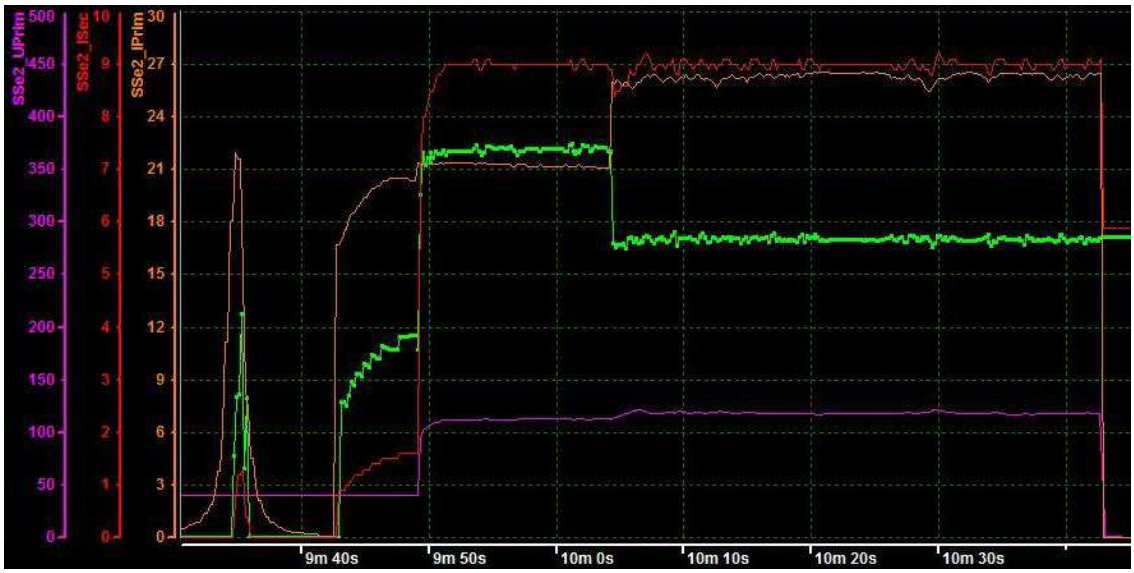

Figure 53: Power delivery start up phase

3.2 Frequency alteration due to system warm up

To achieve a maximum efficiency for the power transfer the major aspect is to operate the system in its resonance frequency. The exact frequency is, amongst other conditions, depending on the gap between the coils and the misalignment in driving and cross direction. As these parameter differ for each parking approach and different loading of the vehicle the resonance frequency is not fixed for a system or vehicle but needs to be determined at the beginning of each charging process. This is done by a frequency sweep and assessment of the actual losses.

Beside the geometrical parameters the electrical values of the resonance circuit are crucial for the resonance frequency. In detail this are mainly the resistance and the capacity of the capacitors and the resistance of the coil.

As the electrical components warm up due to the electric losses during the charging process the actual resonance frequency of the collective inductive system is constantly changing. These changes are not negligible as they may exceed 5% in respect to the inertial frequency. Without consideration of this aspect the system would waste energy as it is not operating in an optimal operating point.

Therefore the control algorithm in the primary side of the system is constantly monitoring the losses and thus the efficiency of the charging process and adapts the frequency if necessary. It is important to consider this when dimensioning the system as one needs to provide a potential frequency band that is wide enough to react to the frequency shifting.

3.3 Dimensioning of the rectifier

On the vehicle side the rectifier is one of the major parts of the inductive charging power system. Its function is to convert the alternating current from the pickup coil to direct current that can be feed into the vehicle power net. It mainly consists of a bridge rectifier build from four diodes.

The nominal Voltage of the Fiat 500 is about 255 V. So the operating voltage of the rectifier and thus the diodes are a little bit higher at about 260 V. During operating the system higher voltages may occur.

These peaks are caused by transient effects like fast load changing. There high is depending on the actual state of the system. Especially during test phase when sometimes no load is applied to the secondary side the risk of high voltage peaks is high. This aspect is important to take into account when dimensioning the components of the rectifier.

Therefore diodes where chosen that are capable to work with 600 V, nearly twice the nominal voltage. Additional a capacitor was applied to filter and thus reduce the maximum peak voltage.

During operation of the system it turned out to be not enough. Figure 54 shows a picture of the burned diodes of the rectifier. As a consequence the diodes where replaced with diodes capable to work at up to 1,200 V.

Figure 54: Burned diodes of the rectifier

3.4 Conclusions of the vehicle integration

Regarding the integration of the charging system two aspects have to be considered: the mechanical and the logical integration. In the UNPLUGGED project the system had to be integrated into an existing vehicle, a Fiat 500. This vehicle has been converted from a conventional, commercial available vehicle equipped with a combustion engine to an electric vehicle before.

Two different aspects follow from this processing of the vehicle. On the one hand for the mechanical integration only the space was available that has not already been used for the components needed for the electrification. The electric power train and the high-voltage battery normally use more space than the original combustion engine. As a result the procedure for mounting (and demounting) the components is quite laborious and some problems with the laying of the cables occurred (s. Figure 55: cable damaged due to a collision with a metal part of the construction).

Figure 55: Damaged cable due to unfavourable mounting construction

On the other hand the data integration of the electric drive train into the vehicle network architecture is not very deep and the logic for the electric charging is quite simple. As for the integration of the inductive charging system the original system needs to be manipulated that is an optimal situation as a simple architecture is easier to manipulate. For the UNPLUGGED project information about the build in conductive charger where available and the inductive system was designed to replace this charger. A simultaneous operation of the conductive and inductive charger presupposes a management instance that coordinates the energy flow. The demand for charging power announced from the high voltage battery needs to be distributed in an efficient way between the two charging system. This was not implemented within the UNPLUGGED project.

These questions are of no interest if the inductive charging system is considered by the car manufacturer and sold with the vehicle or as optional equipment. In this case suitable space will be reserved for an adapted component. In general the space needed for a 3.7 kW secondary side like the one build up in the project is small enough so that it should be available if considered during the design of the vehicle. IT interfaces will be designed to make sure the system integrates with the vehicle functions.

For inductive charging systems aiming for the aftermarket the initial situation is comparable to the UNPLUGGED project or, regarding the data integration, worse. Additionally a system for the aftermarket would be cheaper if it would fit for different vehicles with only few adoptions. The main challenge here is not the coil that can be build quite flat even including the housing. However, the power electronics should be placed near the coil due to EMC and efficiency reasons. As the high voltage battery is often placed at a large area of the underbody it might not be possible to install it.

For the electrical and IT integration for a commercial solution it is not feasible to remove the conductive charger. The customer will not accept to reduce its charging possibilities to only the inductive system in medium term. Thus, a different interface than that of the on-board charger should be used. One possibility would be to use the DC-Charging Interface, both the power and the data part. In that case the secondary side of the inductive system would simulate a standardised DC charging interface, e.g. CHADEMO or CCS.

3.5 Summary and outlook

During the tests with the 3.7 kW System it has proven that it is working not only in a lab but in a real vehicle. It is not only functional but is good to handle by the driver.

The efficiency of the implemented system can be improved by fitting it to the specific vehicle. This applies to the system voltage and the dimensioning of the electric parameters. Additionally the start procedure for the charging can be accelerated by adapting the control parameter. This was not done to be able to monitor the sequence and be able to intervene if necessary due to the prototype character of the system.

The mentioned monitoring of the losses during the charging process can possibly be used to detect foreign objects between the coils. This could help to prevent damage to the vehicle from ignited items or harm of animals. Likewise it is conceivable that it can be used to qualify the exact positioning of the secondary coil above the primary coil. Further investigations are needed here.

The next step to get a commercial system is to analyze the robustness of the secondary side of the inductive charging system in terms of automotive requirements. Especially the mechanical robustness to typical vibrations occurring in vehicles should be tested in a long term test.

3.6 Field measurement procedure and results

3.6.1 Protocol

Our goal was to measure the magnetic induction **B** magnitude inside the vehicle when the charging system is running. We performed measurements at the driver and passenger's seat, at various locations: feet, head and chest. We also performed measurements at the conductor and passenger's seat.

In addition, we performed measurement with the coils misaligned in one or two directions. This kind of measurement assesses the effects of the magnetic flux linkages - if any - on the magnetic induction in the vehicle.

We also checked the shielding effect of the car body by performing some measurements with an opened door, and compared the results with those obtained with all doors closed.

3.6.1.1 Sensor used

We used a Aaronia Spectran high frequency (HF) magnetic sensors, the NF-5035 3 axis magnetometer. The later can measure B fields between the [1 kHz -10 MHz].

This high frequency sensor can perform measurement of the field created by the induction coil (3.7kW, f=140 kHz).

3.6.1.2 Standard used

We compared the measurements with the ICNIRP guidelines [1]. The recommended levels are summarized in tables Table 5 and Table 10.

Frequency range	E-field strength ($V\ m^{-1}$)	H-field strength ($A\ m^{-1}$)	B-field (μT)	Equivalent plane wave power density S_{eq} ($W\ m^{-2}$)
up to 1 Hz	—	3.2×10^4	4×10^4	—
1–8 Hz	10,000	$3.2 \times 10^4/f^2$	$4 \times 10^4/f^2$	—
8–25 Hz	10,000	$4{,}000/f$	$5{,}000/f$	—
0.025–0.8 kHz	$250/f$	$4/f$	$5/f$	—
0.8–3 kHz	$250/f$	5	6.25	—
3–150 kHz	87	5	6.25	—
0.15–1 MHz	87	$0.73/f$	$0.92/f$	—
1–10 MHz	$87/f^{1/2}$	$0.73/f$	$0.92/f$	—
10–400 MHz	28	0.073	0.092	2
400–2,000 MHz	$1.375f^{1/2}$	$0.0037f^{1/2}$	$0.0046f^{1/2}$	$f/200$
2–300 GHz	61	0.16	0.20	10

Table 6. The Spectran magnetometer we used integrates the values related to that standard.

For each measurement, we plotted the data acquired along with the ICNIRP maximum acceptable value.

Frequency range	E-field strength ($V\ m^{-1}$)	H-field strength ($A\ m^{-1}$)	B-field (μT)	Equivalent plane wave power density S_{eq} ($W\ m^{-2}$)
up to 1 Hz	—	1.63×10^5	2×10^5	—
1–8 Hz	20,000	$1.63 \times 10^5/f^2$	$2 \times 10^5/f^2$	—
8–25 Hz	20,000	$2 \times 10^4/f$	$2.5 \times 10^4/f$	—
0.025–0.82 kHz	$500/f$	$20/f$	$25/f$	—
0.82–65 kHz	610	24.4	30.7	—
0.065–1 MHz	610	$1.6/f$	$2.0/f$	—
1–10 MHz	$610/f$	$1.6/f$	$2.0/f$	—
10–400 MHz	61	0.16	0.2	10
400–2,000 MHz	$3f^{1/2}$	$0.008f^{1/2}$	$0.01f^{1/2}$	$f/40$
2–300 GHz	137	0.36	0.45	50

Table 8. Reference levels for occupational exposure to time-varying electric and magnetic fields

Frequency range	E-field strength ($V\ m^{-1}$)	H-field strength ($A\ m^{-1}$)	B-field (μT)	Equivalent plane wave power density S_{eq} ($W\ m^{-2}$)
up to 1 Hz	—	3.2×10^4	4×10^4	—
1–8 Hz	10,000	$3.2 \times 10^4/f^2$	$4 \times 10^4/f^2$	—
8–25 Hz	10,000	$4{,}000/f$	$5{,}000/f$	—
0.025–0.8 kHz	$250/f$	$4/f$	$5/f$	—
0.8–3 kHz	$250/f$	5	6.25	—
3–150 kHz	87	5	6.25	—
0.15–1 MHz	87	$0.73/f$	$0.92/f$	—
1–10 MHz	$87/f^{1/2}$	$0.73/f$	$0.92/f$	—
10–400 MHz	28	0.073	0.092	2
400–2,000 MHz	$1.375f^{1/2}$	$0.0037f^{1/2}$	$0.0046f^{1/2}$	$f/200$
2–300 GHz	61	0.16	0.20	10

Table 9. Reference levels for general public exposure to time-varying electric and magnetic fields

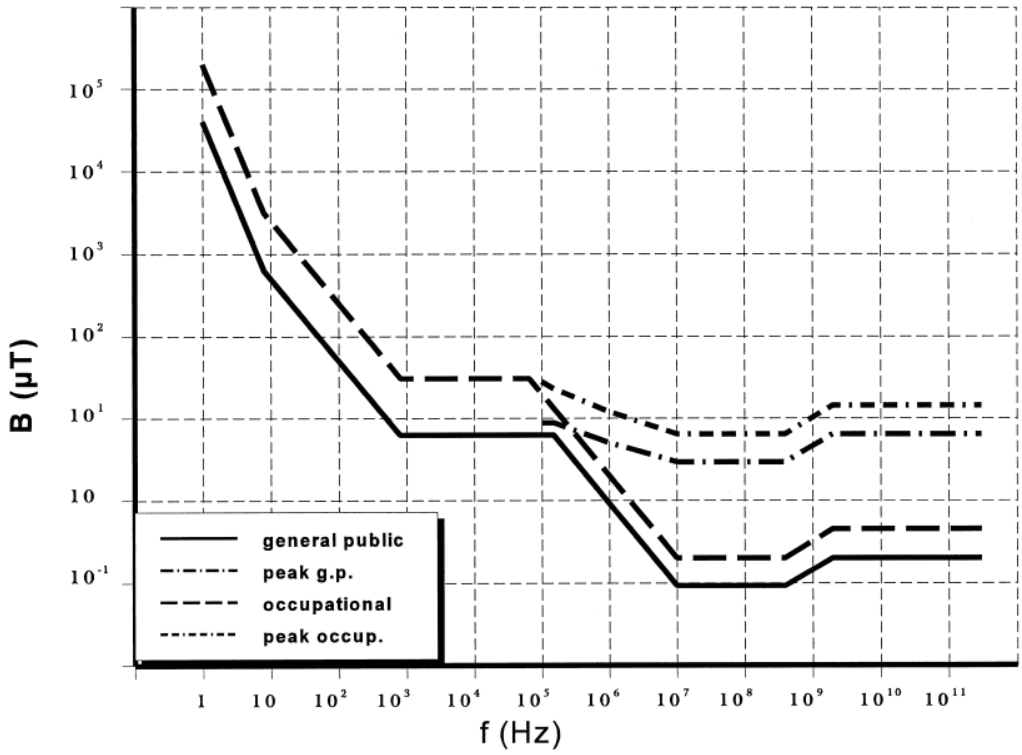

Figure 56 Reference levels for exposure to time varying magnetic fields.

3.6.1.3 Position of the sensor for measurements

The sensor was positioned at 6 places for each configuration: head, seat and feet for both the driver and the passenger seats. We checked that these locations were representative from the value of the magnetic field inside the car. Indeed, we displaced the sensor inside the car, and we could not find a location showing particular magnetic field value peaks.

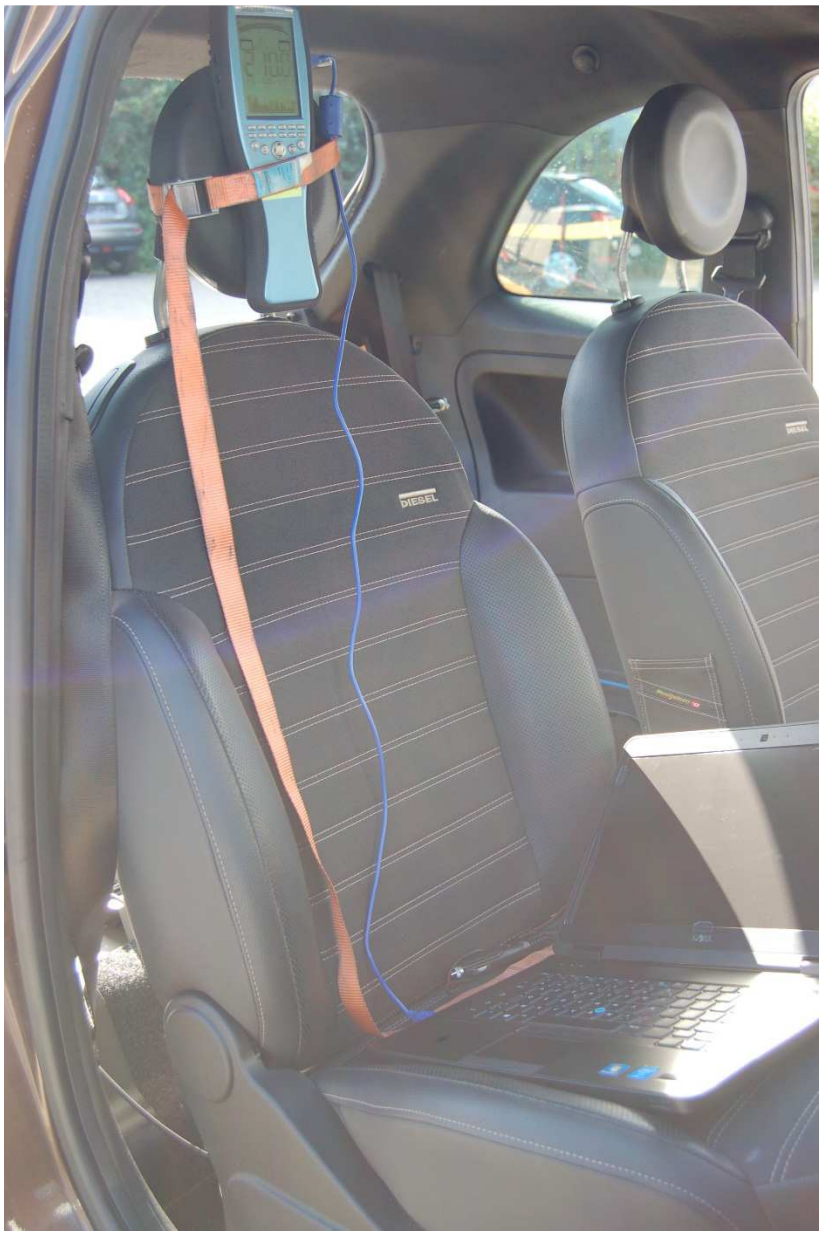

Table 10. Location of the sensor for measurement of B field at the passenger's head.

3.6.1.4 Description of the configurations investigated

We performed several measurements, with parameters as follow:

- location of the sensor (6 locations)
- alignment of the primary and secondary coils in the two directions

- door opened or closed (to assess the shield effect)

It is to note that the inductive charging cannot be turned on if the car power is turned on. This is to avoid the case when the driver would move the car while it is charging.

We defined a car's frame as follow: "X" axis horizontal pointing forward, "Z" axis vertical pointing towards the ground. In that frame, X=0, Y=0 and Z=0 represent the centre of the secondary coil.

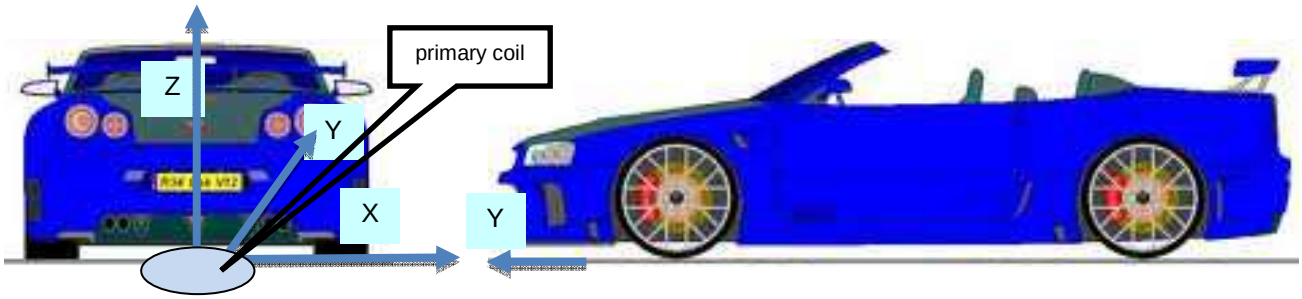

Table 11. Car's frame

To assess the effect of the coils misalignment, we moved the primary coil to the following points:

- X+10 cm : files 1 to 36
- X+20 cm : files 31 to 36
- X+20 cm & Y+10 cm : files 41 to 46
- Y+10 cm : files 51 to 56

3.6.2 Results

3.6.2.1 Precautions to follow by the user with the Aaronia Spectran sensor

We noticed three sources of errors in the measurements

3. The USB extension cable generates a peak @540 kHz.

4. When the arm of the experimenter enters the car by the window, it acts like an antenna, generating a peak at 450 kHz. Consequently, we used an insulating wooden rod to actuate the computer which was driving the sensor.

5. The user must be careful when using the Aaronia sensor the right attenuator value has to be chosen manually particularly with very strong signals to avoid overloading the external SMA input. Possible choices are:

    - Auto = An appropriate attenuator is chosen automatically (10dB and 20dB)
    - 0dB = No attenuator (highest sensitivity)
    - 10dB = Attenuate input signal by 10dB
    - 20dB = Attenuate input signal by 20dB
    - 30dB = Attenuate input signal by 30dB
    - 40dB = Attenuate input signal by 40dB

NOTE: Set the 0dB, 30dB and 40dB attenuator manually. They will not be set with the “Auto” function.

3.6.2.2 The shielding effect cancels the field inside the car

The results of the measurements show that the measured magnetic induction inside the car is far under the maximal acceptable threshold defined by the ICNIRP (6.25 µT). Indeed, the maximal value is 17 nT.

The highest value obtained is measured at the passenger’s seat, when the car is misaligned with the primary coil (X+20 cm Y+10 cm).

This can be explained by the installed shield (metal piece) and the shield effect of the car body. For a frequency of about 150 kHz, the skin depth of steel is about 1 mm. Consequently, there is no magnetic induction inside the car.

The shielding effects were also verified in another way: we performed measurements with one door opened. In that case, the field measured was stronger than with the door closed, as shown Figure 57 and Figure 58.

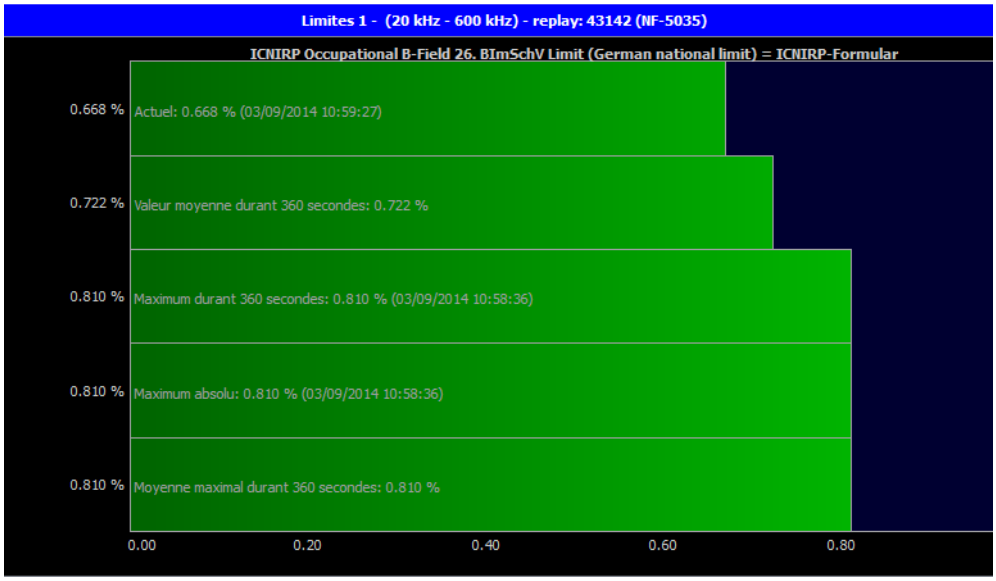

Figure 57. a) Door opened, we measured 13.57 nT at the driver's head (coils aligned). Note the peaks at 450 kHz (antenna effect of the user's arm), and at 534 kHz (USB extension cable) b) In that case, which takes into account the 2 biases, computation shows the value is only 0.81% of the ICNIRP threshold.

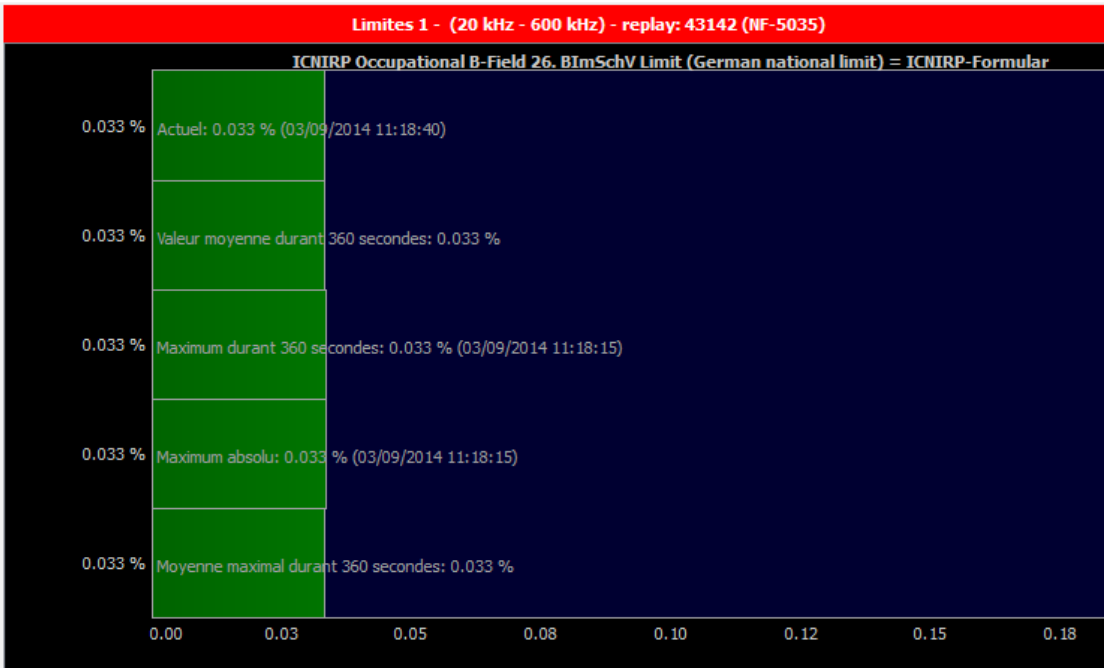

Figure 58: Door closed at the driver's head (coils aligned).. The peak value is now 4.3 nT at 150 kHz. The antenna effect of the arm (450 kHz) is not noticeable, as well as the effect of the USB extension cable at 540 kHz. b) In that case, the maximal value is 0.033% of the ICNIRP threshold.

3.6.2.3 Effect of misalignment

The effect of misalignment is negligible: the maximal value we got in all our measurement was 17.4 nT in the case when the primary coil was misaligned of 20 cm in the X direction. This worst case corresponds to 0.129% of the ICNIRP threshold (Figure 59).

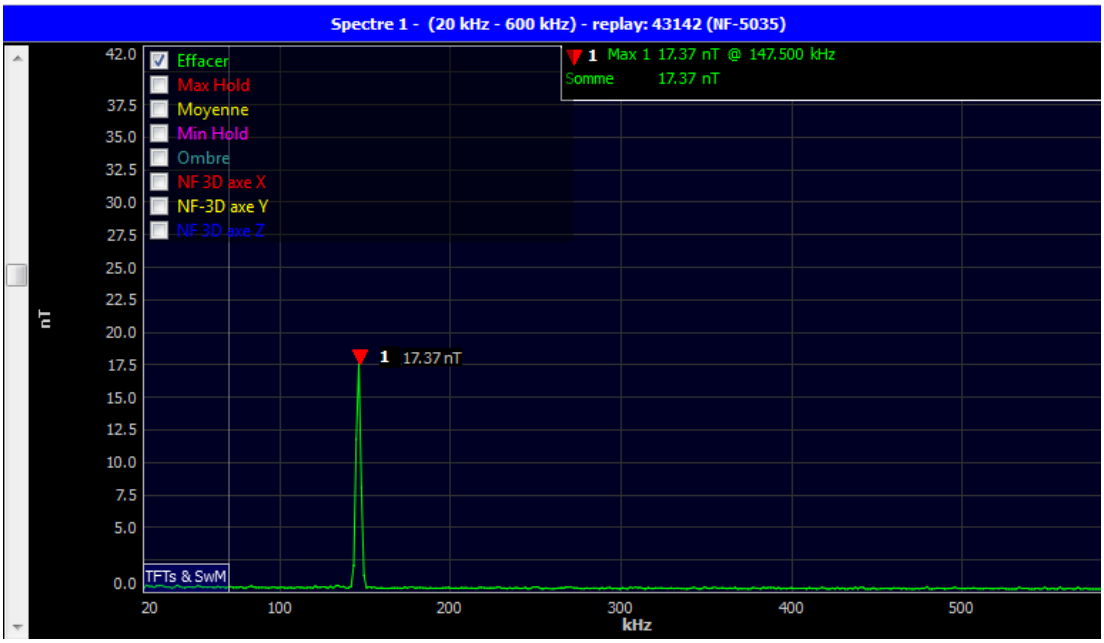

Figure 59. Maximal value obtained during all the measurements. In that case, the primary coil was misaligned of 20 cm in the X direction.

3.6.2.4 Transient state: primary inductive coil turned on then off

We also studied the spectral distribution of the signal when the primary induction coil was turned on and off. Indeed, it is known that inductive currents appear and can lead to strong value of induction. In our case, the effect was negligible (Figure 60 and files 12 and 21).

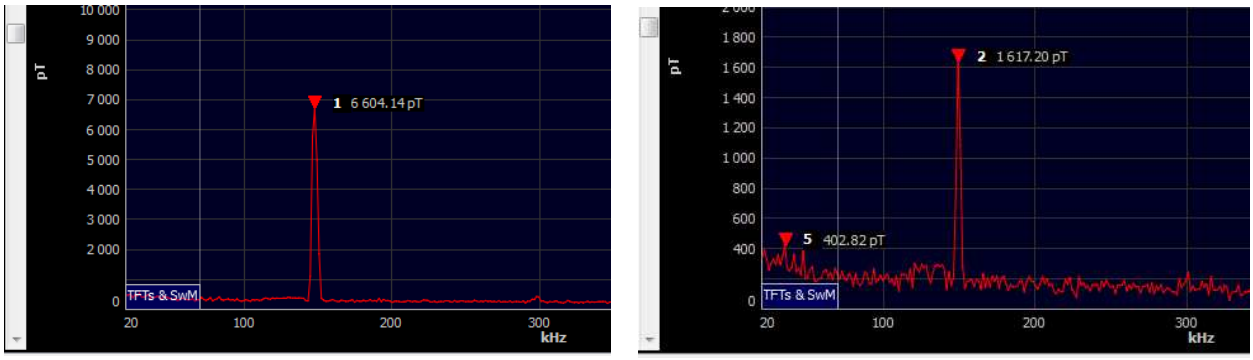

Figure 60. Transient effects. When the inductive system is turned On (left) or Off (right), no induced field is noticeable inside the car. Again, this is due to the shielding effect of the car body.

3.6.3 Conclusion

We have performed a total of 45 measurements inside the Fiat 500. We have assessed the impact of the misalignments of the coils, as well as the shielding effect of the car.

The highest value we obtained was a peak of 18 nT, which is negligible compared to the ICNIRP recommendation. As a reminder, the value of earth Magnetic Field induction is about 50000 nT, and the maximal ICNIRP admissible value is 6.25 µT.

Consequently, the inductive system does not lead to any magnetic induction value in contradiction with the ICNIRP recommendation.

4 Communication System

The communication modules (EVCC and SECC) are part of both inductive charging systems developed by UNPLUGGED. One pair was installed in the 3,7 kW system and one pair in the 50 kW system as well. The communication system is already described detailed in D1.2, D1.3 und D1.4. The requirements regarding installation can be found in D2.2.

Figure 61 - *Prototype of wireless communication system for UNPLUGGED (SECC on left side)*

After finishing the tests with both systems following can be concluded:

The communication modules worked satisfying and reliable in both systems. After some difficulties of adjustment during installation no more problems was detected.

Under common conditions the range of Wi-Fi (WLAN) is completely sufficient for the considered use cases. While the vehicle is approaching to the charging station the Wi-Fi communication will be established and first data will be exchanged. Usually communication is ready for positioning of the car in less than 1 second. Further data, e.g. for identification, authentication and authorization will be exchanged during the car is positioning at the charging station. Commonly positioning takes much more time than communication needs for data transfer.

After the car is positioned and a confirmation by the driver technical data needed for charging procedure will be exchanged and the charging procedure itself could start. During charging a continuous data exchange takes place (cycle time appr. 100 ms). When charging is completed the communication stops and the Wi-Fi channel will be released for other vehicles.

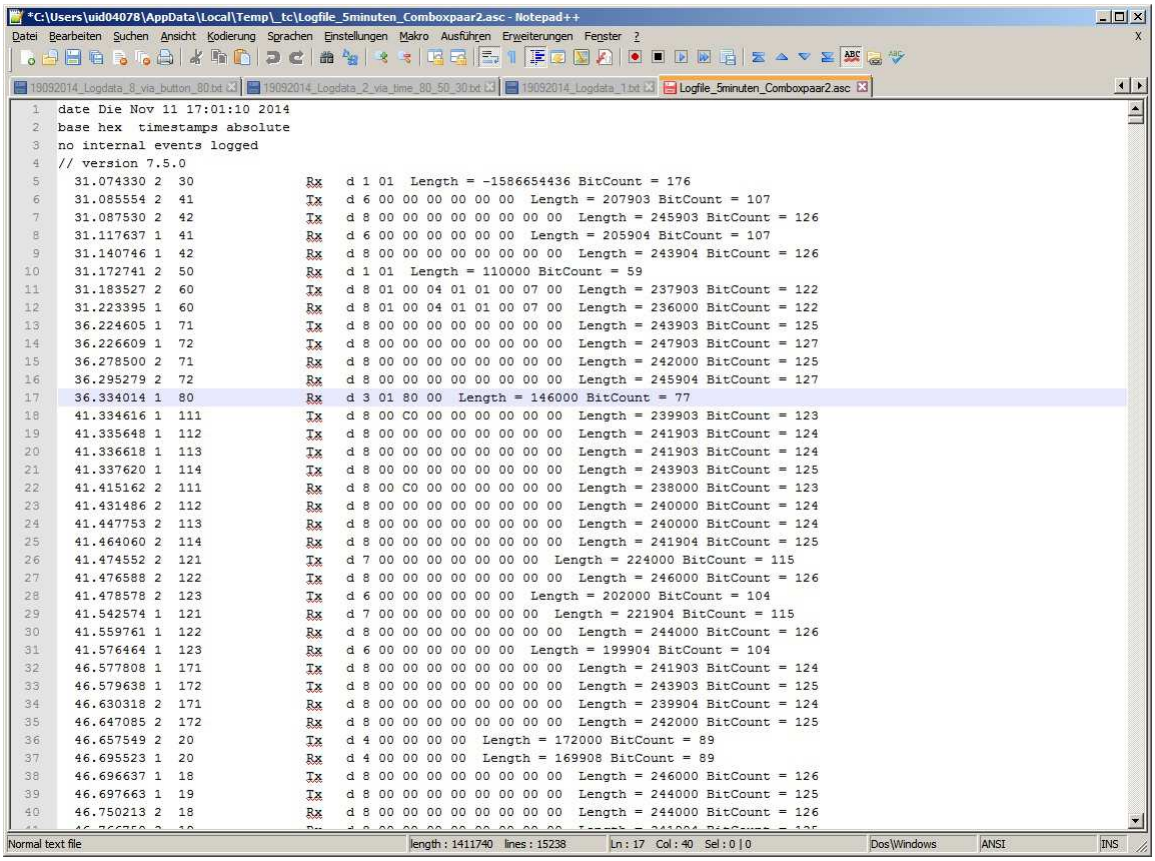

Figure 62 – Example of a communication protocol of wireless communication

For future applications we recommend special attention should be given to fault tolerance of the communication. In general wireless communications can be interfered and thus less reliable than wired communications are.

Following aspects should be considered. For some applications (e.g. huge parking areas, parking garages) can be expected that one base station has to handle many cars and many parking lots for inductive charging. Additionally many other devices not relevant for inductive charging (other vehicles, computers, smartphones and so on) but with Wi-Fi interfaces will be nearby. All these devices have to share the available Wi-Fi channels. This means communication partners have to change their Wi-Fi channel from time to time and this change needs time. Beside these system inherent delays “real” interferences from environment can occur. Summarized interrupts of the Wi-Fi connection from several 100 milliseconds to seconds cannot be excluded.

A measure to mitigate these difficulties would be a second communication channel, e.g. a low level communication directly by the coils. This second communication channel could raise not only availability and reliability, but could be useful also for reasons of safety and security. In this way a secure pairing between user, vehicle and a defined primary charging coil could be realized for instance. Possibly safety and security requirements make a second communication channel indispensable for commercial applications.

5 Positioning System

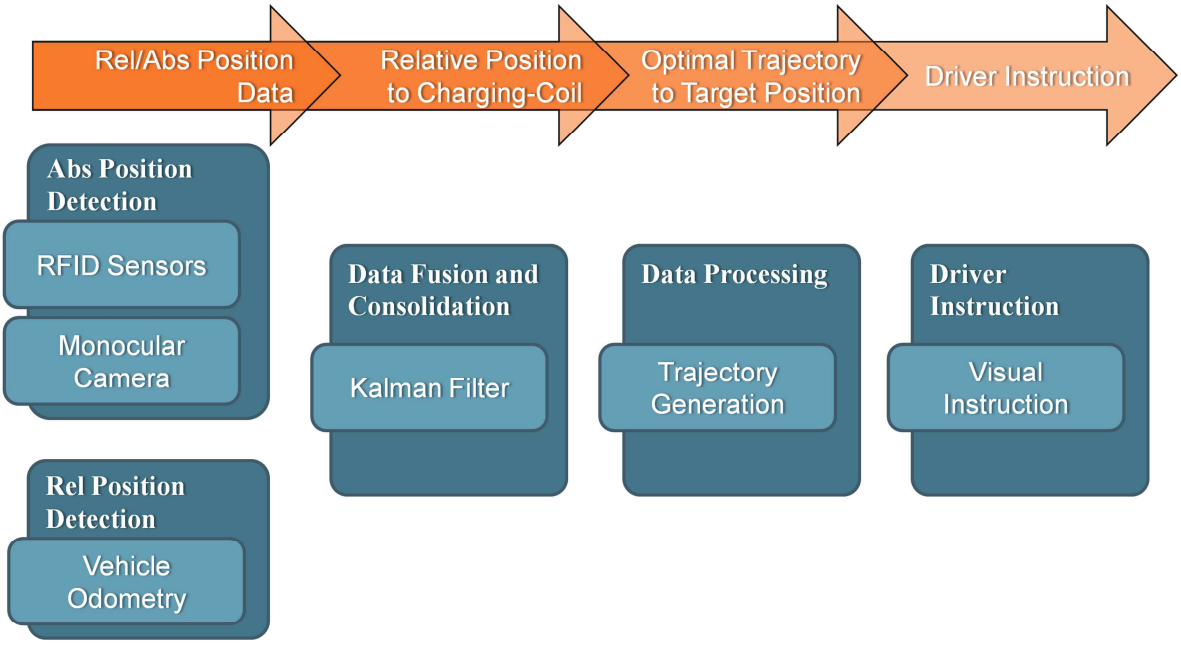

Figure 63: Overall system

The positioning process from gathering sensor information up to displaying instructions to the driver is shown in Figure 63. For absolute position detection, the RFID sensors and the monocular camera are used, while the vehicle odometry (wheel speed and steering angle) is used for relative position detection. The gathered data is merged and consolidated in a kalman filter. The relative position to the charging coil is forwarded to the trajectory generation algorithm, which generates an optimal trajectory to the target position. Finally, the driver is instructed visually and guided to the charging position.

While approaching the positioning area, the monocular camera detects the absolute position of the vehicle to the charging coil. Simultaneously, wheel speed and steering angle are gathered and the data set is merged in the kalman filter based. Timestamp data is also considered to make data coherent, letting all systems work asynchronously. When leaving the section covered by the camera and before entering the RFID section, the position detection and therefore the kalman input is based on odometry only. This is the handover section. When entering the positioning area, both, RFID sensors and odometry provide data for the kalman filter (see Figure 64).

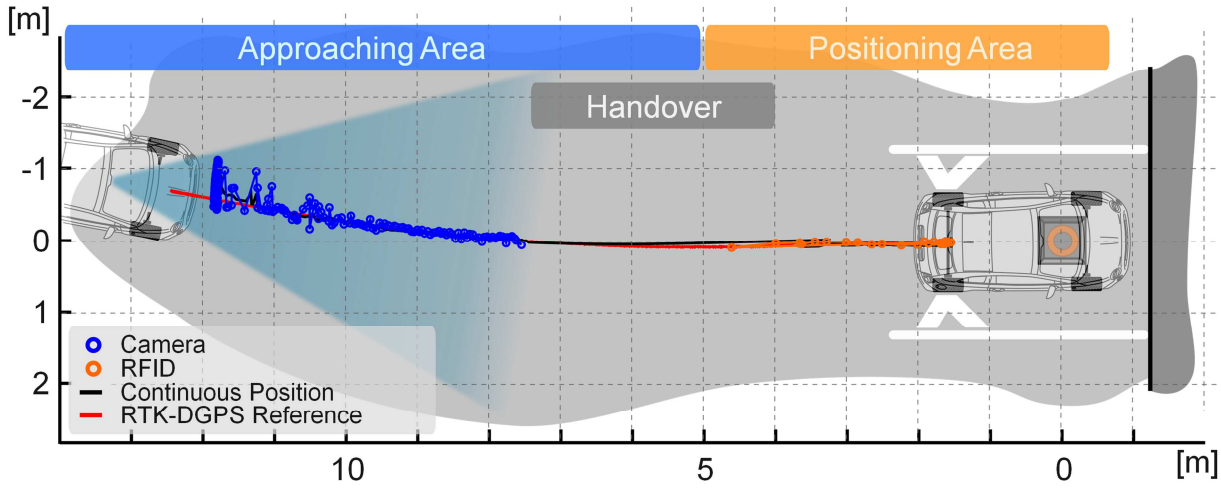

Figure 64: Positioning process

Analysing the gathered data showed that especially varying light conditions and extreme approaching angles were difficult with the camera setup chosen. The camera needs recalibration depending on the actual illumination and roadway colour. This was implemented in the camera algorithm and is now executed automatically. Furthermore the RFID's antenna system was reduced to a single antenna, mounted in the middle of the vehicle. Yet, the second antenna was used to gain information about the vehicle's orientation. Due to technical circumstances, which will be discussed separately in the RFID section, the orientation is now determined by the camera only. In sections without camera information, the last orientation is stored and based on this value, the kalman filter estimates the current position and orientation using information from odometry and the RFID system. The tablet used for displaying information to the driver was changed to a different model because of limitations in speed.

5.1 Camera

The hardware is fitted at the front window in place of the rearview mirror. Different from the test setup described in former deliverables, a new bracket with adjustable tilt angle was designed. This simplifies the calibration process necessary for different passenger load situations. The field test showed that passengers on the back seat affect the tilt angle of the vehicle more than expected which causes problems with the detection of the optical markers due to distortion. Furthermore, the detection of markers and therefore the accuracy of the position estimation is dependent on illumination and the surface colour. In each scenario, recalibration is necessary.

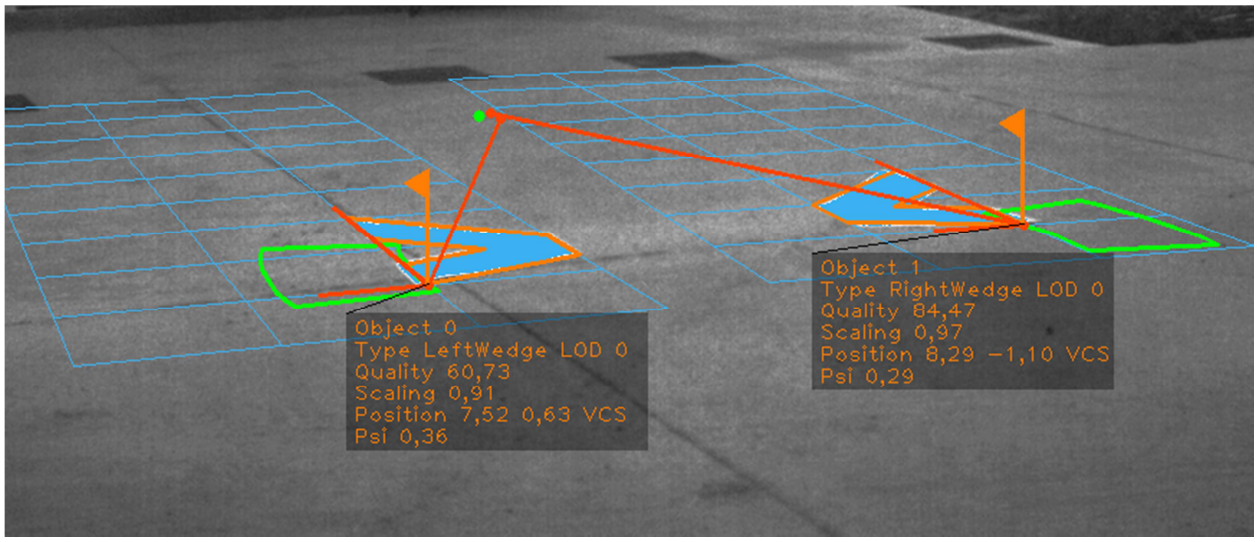

Figure 65: Snapshot camera module

Figure 65 shows a snapshot from the camera module. Two markers have been detected and the quality of detection has been rated. The angle psi, which describes the position of the vehicle's longitudinal axis to the x-axis of the local coordinate system is acquired. Only if both markers are detected, the estimation of the primary coil position in the local coordinate system is accepted and processed by the kalman filter. Data sets with a single detected optical marker are neglected.

Problems with the detection of markers during the field tests were caused by

- Reflections in the front window
- Dirty front window
- Front lighting
- Polluted optical markers
- Extreme approach angle (most of the time only one marker detected)
- Shades, changes in illumination
- Different load situations (also co-driver dependent, side tilting)

Although the camera is capable of 50fps in Full HD, the algorithm which detects and rates the markers has an output rate of only 20Hz. The algorithm contains three major steps, beginning with the

segmentation followed by the contour detection and finally the position detection. Each step contains several substeps.

5.1.1 Segmentation

Before entering the segmentation process, the recorded picture's resolution is reduced to 1/10 of the original resolution. Using a "Moving window filter", the grey-scale values are determined line by line (see Figure 66), followed by a column by column determination of the grey-scale values using the same filter. The resulting grey-scale picture is subtracted from the unfiltered picture. Finally, a threshold, which depends on the surrounding illumination and surface colour is applied to separate bright areas form dark areas (see Figure 67). The result is a digital picture which contains only the values black (0) and white (1).

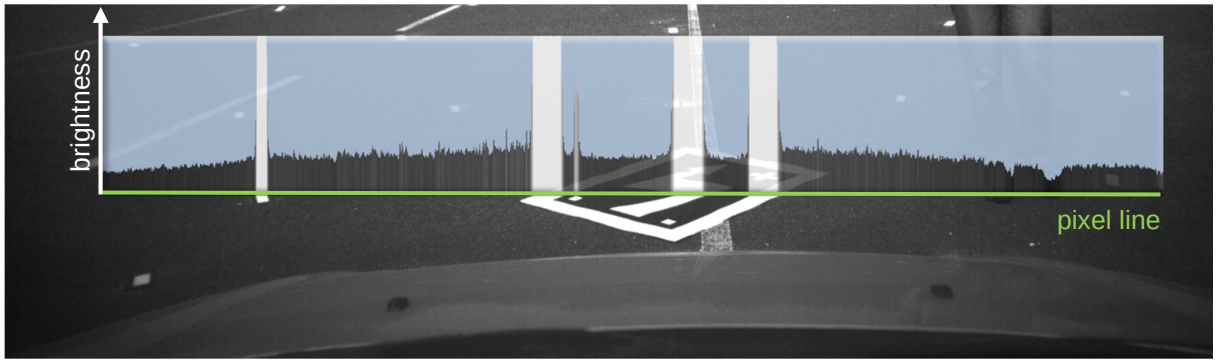

Figure 66: Brightness behaviour of a pixel line

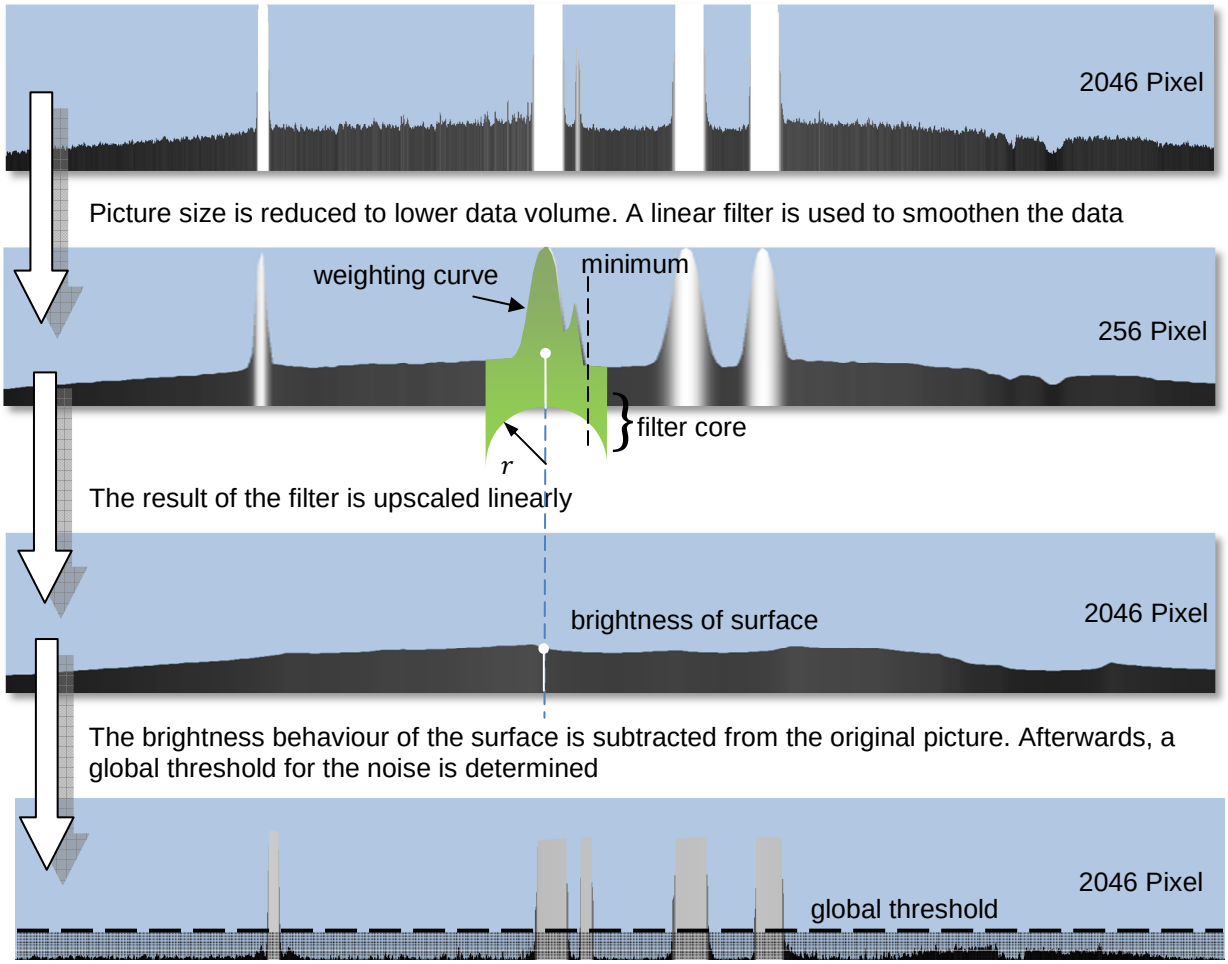

Figure 67: Filtering of a picture with a semi-circle shaped weighting curve explained for a single pixel line

5.1.2 Contour detection

The digital picture, which contains only black and white areas is taken and white areas and their contours are identified. A comparison in size to the known marker size identifies areas which are too large or too small to be the marker and are therefore eliminated. The moments of the remaining contours are calculated. The resulting moments are used to calculate the Hu moments, which are compared to the Hu moments of the reference contour and a matching is possible. The probability of detecting the correct marker is expressed as quality (see Figure 68, Figure 69 and Figure 70).

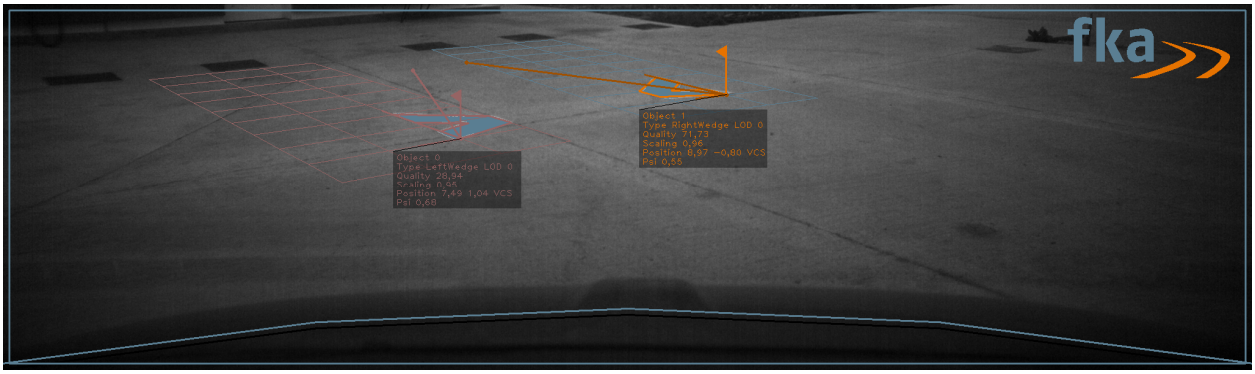

Figure 68: contour detection, one marker good quality, one marker poor quality, no cross validation

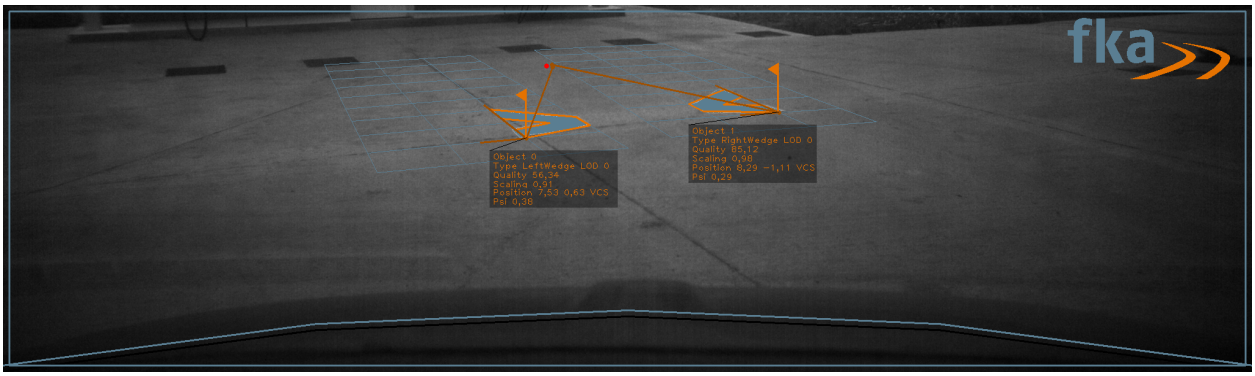

Figure 69: contour detection, both markers good quality, no cross validation

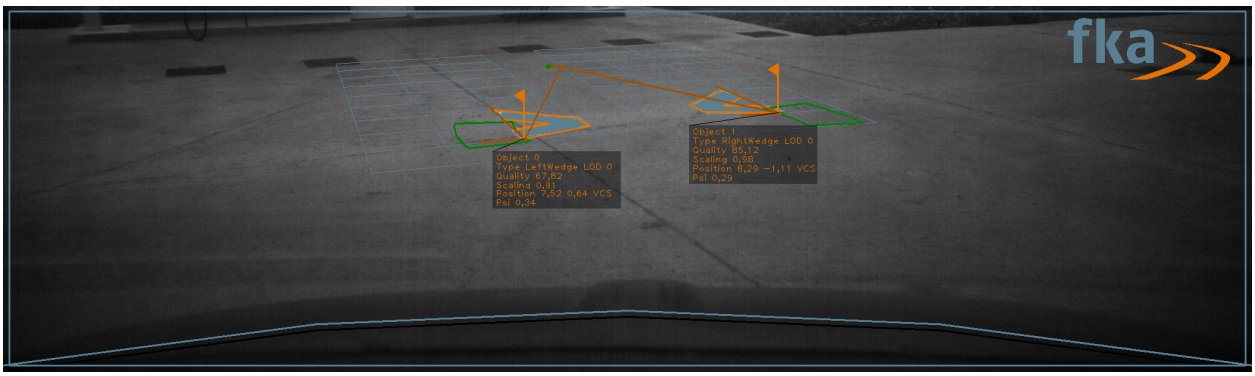

Figure 70: contour detection, both markers good quality, cross validation positive

5.1.3 Position detection

Within the contour detection process, the markers have been matched and identified. This means, that the picture contains the marker without any information about distance and orientation to the marker. Consequently the positions of the different markers are determined, the data is synthesized and the position of the primary coil is propagated. The entire processing chain from the taken picture to the final position determination is shown in Figure 71.

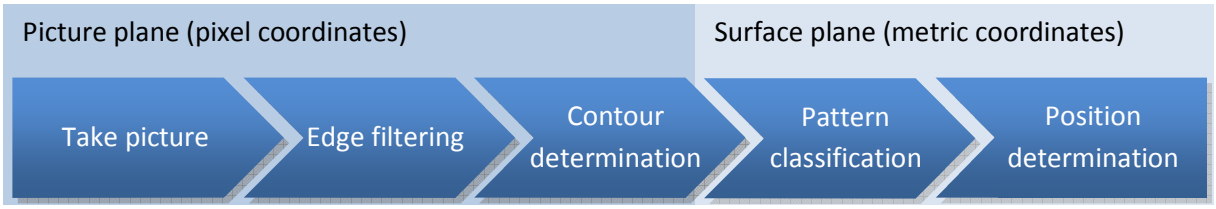

Figure 71: Process of position determination

The problems in marker detection result from weaknesses in the segmentation process. The used filter is not the optimal choice and can be optimized. Furthermore, the global threshold is not self-adapting to the surrounding illumination and surface colour.

5.2 RFID

Different than originally planned, the RFID system was converted to a single antenna setup. Using both antennas in order to determine the actual position and orientation in the local coordinate system caused several problems during the field tests. These were caused by a variety of effects that are described in the following section.

5.2.1 Coupling effects of the antennas

The idea of determining the antenna position in the local coordinate system is based on the assumption, that only tags close to the antenna answer the antennas request for inventory. Depending on the preset transmitting power, more or less tags are acquired in an area which is covered by the antenna. For weak transmitting power, the covered area resembles the antenna shape, for higher transmitting power, the area grows and looses the antenna shape. The tags acquired and their positions in the local coordinate system are deposited in a look-up table and used to calculate the centroid. This centroid represents the center of the antenna and therefore the antennas position in the local coordinate system. Using a second antenna also delivering its position in the local coordinate system, a statement about the vehicles orientation is possible (see Figure 72).

Figure 72: vehicle integration of RFID system (two antenna setup)

The two antennas request the inventory asynchronously due to the working principle of the used multiplexer. Thus, the antennas read the tags individually and only tags close to the active antenna should answer the request. Due to a coupling effect, also tags underneath the non-active antenna answer and therefore wrong tags are acquired. Even though the tags show a decreasing signal strength and can be filtered by this value, data collision causes longer and unpredictable reading times. The coupling is caused by the antennas close mounting position and the metal frame of the vehicle itself.

5.2.2 Impedance detuning

A magnetic field cannot penetrate metal or other magnetically conductive materials. The course of the lines of electric flux and the inductivity of the antenna is changed and has therefore a considerable influence on the reading range. Furthermore, the field is weakened by the mutual inductance response of the eddy current within the metal. The change of inductivity must be compensated with the help of tuning electronics.

- The minimum distance between metal and antenna is 5cm. A distance up to 30cm will lead to a considerable reduction in the reading range. At a distance of 50cm to metal parts, there will be almost no influence to be measured.
- Metal parts must not form closed loops or electric circuits. These have to be electrically separated at one point.
- Metal parts in close vicinity to the antenna have to be grounded in star configuration with a good HF-connection.

Regarding the Fiat 500, the ground clearance of the vehicle is the limiting factor, forcing the antennas to be mounted close to the vehicle's metal body. This results in a loss of reading range and impedance detuning of the impedance. The impedance has been retuned using external electronics, while the distance to metal cannot be improved.

5.2.3 Asynchronous reading of antennas

The OBID reader has a single input channel which makes the use of a multiplexer necessary. This way, the reader is capable of reading up to four antennas asynchronously. The time for reading the inventory therefore not only depends on the number of tags acquired, but also on the switching time of the multiplexer.

When entering the parking lot at a moderate speed, the first antenna (left) is active and the inventory is determined. While switching to the next antenna (right), the vehicle keeps moving and at the moment of determining its inventory, has moved a distance in x-direction. Calculating the center of each antenna out of this data set and concluding and orientation information is thus only possible, if the actual speed, the steering angle and the reading time (reading time left antenna, switching time, reading time right antenna) are known.

Since the reading time is not very constant due to the above mentioned coupling effect, the determination of orientation by using the established RFID system is difficult and inaccurate.

5.2.4 Final setup

The observation of inaccurate orientation determination led to the decision to move this process to the responsibility of the camera system. The orientation is determined once both markers are detected and from that point pursued and adjusted by odometry.

Moving the orientation determination process to a different module made the use of a second antenna unnecessary. This eliminates the problems caused by coupling effects and also lowers reading times, since the use of the multiplexer is obsolete. The effect of impedance detuning is still present.

5.3 Human Machine Interface (HMI)

Figure 73: Human machine Interface showing a planned trajectory

The determined position of the primary coil and the trajectory leading to the desired charging station are presented to the driver graphically (see Figure 73). For this purpose, a simple ASUS tablet running Microsoft Windows 8, which is connected via WLAN to the main PC, is used. In the following section the different screens while approaching a charging station are explained in detail.

Generally, there are two different ways of charging selectable, the stationary charging and on–road charging while driving. In a first step, the HMI asks the driver to choose, if charging is desired and if so, which charging mode to use (see Figure 74).

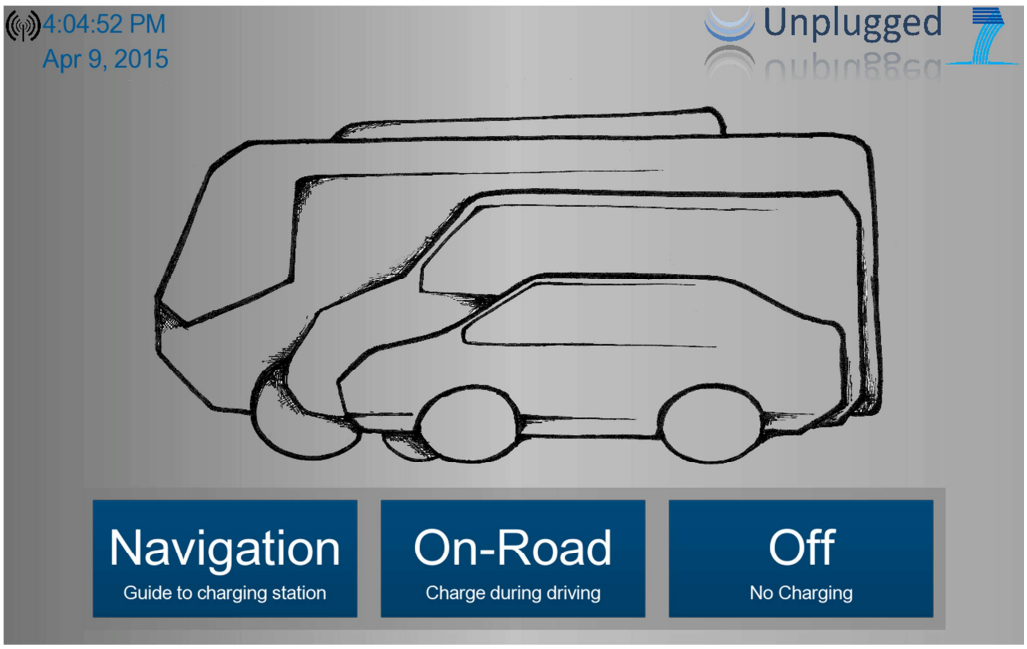

Figure 74: HMI Charge select

In case of navigation button is pressed, the driver is guided via GPS to the next charging system. Additionally to a map, relevant values like the state of charge (SOC) and autonomy (range) are displayed to the driver, helping to estimate in advance how long charging will be necessary to safely reach the next destination (see Figure 75).

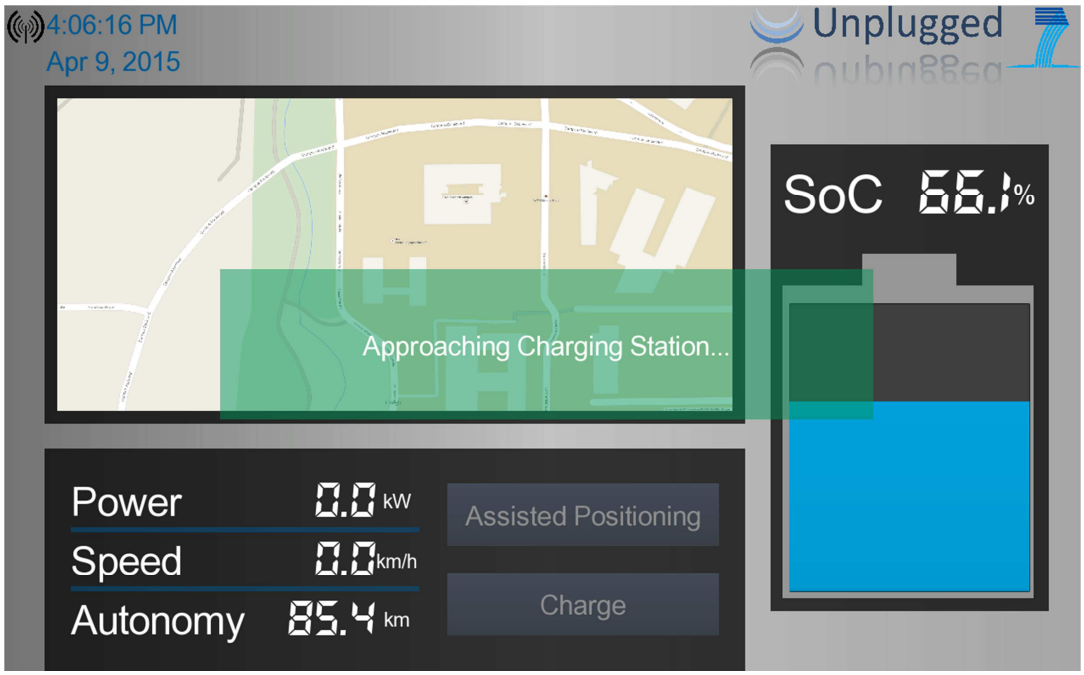

Figure 75: Navigation screen

As soon as the charging station is reached and the camera acquires the first marker, the position of the charging station is estimated and a trajectory is planned. The result is displayed to the driver in the positioning screen, which switches the viewing angle in dependence of the distance to the coil. The white lines show the trajectory to the charging station (yellow spot). The red lines represent the cars predicted driving path with the actual steering angle (see Figure 76**Error! Reference source not found.**). Additionally the distance to the charging station is given in meters. The positioning process can be cancelled at any time.

By turning the steering wheel, the driver needs to match the red (predicted driving path) and the white (trajectory) lines to follow the indicated trajectory (see Figure 76).

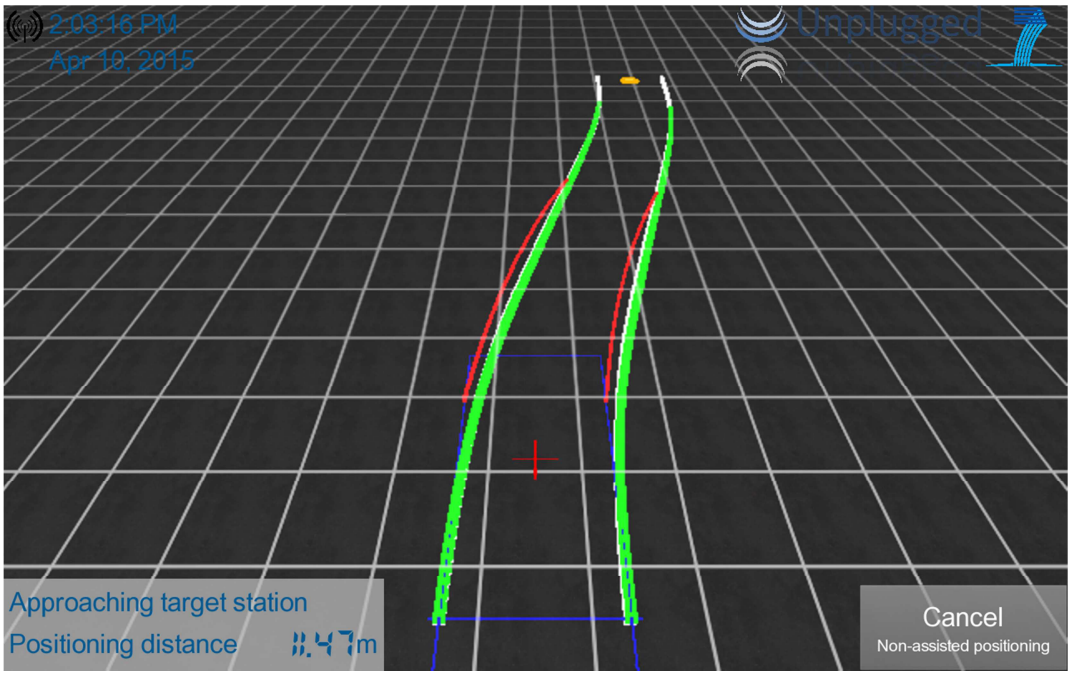

Figure 76: Matching predicted path (red) and trajectory (white)

Close to the charging station, the viewing angle switches into bird view. The vehicles secondary coil is represented as a cross which has to be matched with the charging station (yellow circle). Once the charging station is reached and the deviation from actual to desired position is less than 10cm, the driver is instructed to press the brakes and turn off the vehicle (see Figure 77).

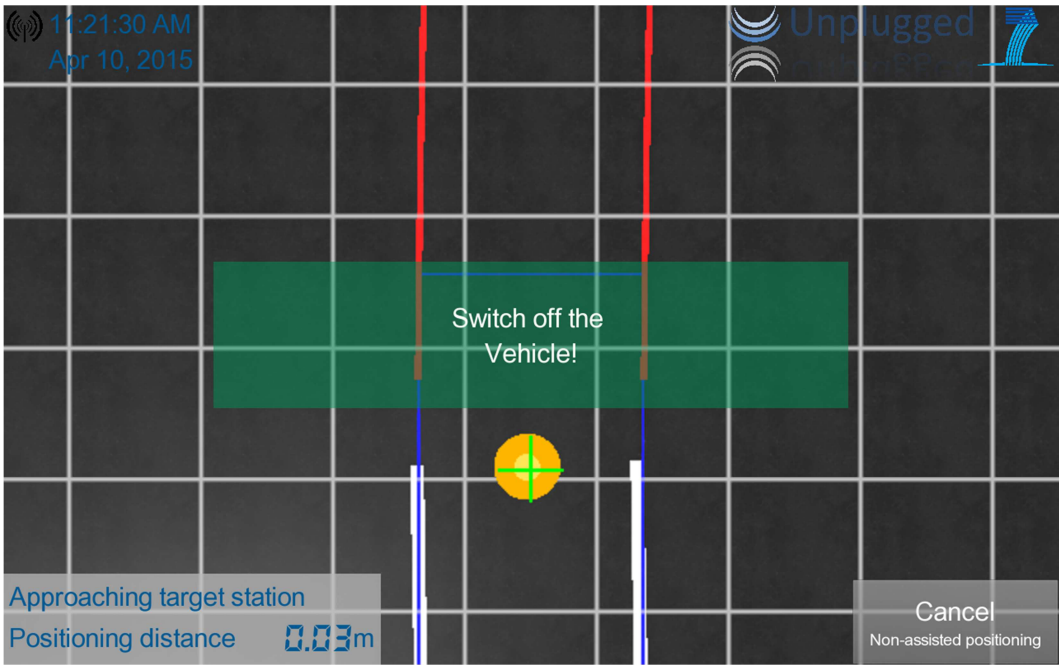

Figure 77: Charging position reached

With turning off the ignition, charging process starts automatically.

5.4 Trajectory-planning

The task of the trajectory planning algorithm is to find a suitable steering trajectory from the vehicle's current to the detected target position. As the system is not used in fully automated mode, it is the driver's job to follow the resulting path - therefore, this path has to correlate with his natural behaviour for him to accept it. Further on, the generator has to be applicable in all three different scenarios, resulting in a broad range of different use cases. In case of the static scenario, maneuvers with large steering angles are probable; the resulting trajectory has to be continuously checked against exceedance of the maximal steering angle. On the other hand in the dynamic scenarios, the steering dynamics have to be limited. Another difference results from the optimization criterion: Whereas in static scenario oscillations and overshoots in the steering trajectory have to be avoided, the dynamic scenarios ask for a comfortable steering style, i.e. a minimal jerk caused by abrupt angle changement.

In summary, the following requirements were identified:

- The driver has to accept the generated trajectory
- All scenarios have to be covered
- The planner has to be stable by means of generation time and plausibility
- Optimization criterion has to be dynamically adaptable
- Constraints have to be checked continuously

The resulting trajectory generator is based on a nonlinear minimization problem (NLP), which is itself used to solve an optimal control problem. The vehicle's steering angle is utilized as control input u(t); constraints are defined by reaching the target position and limiting u(t) to kinematic constraints of the car. The NLP itself optimizes the parameters of a base function defining u(t) – usually a polynomial of n-th degree is used for this purpose and the NLP searches for the best parameters.

During the field test, different kinds of control and cost functions for the static scenario were evaluated and checked against the driver's acceptance. It was observed that a single polynomial is not suitable to define u(t) for the following reasons:

- Changes are not limited to be local and therefore the convergence in extreme situations could not be guaranteed
- A large amplitude, which is typical for parking scenarios, results in large overshoots and oscillations, both of which are not accepted by the driver
- The number of changes is limited by the polynomial degree. High degrees intensify oscillations, low degrees limit the maneuver space.
- As a single polynomial is limited to a specific degree, it cannot change to linear behaviour to represent a constant steering angle. Therefore, the steering wheel is always in motion.

To eliminate the mentioned problems, a special shape preserving spline interpolation with an arbitrary number of sample points was developed. A comparison of the two approaches is given by the following figures.

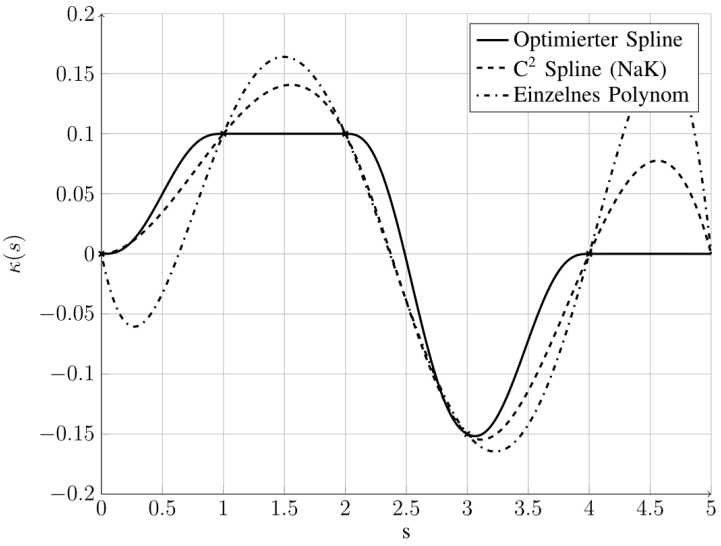

Figure 78: Comparison of single polynomial and different spline interpolations

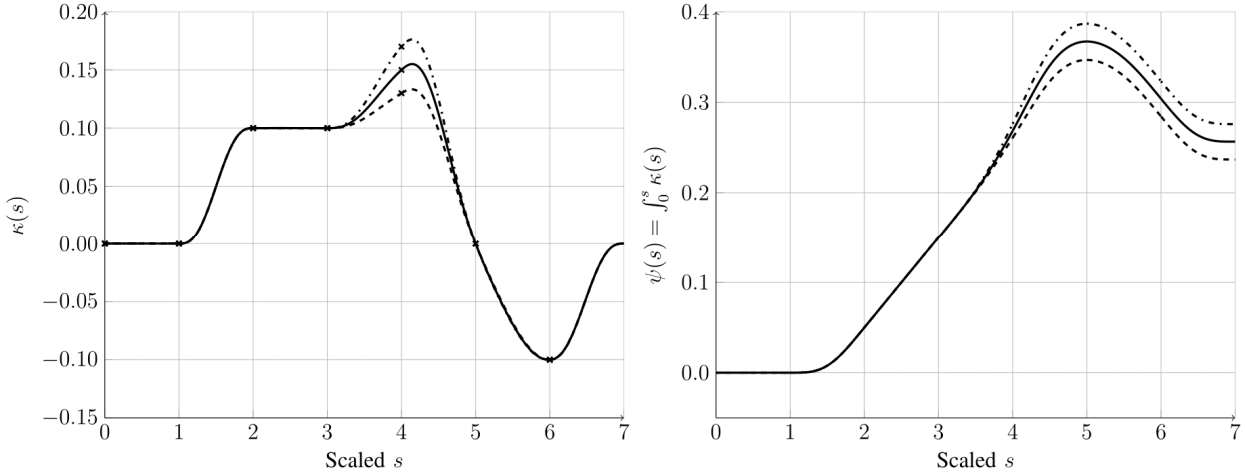

Figure 79: Local influence of single parameter variation

The spline interpolation utilizes a local optimization of the steering behavior on a micro layer, the NLP itself chooses the single parameters and therefore optimizes on a different level. This way, a far more natural way of steering motions could be established.

Different optimization criterions were also evaluated in the field test. As the resulting function has to be two times continuously differentiable, analysis started with a simple minimization of $\int x^2$, whereas the meaning of x was varied between the steering angle itself, as well as several of its derivatives. The utilization of the squared function did not lead to satisfying results, motivating the usage of a more sophisticated function approximating the absolute value $\int |x| \approx \int \sqrt{1e^{-5} + x^2}$. For the static scenario the

minimization of the overall steering motion was finally identified to be well accepted by the drivers, resulting in simple to follow and “visually pleasant” trajectories.

To enable the consideration of obstacles during trajectory generation, a distance metrics was developed (cmp. Figure 80). As no detection of obstacles was implemented for the camera, this metric could only be analyzed in simulation.

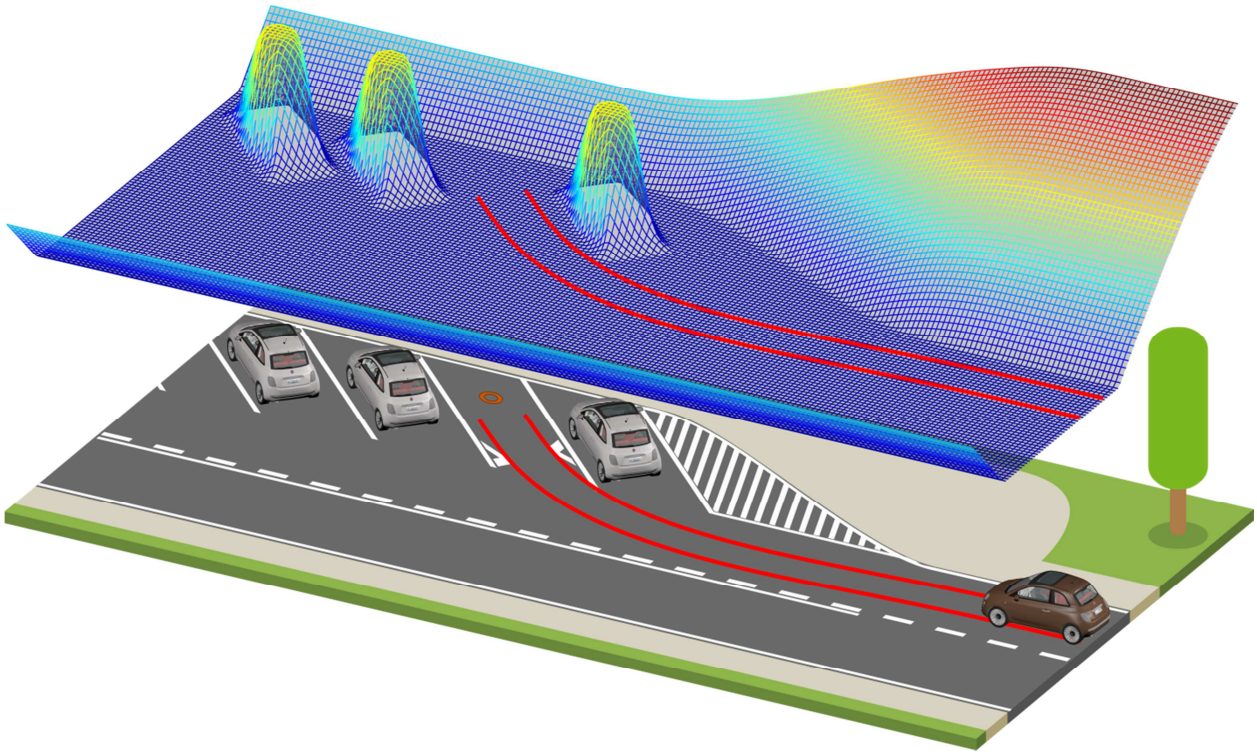

Figure 80: Visualization of the distance metrics

5.5 Summary

Differing from former deliverables, which stated the technical setup of the newly developed overall system, minor changes have been necessary due to the observed system behaviour throughout the field test.

6 Combined conductive/inductive charging

As already described in the Deliverable D2.1, taking into account current market scenario, it is useful to evaluate an integration between the wired and the wireless charging.

Needs for the integration of both systems in one vehicle can be due to different reasons, and being not costly effective, it must be justified by technical and functional motivations.

A possible application is to consider the wired solution as a backup or service system of the wireless solution (with significantly different power levels).

With the combination of both systems, user can have the possibility use wireless charging for standard use, but it has the opportunity to recharge with a standard connection for emergency or if wireless charging infrastructure is missing.

Taking into account this option, for the project testing purposes, a Test Bench has been developed.

It has been already described in other deliverables; mainly it is a vehicle subsystem and it is constituted by a Battery System connected to a Vehicle Management Unit and it provides power connection for wireless charging secondary side system.

On this Test Bench, a conductive charger has been installed, as shown in the next figure.

The charger used has 3.7 kW maximum power, and aim of this integration was mainly to allow the management of cells balancing, performed automatically on request by Battery Management System or controlled by Vehicle Management Unit.

Considering this function, the conductive charge becomes a backup system for service purposes.

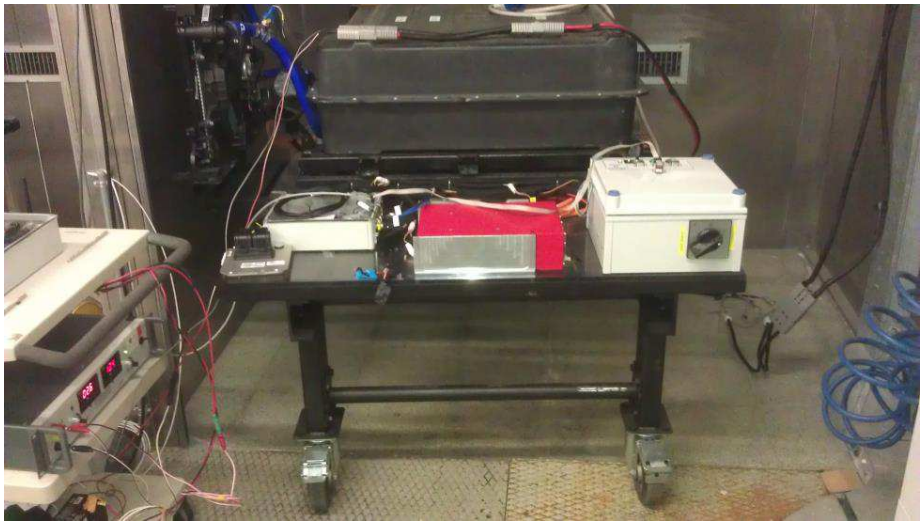

Figure 81: Test Bench equipped with conductive charger

As already discussed in the deliverable 2.1, integration of conductive and inductive system is possible from the technical point of view taking into account following aspects:

- communication integration between system
- the vehicle management unit must control and interact with both systems
- one system must exclude the other from operating
- the Valued Added Services (VAS) can be shared by both systems offering user a wide variety of opportunity for example related to charging booking and payment

Integration is technically possible from communication and power systems point of views, but it constitutes a complex system on vehicle side, adding costs and weight to the vehicle; for these reasons, installation of both systems must be evaluate according to vehicle mission and application.

7 Assessment on the impact on the grid by simulations in virtual grids and by real tests.

7.1 Introduction

The aim of this document is to calculate the impact on the grid network for the inductive charging built up during the project.

Starting from the results of the real test performed in the CIRCE lab, those have been given as input data for the simulation on a real Italian grid network and they have been considered in addition to the real consumption values recorded on one day in November 2013.

The results compared with the international standards limits show how the examined inductive charging station does not influence the network quality and the THD values are fully compliant to the limits. These results can be pinpointed to the great design of the inductive charging station.

7.2 Standard for the evaluation of the impact on the grid

In order to evaluate the impact on the low voltage grid of each equipment or electronic device the results in terms of voltage and current values have to be compared to the limits required by international standards.

The first standard is the IEC 50160 describes the voltage characteristics of electricity supplied by public distribution networks. In case of low voltage the main requirements are:

- Nominal voltage U_n 230 V, either between phase and neutral, or between phases:
  1. For four-wire three phase systems: U_n = 230 V between phase and neutral
  2. For three-wire three phase systems: U_n = 230 V between phases
- Under normal operating conditions excluding the periods with interruptions, supply voltage variations should not exceed ± 10 % of the nominal voltage U_n
- The THD of the supply voltage (including all harmonics up to the order 40) shall be less than or equal to 8 %.
- Under normal operating conditions, during each period of one week, 95 % of the 10 min mean r.m.s. values of each individual harmonic voltage shall be less than or equal to the values given in Table 12.

Odd harmonic				Even harmonics	
Not Multiples of 3		Multiples of 3			
Order h	Relative Amplitude U_n	Order h	Relative Amplitude U_n	Order h	Relative Amplitude U_n
5	6,00%	3	5,0%	2	2,0%
7	5,00%	9	1,5%	4	1,0%
11	3,5%	15	0,5%	6…24	0,5%
13	3,0%	21	0,5%		
17	2,0%				
19	1,5%				
23	1,5%				
25	1,5%				
Note No values are given for harmonics of order higher than 25, as they are usually small, but largely unpredictable due to resonance effects					

Table 12 Values of individual harmonic voltages at the supply terminals for orders up to 25 given in percent of the fundamental voltage U_1

The second one is the IEC 61000-3-12. This standard is focused on the limits for harmonics currents produced by each equipment that has to be connected to public low voltage network for current values greater than 16 A and lower than 75 A for each phase. In addition to the harmonics limits, this standard also indicates the value of the THD of the current.

Considering the charging system as a balanced three-phase equipment the Table 15 reports the limits for the harmonics current and THD values:

Minimal R_{sce}	Admissible individual harmonic current I_n/I_1 ([a])[%]				Admissible harmonic current distortion factor [%]	
	I_5	I_7	I_9	I_{11}	THD	PWHD
66	10,7	7,2	3,1	2	13	22
33	14	9	5	3	16	25
120	19	12	7	4	22	28
250	31	20	12	7	37	38
≥350	40	25	15	10	48	46
The relative values of even harmonics up to order 12 shall not exceed $16/n$ %. Even harmonics above order 12 are taken into account in THD and PWHS in the same way as odd order harmoncs. Note Linear interpolation between successive R_{sce} values is permitted.						
(a) I_1 Reference fundamental current, I_n harmonic current component.						

Table 13 Current emission limits for balanced three-phase equipment

The value of R_{sce} is set equal to 33, since the standard indicates that all equipment comply with the emission limits of harmonic current in R_{sce} equal to 33 are suitable for connecting to each point of the grid.

The document also reports the requirements for getting the measurements, in detail:

- For each harmonic order, measure the 1,5 s smoothed r.m.s. harmonic current in each DFT time window as defined in IEC 61000-4-7
- For each harmonic order, calculate the arithmetic average of the measured valued from the DFT, over the entire observation period

7.3 Real test in the laboratory in Circe

The first step of this work was focused on the measurements of voltage and current parameters during a real transfer of energy with the system at 50 kW. The power of the primary circuit was modified starting from the 50 kW to 15 kW, passing at 25 kW, with an accurate sampling timing of 6 µs using an oscilloscope, and the values recorded were voltage and current for each phase.

The oscilloscope was directly connected to the entrance of cabinet of the inductive charging system during the test, while the cabinet connected to the grid of the laboratory in Circe. It was not possible to measure the nuisance and status of all equipment present in laboratory grid without the inductive charging load. Surely it would be helpful to understand the real impact of the inductive charging.

The next three figures depict the behavior of the voltage and current on the 1st and 2nd phase for the three different power levels, and they show how these parameters are in perfect phase as a resistive load and not a typical inductive load.

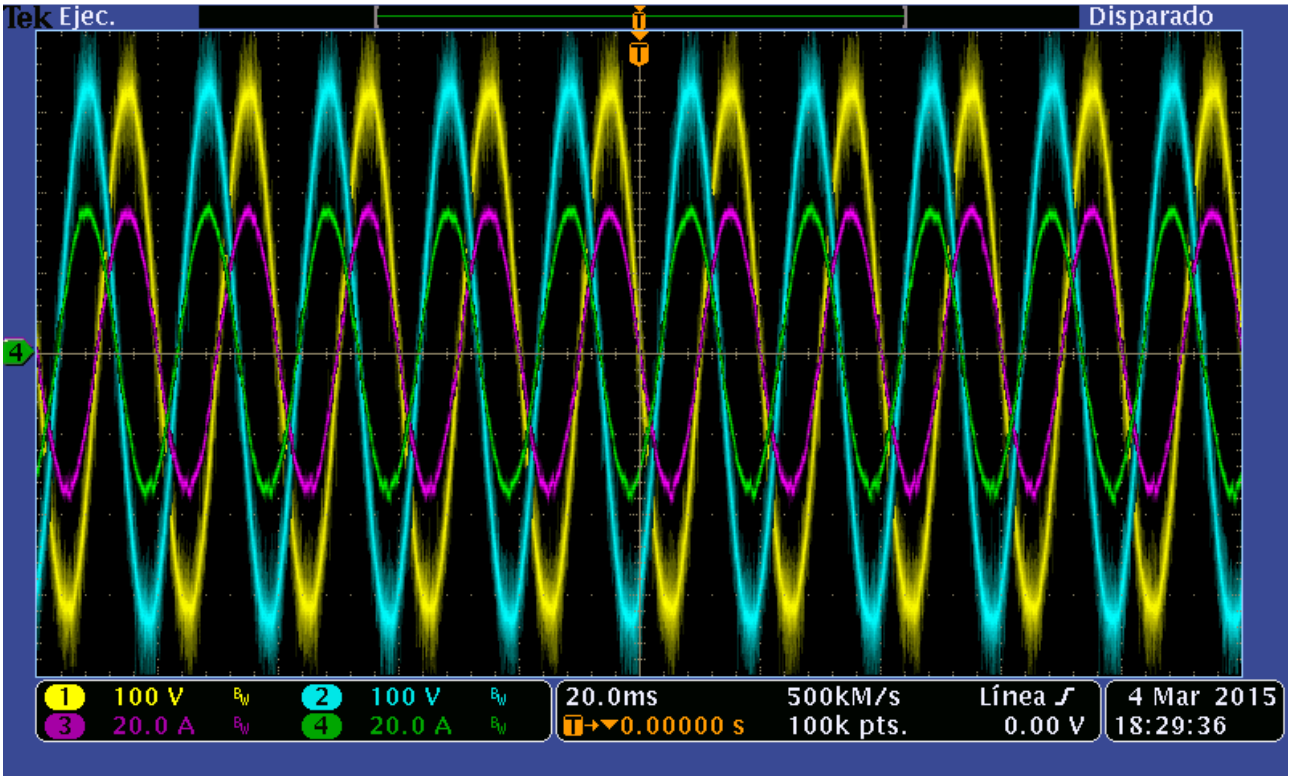

Figure 82 Voltage and current behaviour with the system at 15 kW

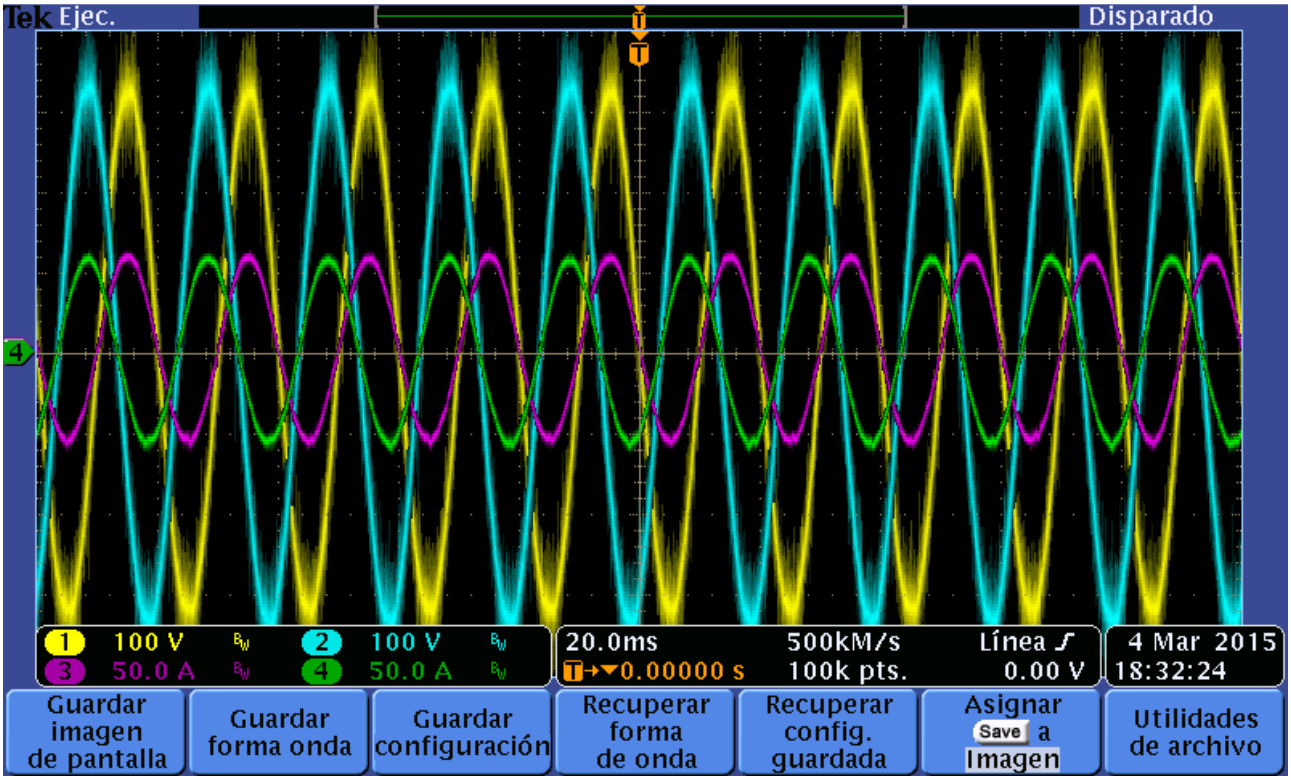

Figure 83 Voltage and current behaviour with the system at 25 kW

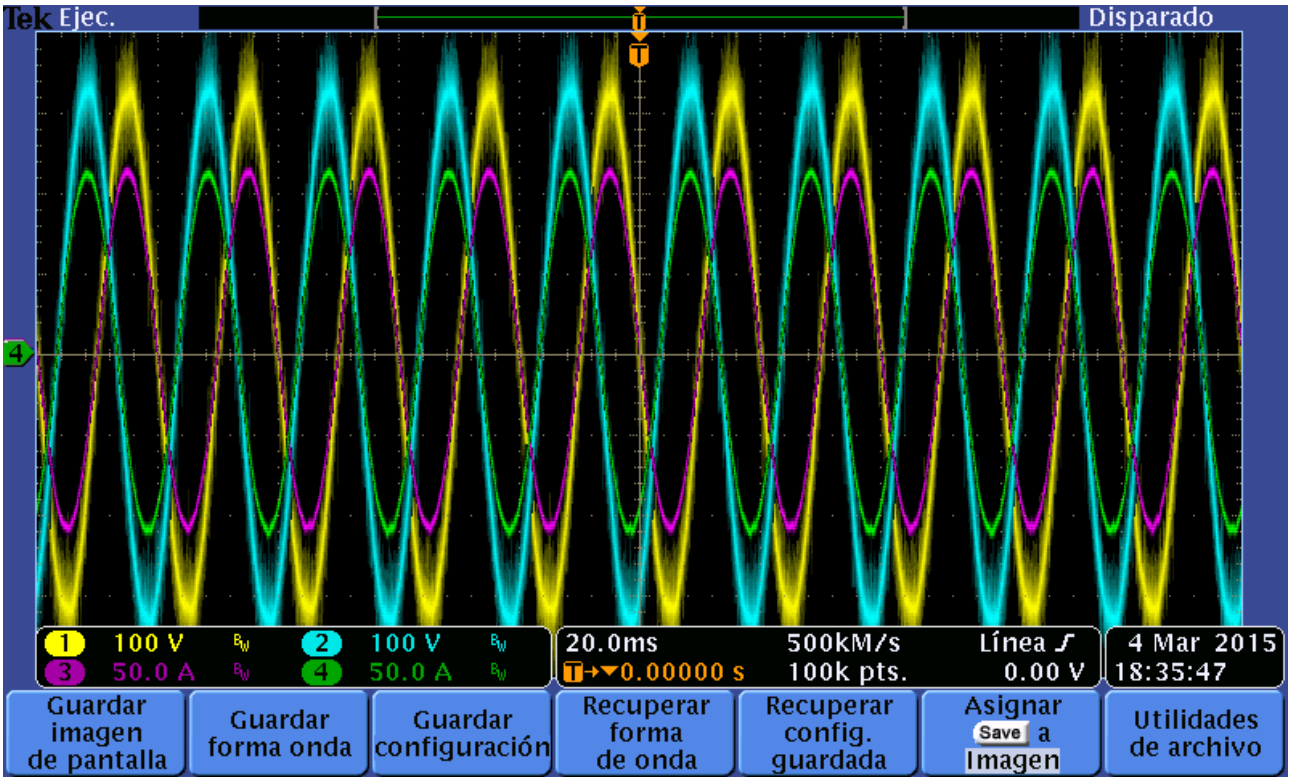

Figure 84 Voltage and current behaviour with the system at 50 kW

From the voltage and current values with the DFT analysis the harmonics for voltage and current have been calculated and these values compared to the limits as for IEC 61000-3-12 and IEC 50160.

The next three histogram describes the behavior of the harmonics current for each phase for the three different level of power, respectively Figure 85 for the system at 15 kW, Figure 86 for 25 kW system and Figure 87 for 50 kW system.

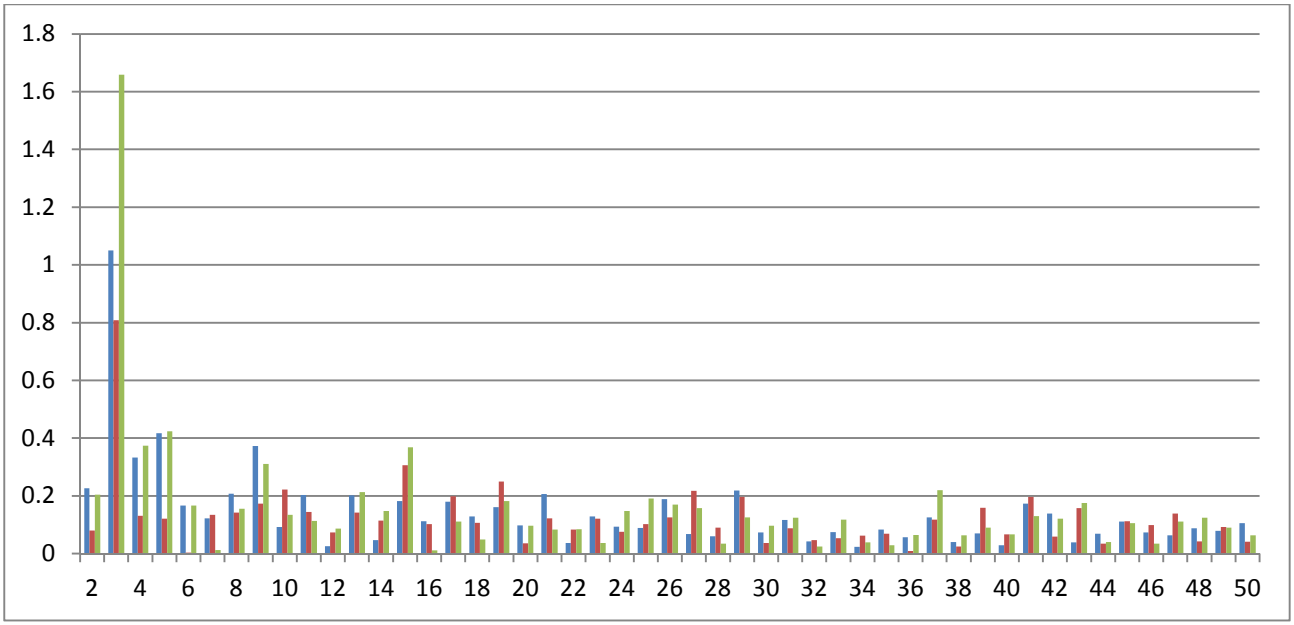

Figure 85 Amplitude of harmonic current for the system at 15 kW

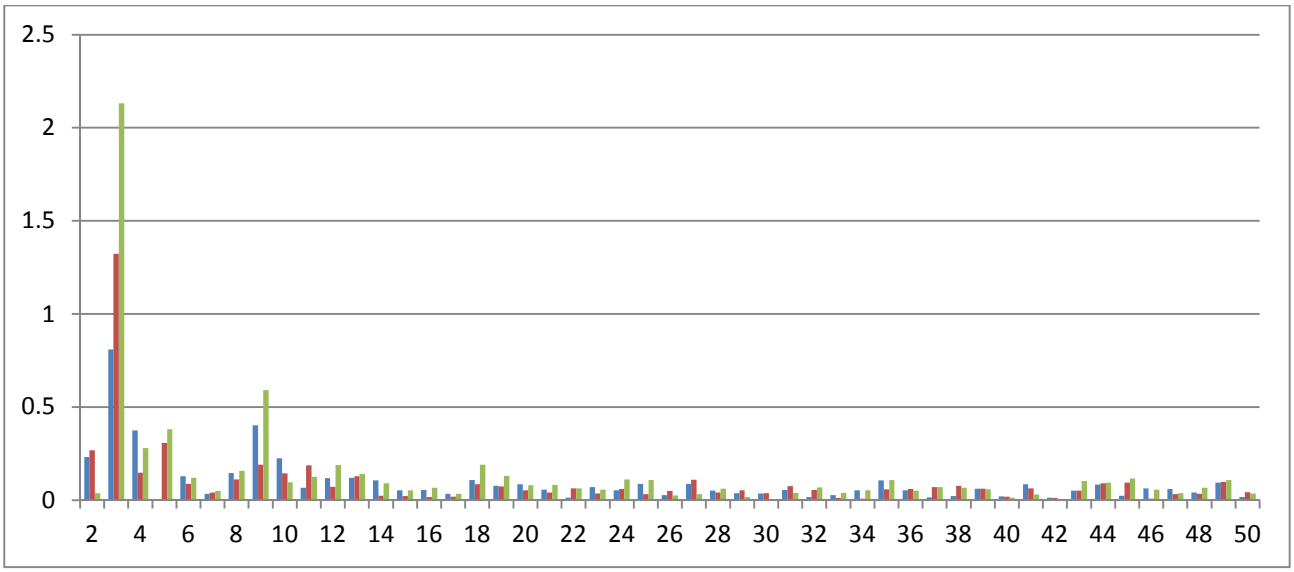

Figure 86 Amplitude of harmonic current for the system at 25 kW

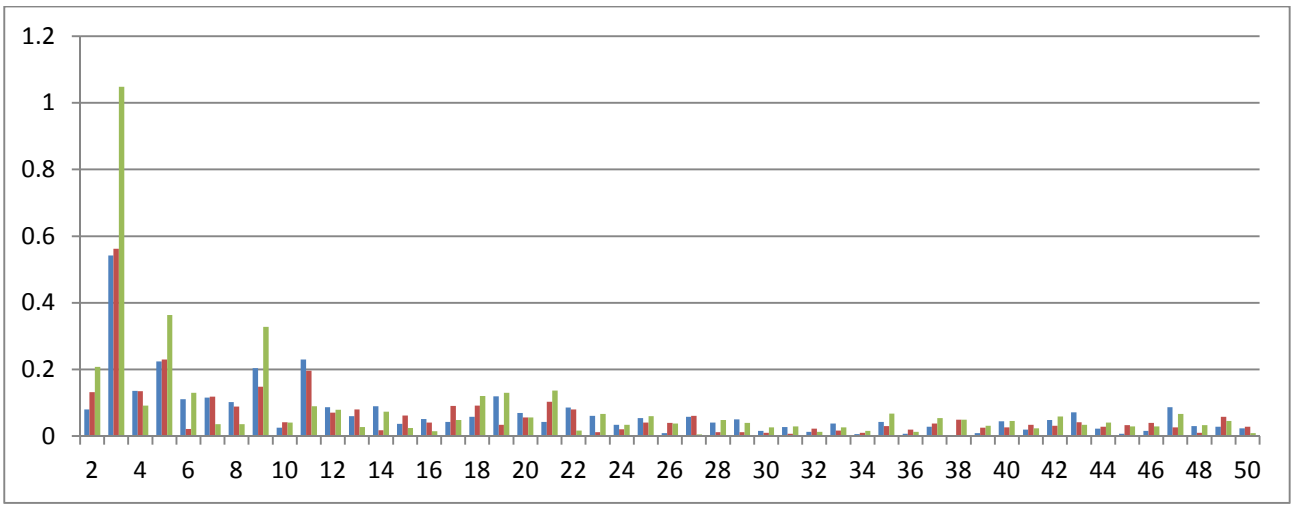

Figure 87 Amplitude of harmonic current for the system at 50 kW

Each histogram corresponds a single value of harmonic during the whole charging and separated for each phase (blue for the 1st phase, red for the 2nd phase and green for the 3rd phase). As required by the standard each value is in percentage of the 1st harmonic.

The three figures above show how the harmonic current do not exceed the limit, assuring for the system the compliance with the international standard.

Moreover the calculated THD values for current and voltage show the compliant to the limits:

- THD of the voltage less than 8%
- THD of the current less than 23%

Power [kW]	THD voltage			THD current		
	Phase u	Phase v	Phase w	Phase u	Phase v	Phase w
15	1.314583	1.097440	1.863563	1.488921	1.199146	1.982228
25	1.364727	1.156842	1.983905	1.220737	1.479774	2.334171
50	1.346627	1.173881	1.986359	0.773160	0.756352	1.238896

Table 14 THD voltage and current values obtained from the measurements

7.4 Simulation in the real Italian power network

Based on the measurement achieved on the real system, to evaluate the impact on the grid network of the inductive charging, those data have been given as input for the grid simulation using the RTDS, a commercial software with different features for controlling and monitoring the power grid.

To obtain an evaluation of the impact as close as possible to the reality, the analysis was focused on the real line of the Italian network, located in Bari, for which the real consumptions of the active and reactive power have been recorded during one day in November 2013. So adding the measurements of the inductive charging gathered during the test to the real Italian grid and looking at the voltage values and THD values, the impact on the grid of the inductive charging designed during this project has been identified.

Main characteristics of the analyzed line are detailed below :

- Nominal power of the transformer 630 kVA with 3 exiting lines, of which the 3rd line under analysis
- Length of the line 250 m
- Nominal current for the line 250 A
- Percentage of single-phase users 83,6% and the three-phase ones 16,4%

Figure below indicates the characteristics of the line with 7 dorsal lines, with different single phase users indicated with U1_i and three-phase users indicated with U3_i.

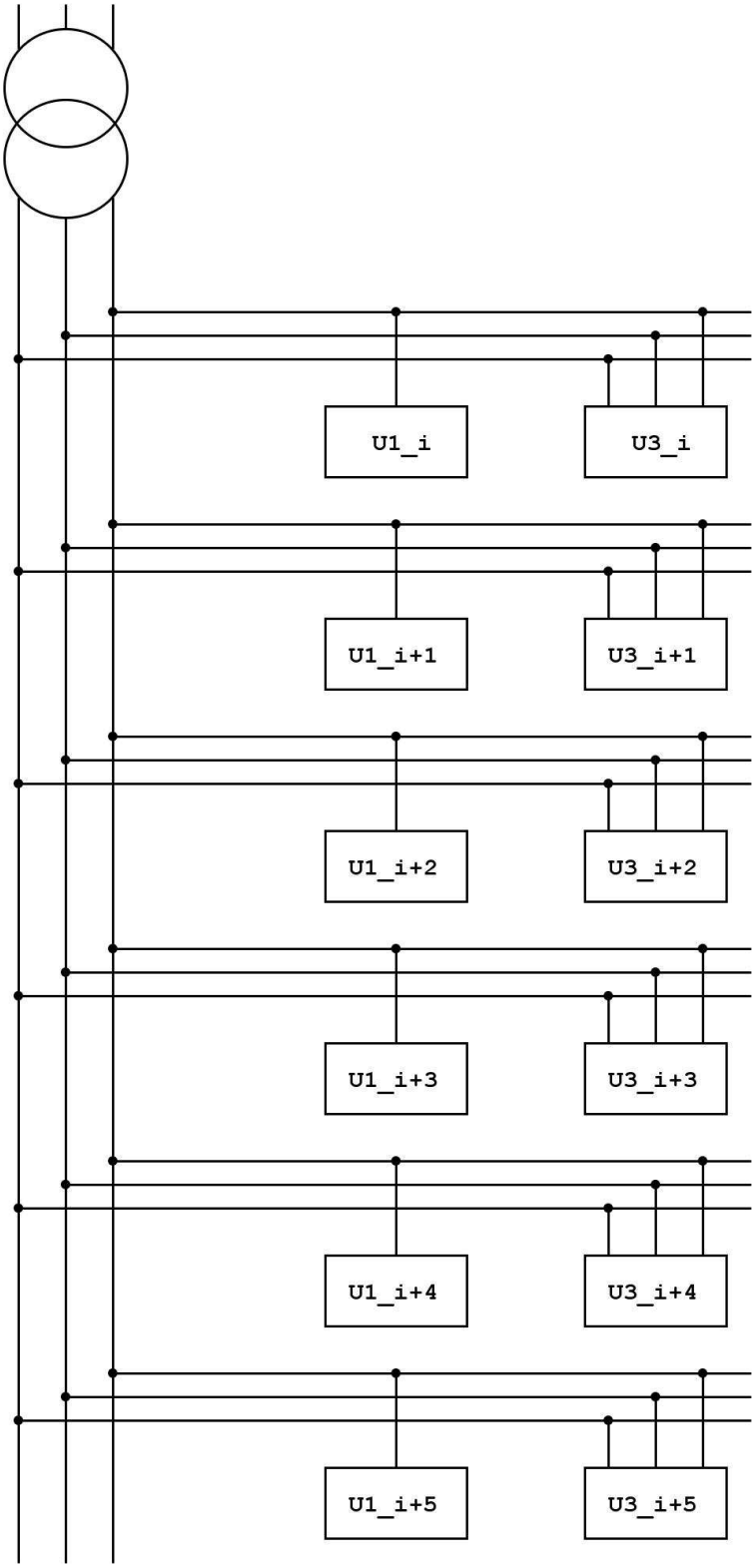

Figure 88 Line of the analyzed grid

The real active and reactive power behavior have been recorded in one day in November 2013 and the behaviour indicates in Figure 89. The data are recorded every 15 minutes starting from 00:00 for a total of 96 meter readings in one day.

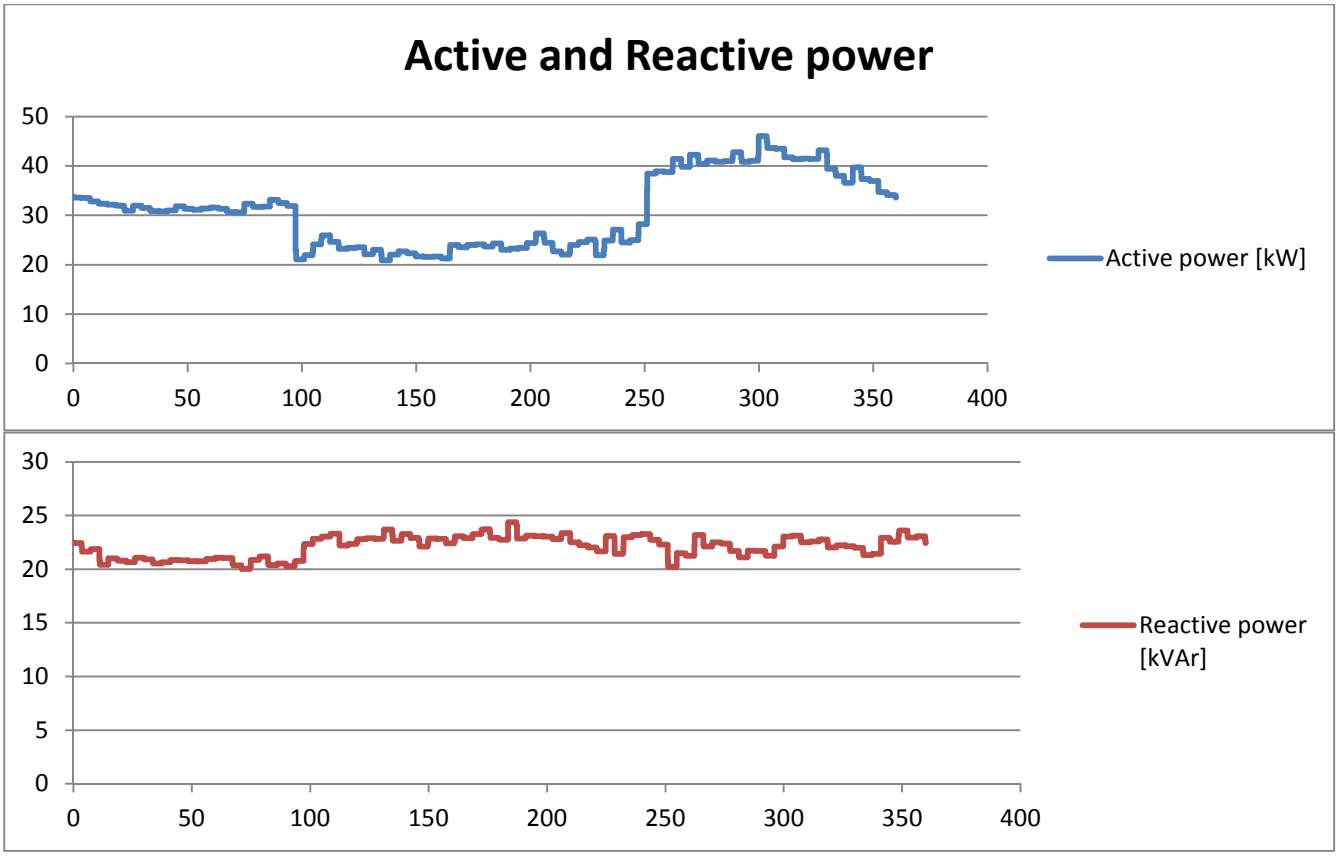

Figure 89 Active and reactive power recorded data

Based on the recorded data for the consumption of the active and reactive power of all users, three different timings have been fix:

- 1st point: 12th quarter hour – time 3:00
- 2nd point: 52nd quarter hour – time 13:00
- 3rd point: 80th quarter hour – time 20:00 (the worst case)

Thus the analysis is carried out for these 3 different timings during the day with different consumptions of active and reactive power.

Moreover to estimate the worst and best scenario for connecting the inductive charging stations in addition to the existing loads, its position among the line is analyzed in three different locations.

The hypotheses for the analysis are detailed below:

- Voltage constant during each line
- 3 different power levels: 15 kW, 25 kW and 50 kW
- 3 different timings during the day
- 3 different positions in the line: at the beginning of the line downstream to the transformer, in the middle of line and at the end of the line.

Figure 90 indicates all the positions of the charging station as a three-phase load in addition to the other loads present in the line.

The single-phase load has been connected always to the same line just for the graph. This kind of load is usually connected to different line to assure the balancing of the load in the grid.

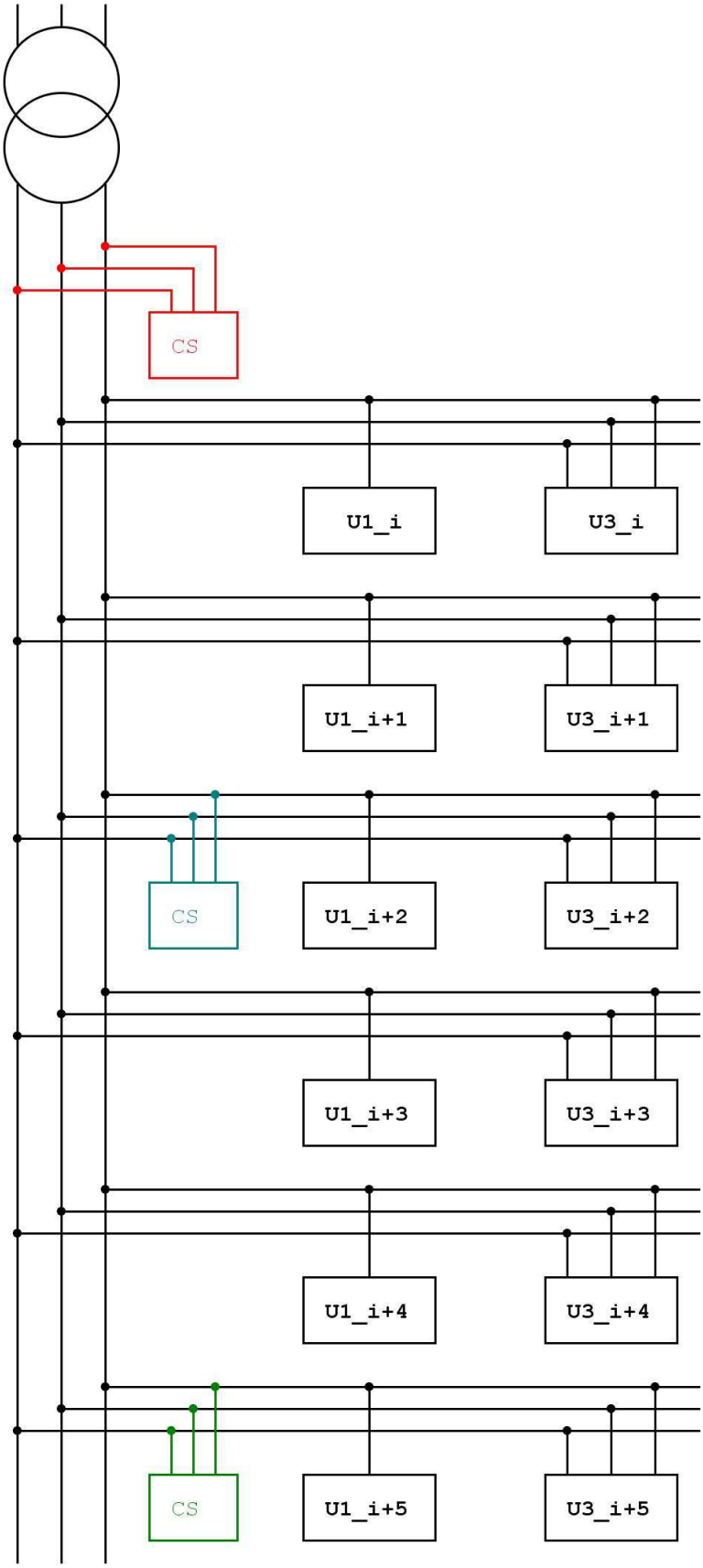

Figure 90 Different positions of the inductive charging station

Table 15 reports the set points for the simulation, considering the different values of power of the inductive charging station, location of the inductive charging station in the line and different timings during the day.

Case	Power [kW]	Position of the charging station	Time [hh:mm]
1	15	At the beginning of the line	03:00
2	15	At the beginning of the line	13:00
3	15	At the beginning of the line	20:00
4	15	In the middle of the line	03:00
5	15	In the middle of the line	13:00
6	15	In the middle of the line	20:00
7	15	At the end of the line	03:00
8	15	At the end of the line	13:00
9	15	At the end of the line	20:00
10	25	At the beginning of the line	03:00
11	25	At the beginning of the line	13:00
12	25	At the beginning of the line	20:00
13	25	In the middle of the line	03:00
14	25	In the middle of the line	13:00
15	25	In the middle of the line	20:00
16	25	At the end of the line	03:00
17	25	At the end of the line	13:00
18	25	At the end of the line	20:00
19	50	At the beginning of the line	03:00
20	50	At the beginning of the line	13:00
21	50	At the beginning of the line	20:00
22	50	In the middle of the line	03:00
23	50	In the middle of the line	13:00
24	50	In the middle of the line	20:00
25	50	At the end of the line	03:00
26	50	At the end of the line	13:00
27	50	At the end of the line	20:00

Table 15 Different scenarios for the analysis

8 Annex

Next paragraphs report for each case the graphs for the behavior of the harmonic current and the current and a table stating the value of voltage value recorded in the three different locations where the inductive loads is added.

8.1.1 Case 1 – Power at 15 kW – at the beginning of the line – 03:00

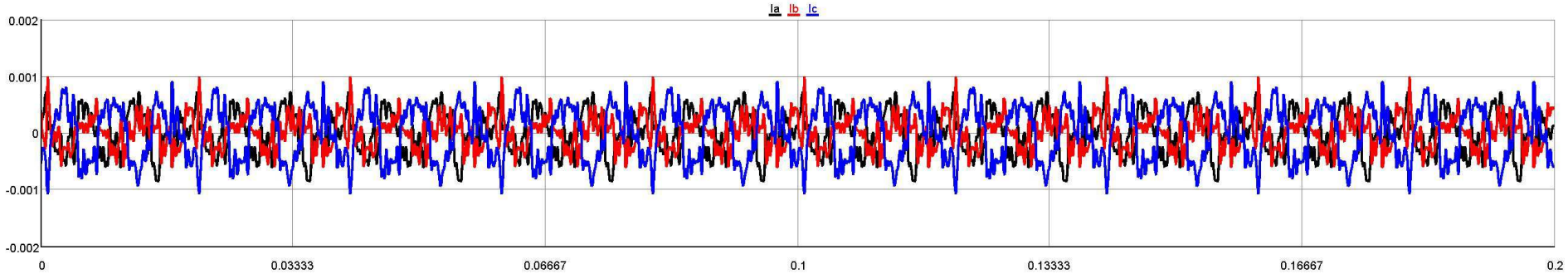

Figure 91 Harmonic current – case 1

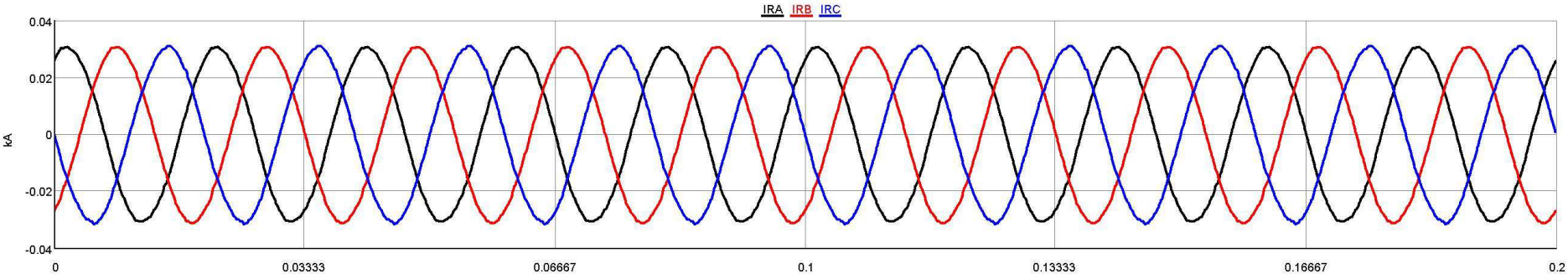

Figure 92 Current – case 1

	Voltage at the beginning of the line [V]			Voltage in the middle of line [V]			Voltage at the end of the line [V]		
Case	Line a	Line b	Line c	Line a	Line b	Line c	Line a	Line b	Line c
1	230,4	230,5	230,7	228,8	229,2	229,6	228,4	228,7	229,2

Table 16 Voltage values – case 1

8.1.2 Case 2 – Power at 15 kW – at the beginning of the line – 13:00

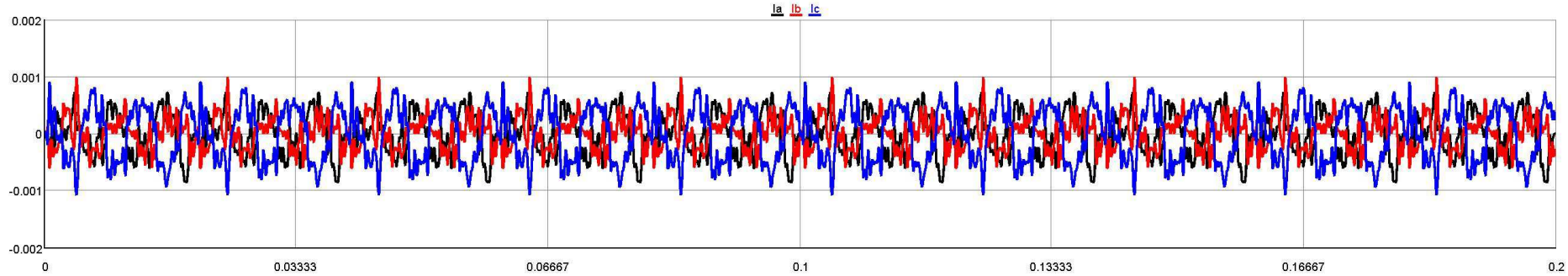

Figure 93 Harmonic current – case 2

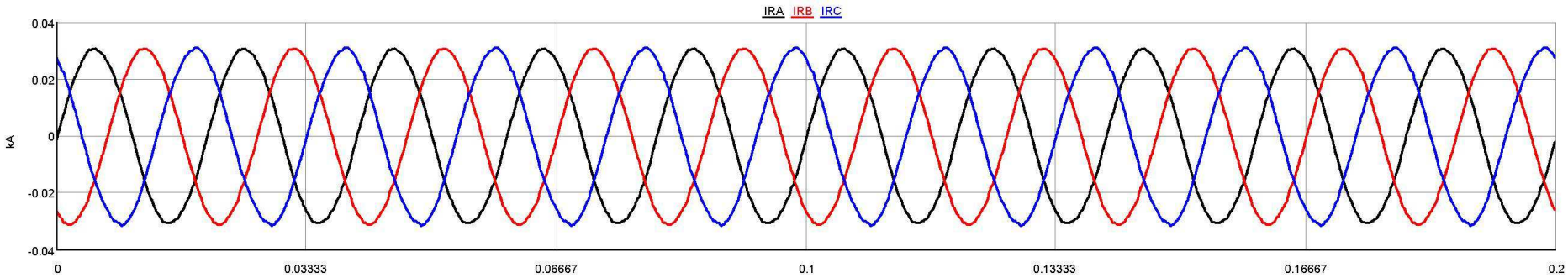

Figure 94 Current – case 2

	Voltage at the beginning of the line [V]			Voltage in the middle of line [V]			Voltage at the end of the line [V]		
Case	Line a	Line b	Line c	Line a	Line b	Line c	Line a	Line b	Line c
2	230,6	230,6	230,4	229,3	229,5	229,8	229	229,2	229,6

Table 17 Voltage values – case 2

8.1.3 Case 3 – Power at 15 kW – at the beginning of the line – 20:00

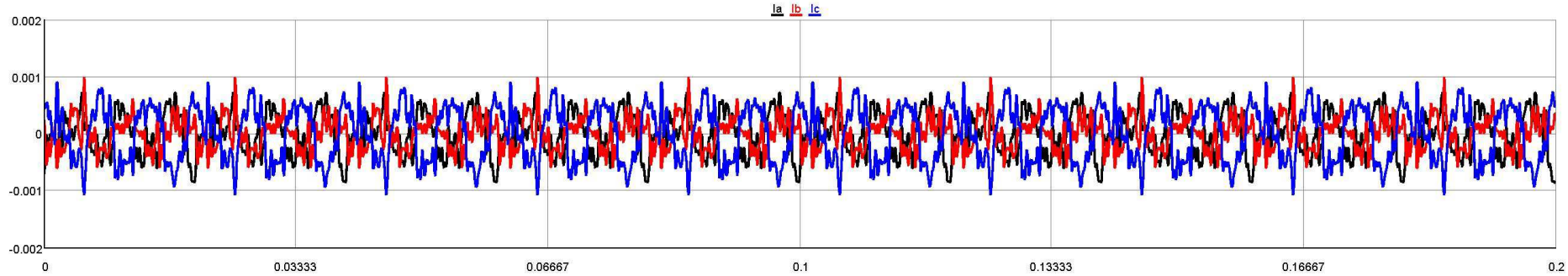

Figure 95 Harmonic current – case 3

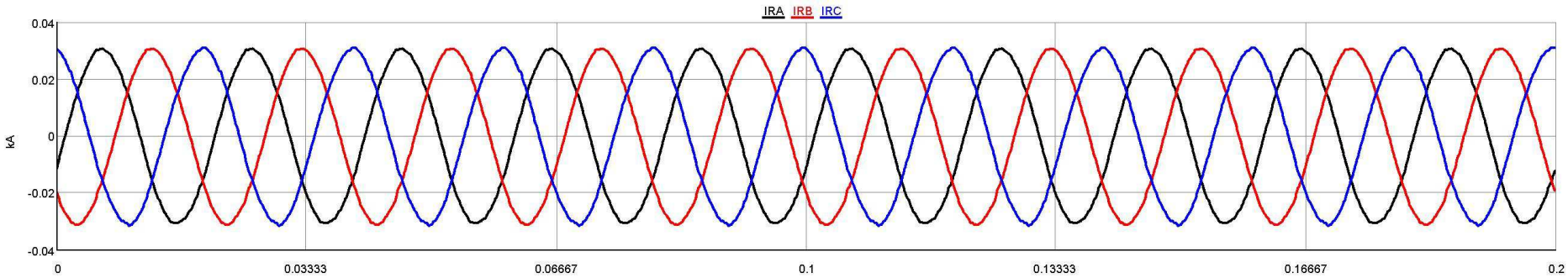

Figure 96 Current – case 3

	Voltage at the beginning of the line [V]			Voltage in the middle of line [V]			Voltage at the end of the line [V]		
Case	Line a	Line b	Line c	Line a	Line b	Line c	Line a	Line b	Line c
3	230,5	230,6	230,4	228,1	229,1	229,5	227,7	228,6	229,1

Table 18 Voltage values – case 3

8.1.4 Case 4 – Power at 15 kW – in the middle of the line – 03:00

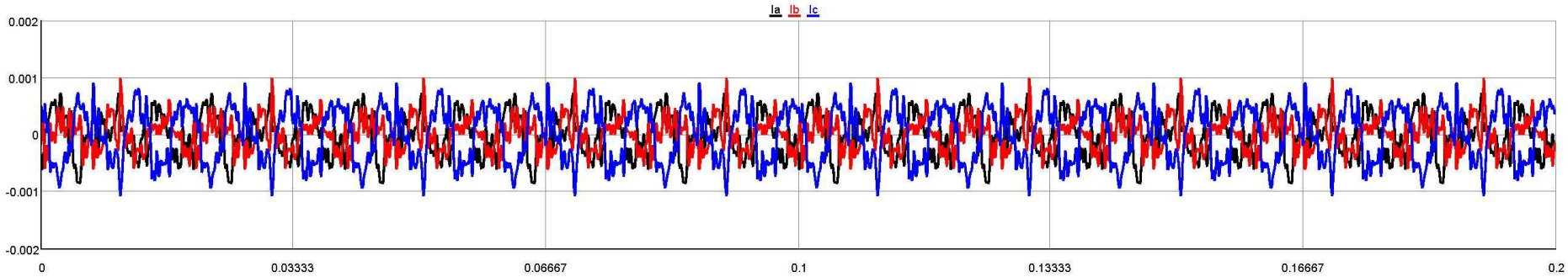

Figure 97 Harmonic current – case 4

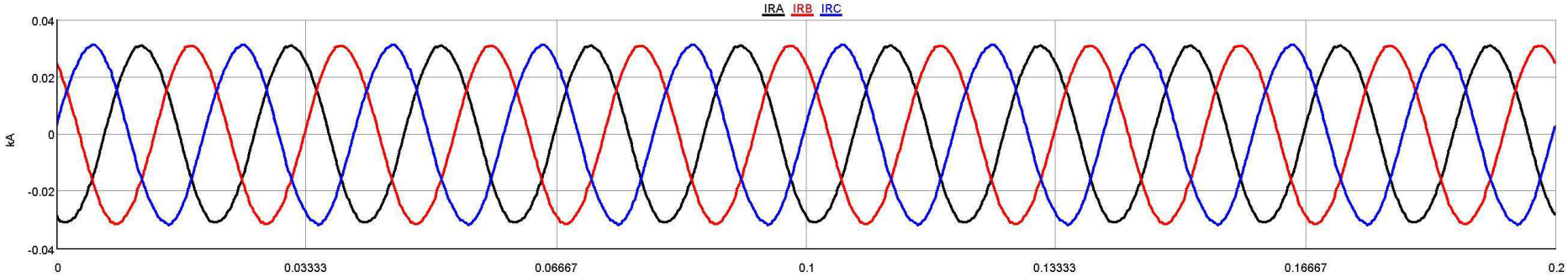

Figure 98 Current – case 4

	Voltage at the beginning of the line [V]			Voltage in the middle of line [V]			Voltage at the end of the line [V]		
Case	Line a	Line b	Line c	Line a	Line b	Line c	Line a	Line b	Line c
4	230,5	230,7	230,4	228,4	228,7	228,8	228	228,3	228,3

Table 19 Voltage values – case 4

8.1.5 Case 5 – Power at 15 kW – in the middle of the line – 13:00

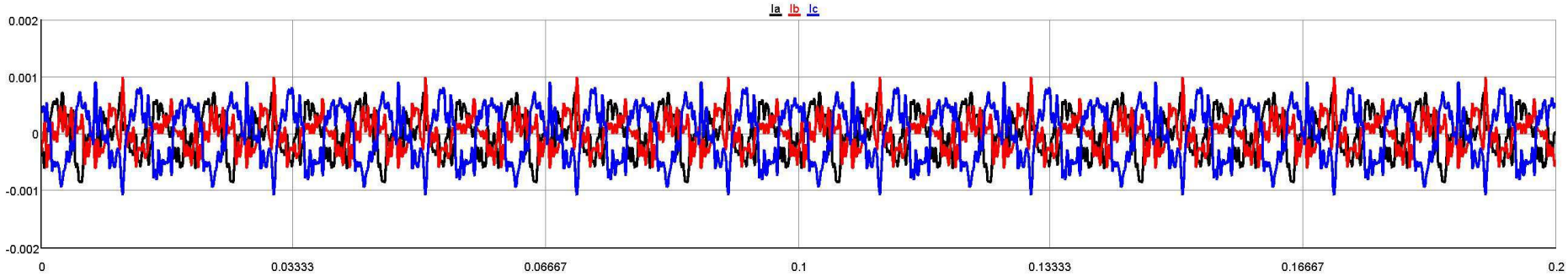

Figure 99 Harmonic current – case 5

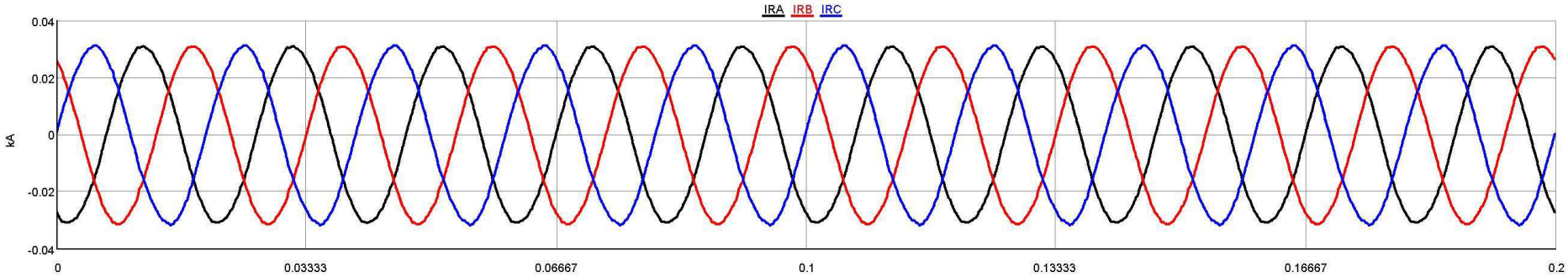

Figure 100 Current – case 5

	Voltage at the beginning of the line [V]			Voltage in the middle of line [V]			Voltage at the end of the line [V]		
Case	Line a	Line b	Line c	Line a	Line b	Line c	Line a	Line b	Line c
5	230,6	230,4	230,6	228,7	228,7	229,4	228,5	228,4	229,2

Table 20 Voltage values – case 5

8.1.6 Case 6 – Power at 15 kW – in the middle of the line – 20:00

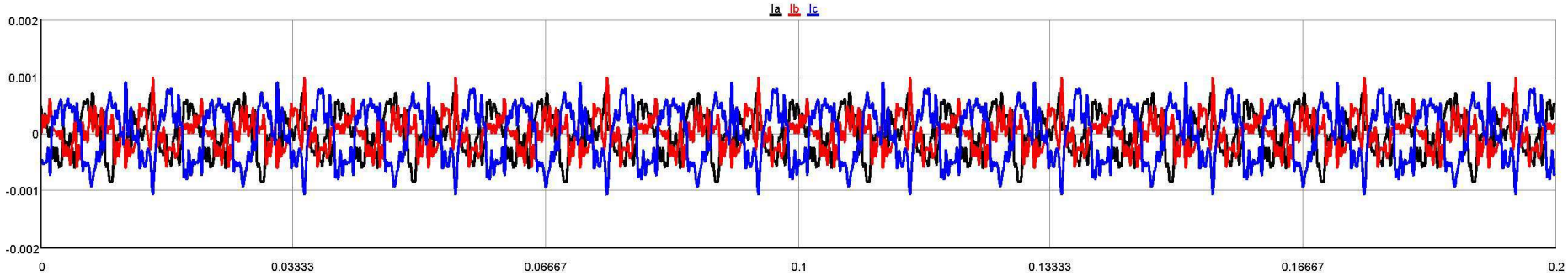

Figure 101 Harmonic current – case 6

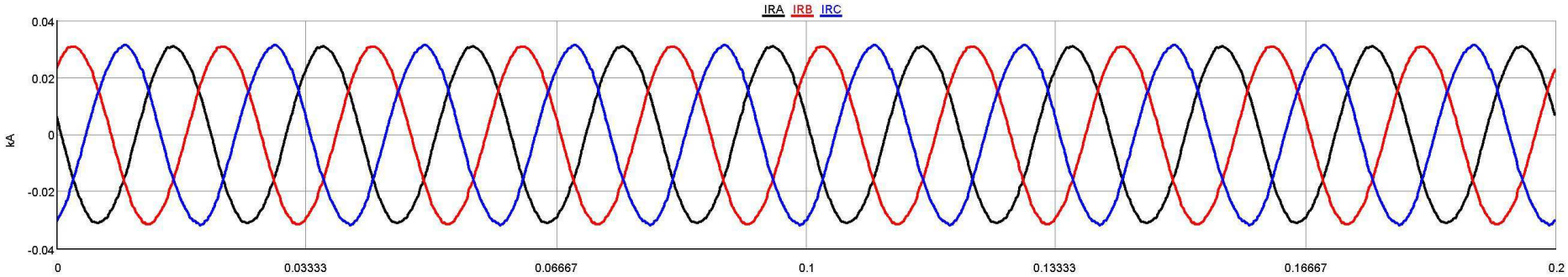

Figure 102 Current – case 6

	Voltage at the beginning of the line [V]			Voltage in the middle of line [V]			Voltage at the end of the line [V]		
Case	Line a	Line b	Line c	Line a	Line b	Line c	Line a	Line b	Line c
6	230,6	230,5	230,4	227,6	228,4	228,9	227,2	227,9	228,5

Table 21 Voltage values – case 6

8.1.7 Case 7 – Power at 15 kW – at the end of the line –03:00

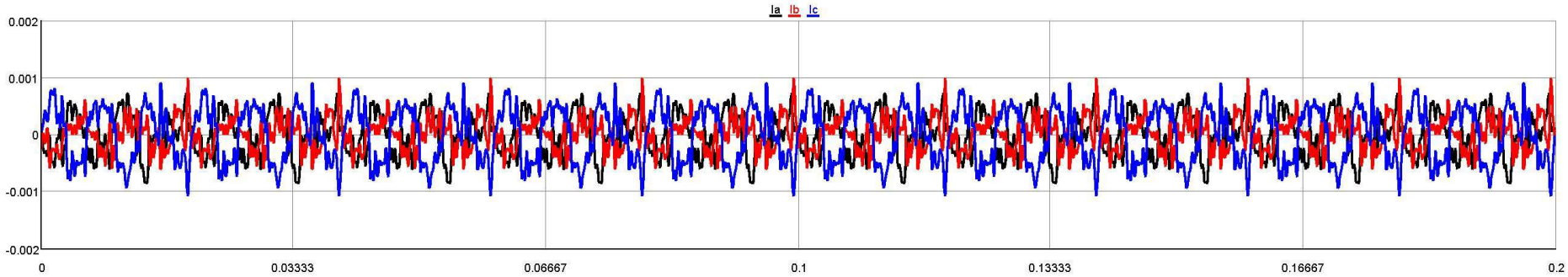

Figure 103 Harmonic current – case 7

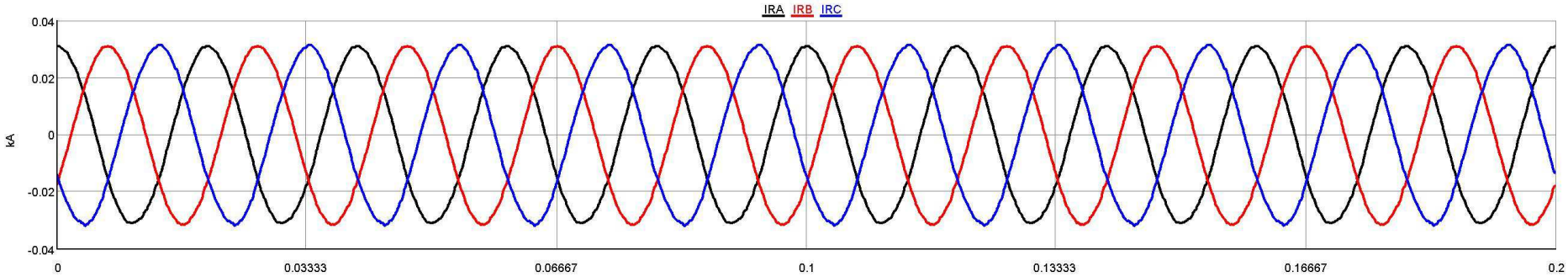

Figure 104 Current – case 7

	Voltage at the beginning of the line [V]			Voltage in the middle of line [V]			Voltage at the end of the line [V]		
Case	Line a	Line b	Line c	Line a	Line b	Line c	Line a	Line b	Line c
7	230,4	230,6	230,7	228,2	228,6	290	227,4	227,8	228,2

Table 22 Voltage values – case 7

8.1.8 Case 8 – Power at 15 kW – at the end of the line –13:00

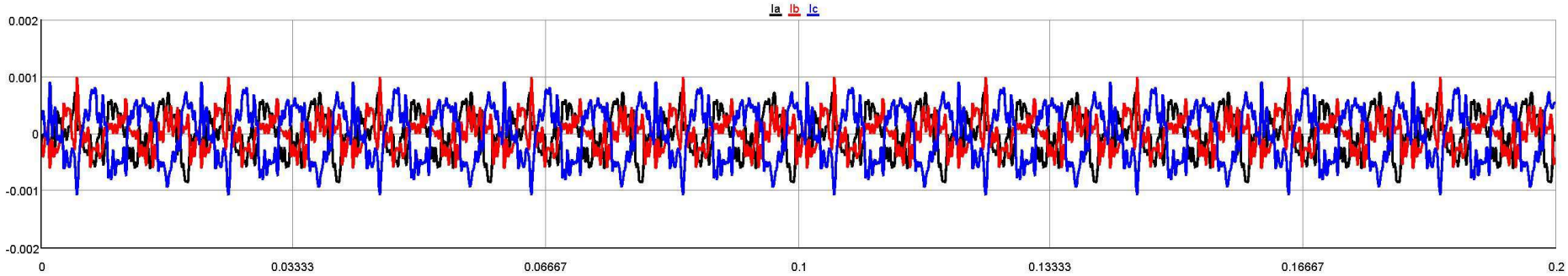

Figure 105 Harmonic current – case 8

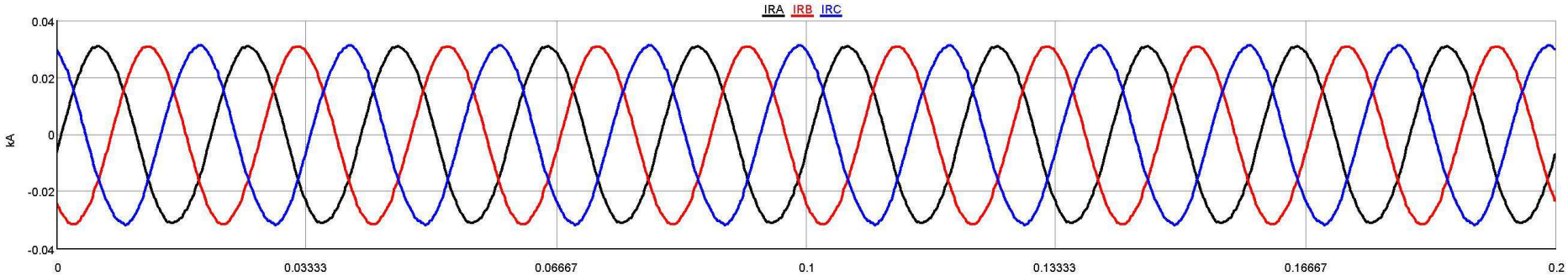

Figure 106 Current – case 8

	Voltage at the beginning of the line [V]			Voltage in the middle of line [V]			Voltage at the end of the line [V]		
Case	Line a	Line b	Line c	Line a	Line b	Line c	Line a	Line b	Line c
8	230,6	230,6	230,5	228,8	228,8	229,3	228,1	228,1	228,6

Table 23 Voltage values – case 8

8.1.9 Case 9 – Power at 15 kW – at the end of the line –20:00

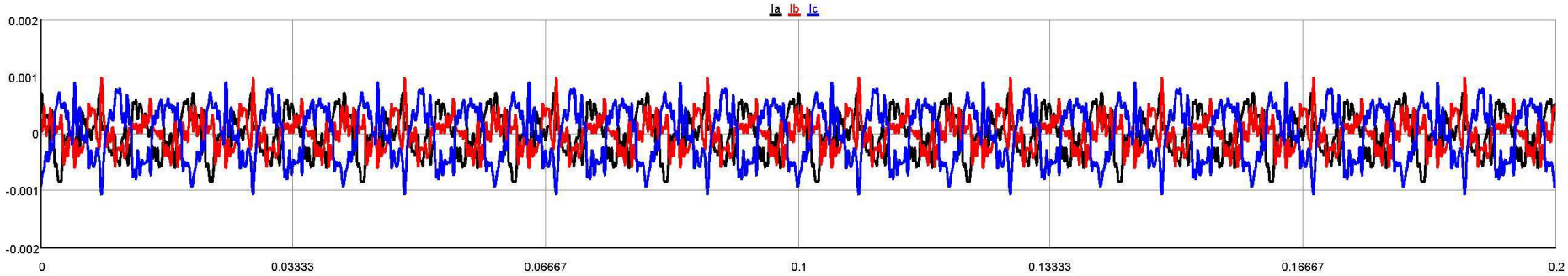

Figure 107 Harmonic current – case 9

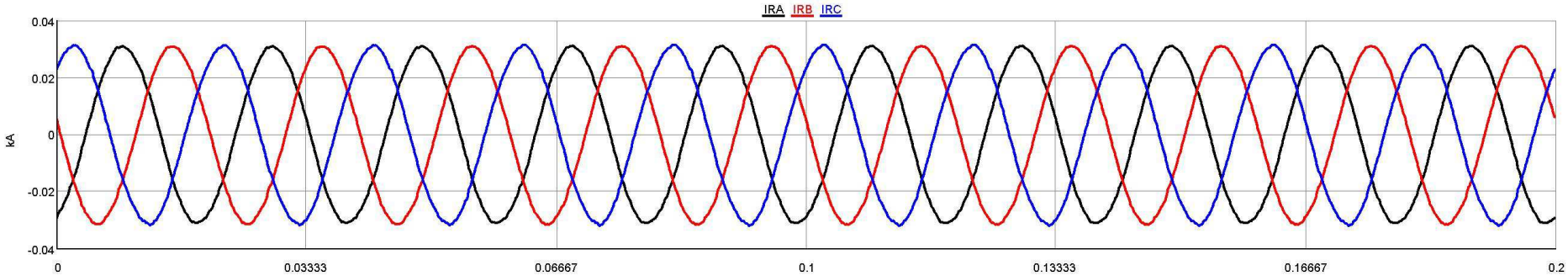

Figure 108 Current – case 9

	Voltage at the beginning of the line [V]			Voltage in the middle of line [V]			Voltage at the end of the line [V]		
Case	Line a	Line b	Line c	Line a	Line b	Line c	Line a	Line b	Line c
9	230,3	230,6	230,5	227,4	228,6	229	226,6	227,6	228,2

Table 24 Voltage values – case 9

8.1.10 Case 10 – Power at 25 kW – At the beginning of the line – 03:00

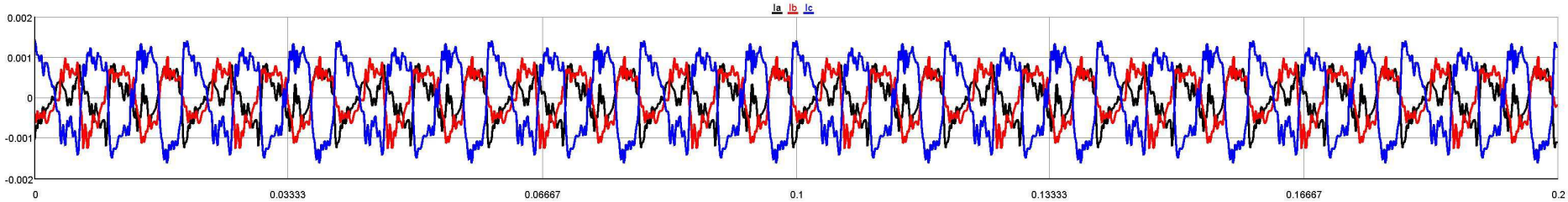

Figure 109 Harmonic current – case 10

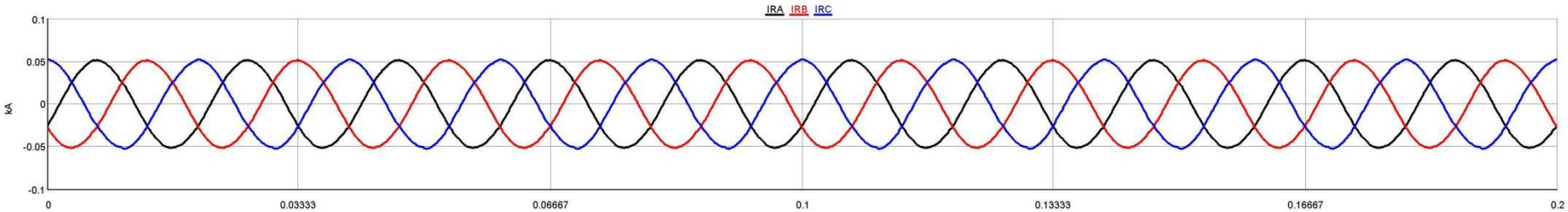

Figure 110 Current – case 10

	Voltage at the beginning of the line [V]			Voltage in the middle of line [V]			Voltage at the end of the line [V]		
Case	Line a	Line b	Line c	Line a	Line b	Line c	Line a	Line b	Line c
10	230,5	230,4	230,6	229	229	229,5	228,6	228,6	229,1

Table 25 Voltage values – case 10

8.1.11 Case 11 – Power at 25 kW – At the beginning of the line – 13:00

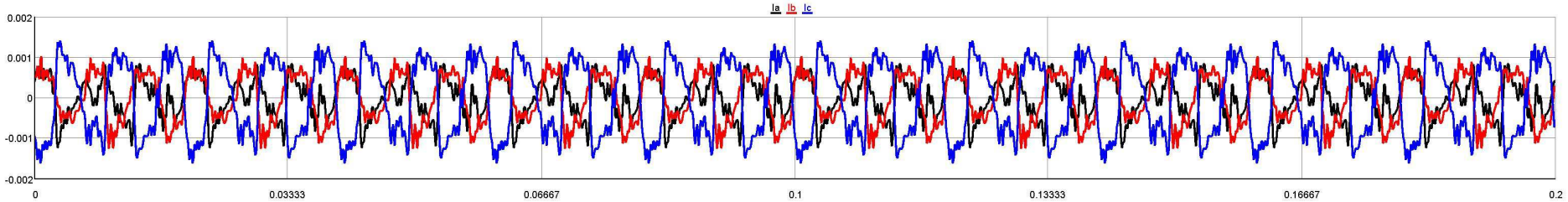

Figure 111 Harmonic current – case 11

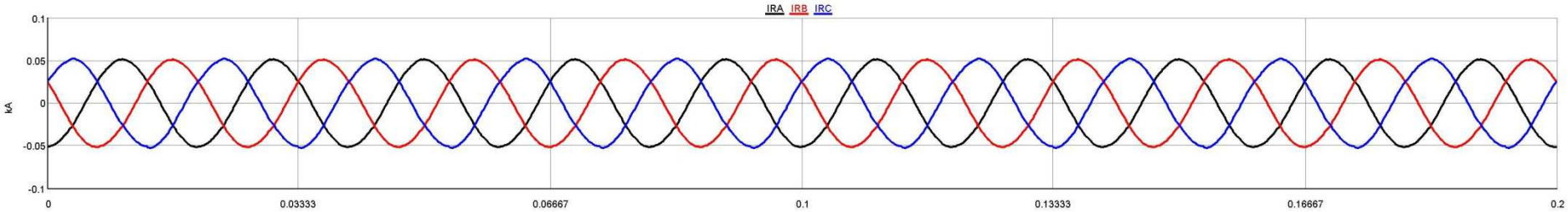

Figure 112 Current – case 11

	Voltage at the beginning of the line [V]			Voltage in the middle of line [V]			Voltage at the end of the line [V]		
Case	Line a	Line b	Line c	Line a	Line b	Line c	Line a	Line b	Line c
11	230,6	230,4	230,5	229,3	229,3	229,9	229	229	229,7

Table 26 Voltage values – case 11

8.1.12 Case 12 – Power at 25 kW – At the beginning of the line – 20:00

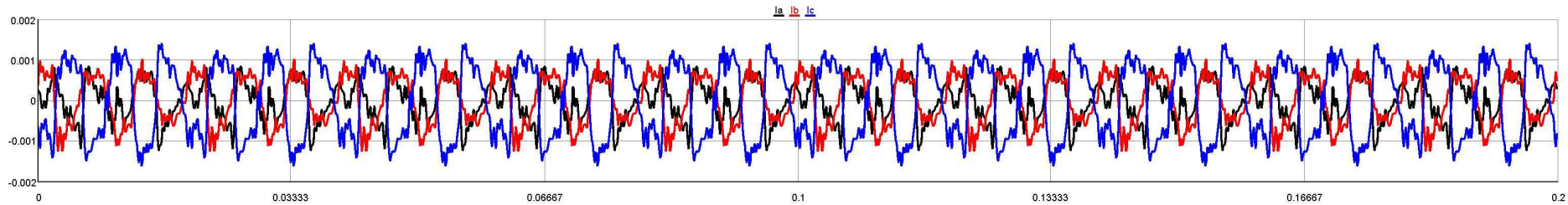

Figure 113 Harmonic current – case 12

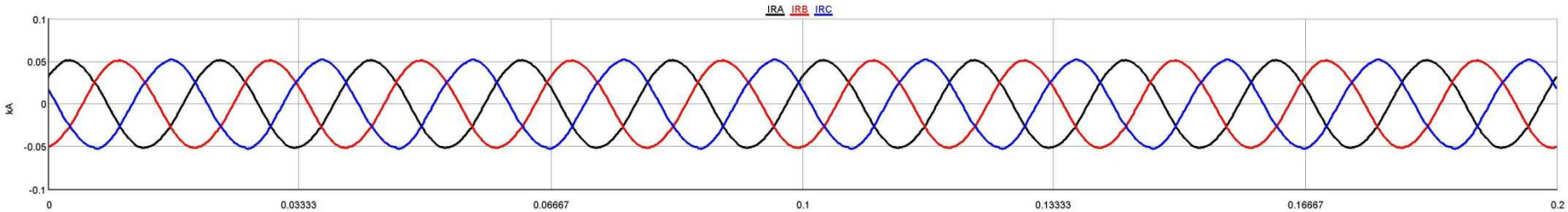

Figure 114 Current – case 12

	Voltage at the beginning of the line [V]			Voltage in the middle of line [V]			Voltage at the end of the line [V]		
Case	Line a	Line b	Line c	Line a	Line b	Line c	Line a	Line b	Line c
12	230,4	230,5	230,7	227,8	228,1	228,6	227,4	227,7	228,2

Table 27 Voltage values – case 12

8.1.13 Case 13 – Power at 25 kW – In the middle of the line – 03:00

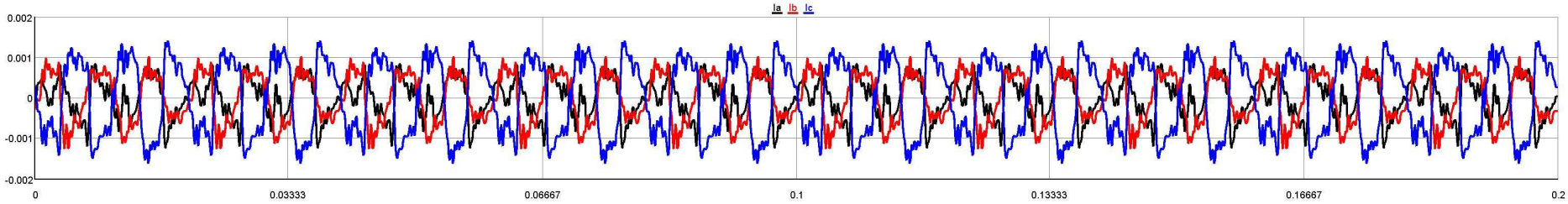

Figure 115 Harmonic current – case 13

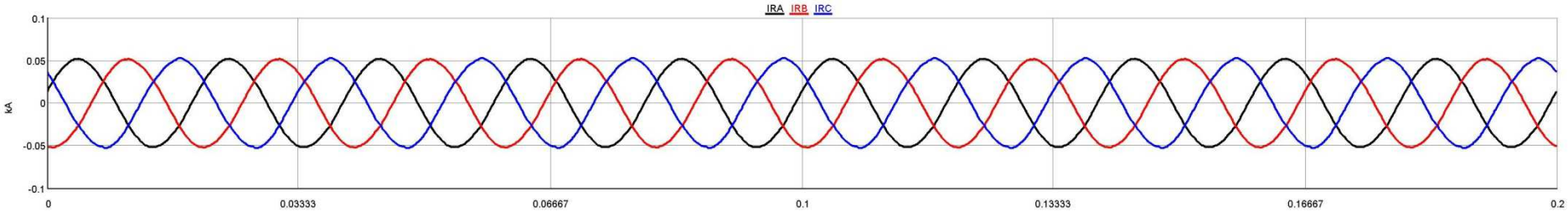

Figure 116 Current – case 13

	Voltage at the beginning of the line [V]			Voltage in the middle of line [V]			Voltage at the end of the line [V]		
Case	Line a	Line b	Line c	Line a	Line b	Line c	Line a	Line b	Line c
13	230,4	230,7	230,5	227,8	228,3	228,4	227,4	227,9	228

Table 28 Voltage values – case 13

8.1.14 Case 14 – Power at 25 kW – In the middle of the line – 13:00

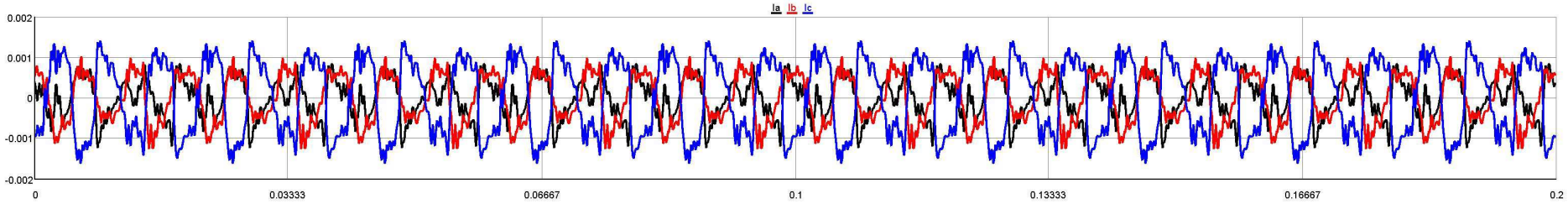

Figure 117 Harmonic current – case 14

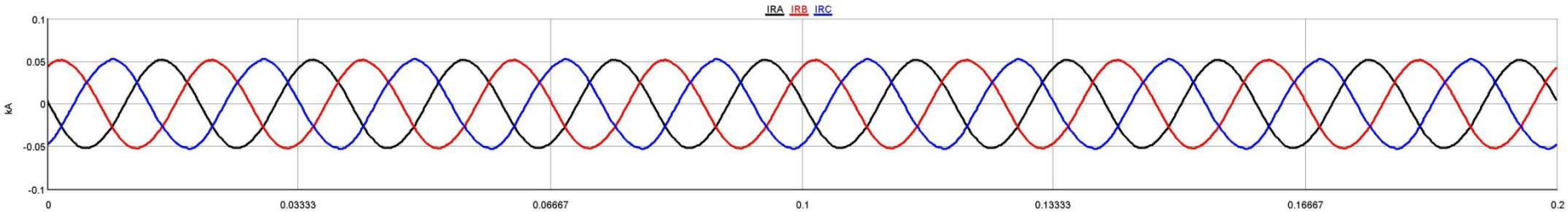

Figure 118 Current – case 14

	Voltage at the beginning of the line [V]			Voltage in the middle of line [V]			Voltage at the end of the line [V]		
Case	Line a	Line b	Line c	Line a	Line b	Line c	Line a	Line b	Line c
14	230,6	230,5	230,5	228,3	228,3	228,9	228,1	228	228,6

Table 29 Voltage values – case 14

8.1.15 Case 15 – Power at 25 kW – In the middle of the line – 20:00

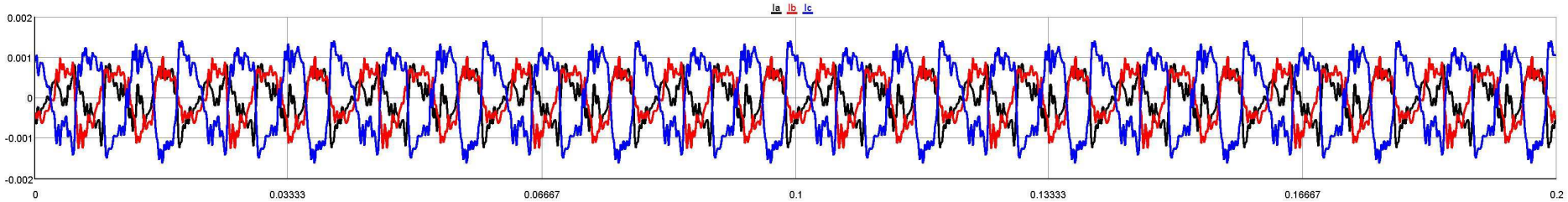

Figure 119 Harmonic current – case 15

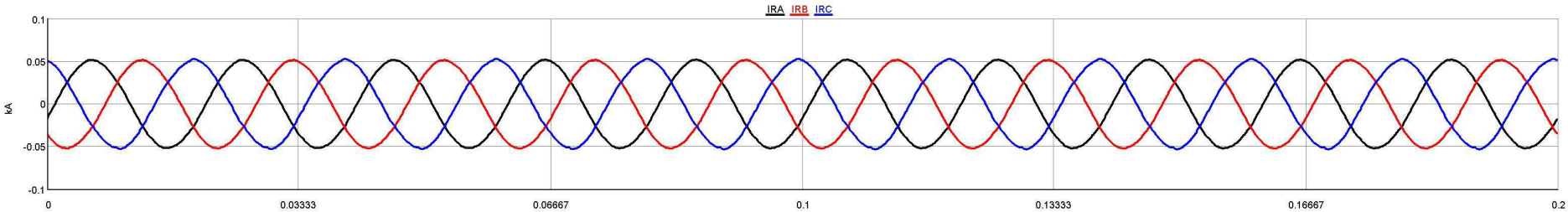

Figure 120 Current – case 15

	Voltage at the beginning of the line [V]			Voltage in the middle of line [V]			Voltage at the end of the line [V]		
Case	Line a	Line b	Line c	Line a	Line b	Line c	Line a	Line b	Line c
15	230,4	230,6	230,4	227	228,1	228,5	226,6	227,6	228,1

Table 30 Voltage values – case 15

8.1.16 Case 16 – Power at 25 kW – At the end of the line –03:00

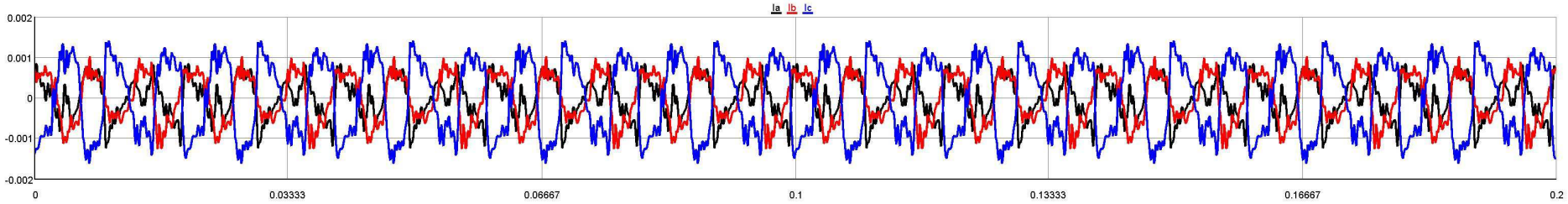

Figure 121 Harmonic current – case 16

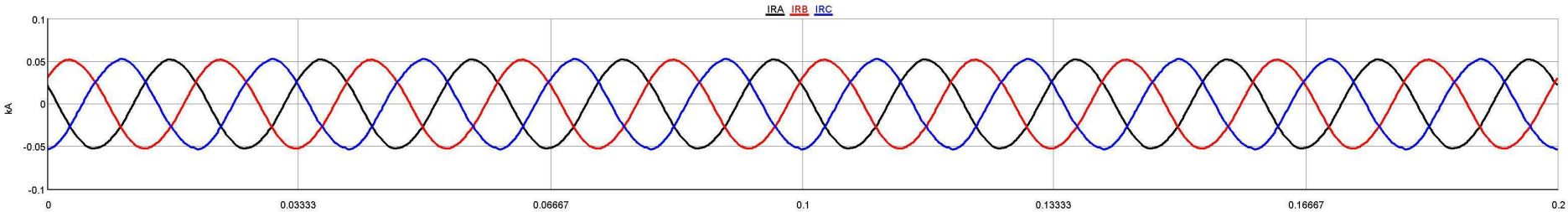

Figure 122 Current – case 16

	Voltage at the beginning of the line [V]			Voltage in the middle of line [V]			Voltage at the end of the line [V]		
Case	Line a	Line b	Line c	Line a	Line b	Line c	Line a	Line b	Line c
16	230,3	230,6	230,6	227,8	228,3	228,5	226,7	227,1	227,4

Table 31 Voltage values – case 16

8.1.17 Case 17 – Power at 25 kW – At the end of the line –13:00

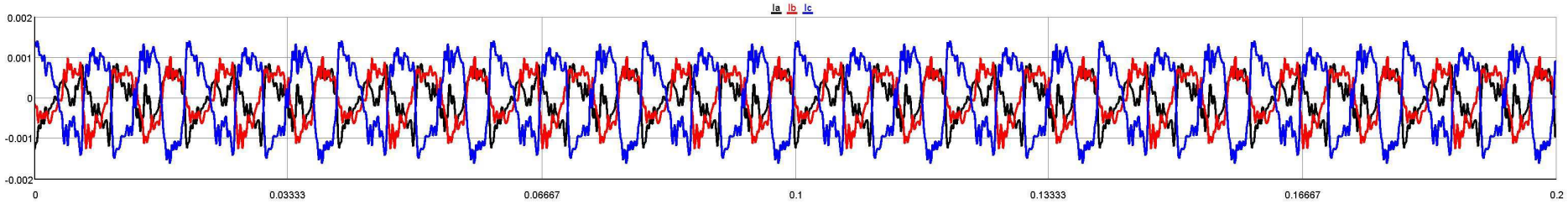

Figure 123 Harmonic current – case 17

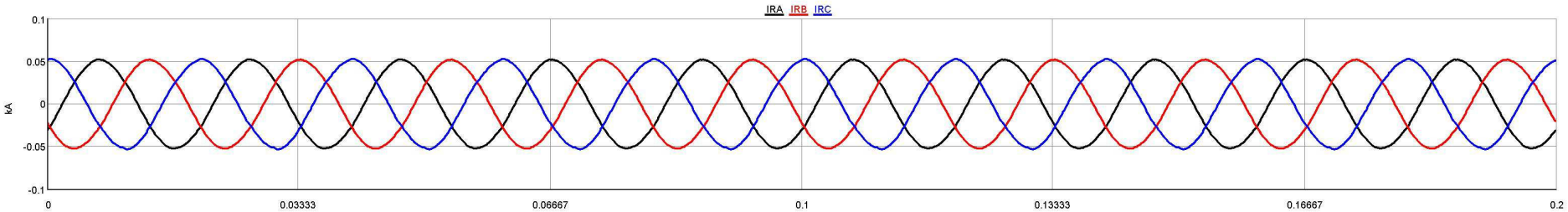

Figure 124 Current – case 17

	Voltage at the beginning of the line [V]			Voltage in the middle of line [V]			Voltage at the end of the line [V]		
Case	Line a	Line b	Line c	Line a	Line b	Line c	Line a	Line b	Line c
17	230,6	230,5	230,4	228,3	228,4	228,8	227,4	227,4	227,9

Table 32 Voltage values – case 17

8.1.18 Case 18 – Power at 25 kW – At the end of the line –20:00

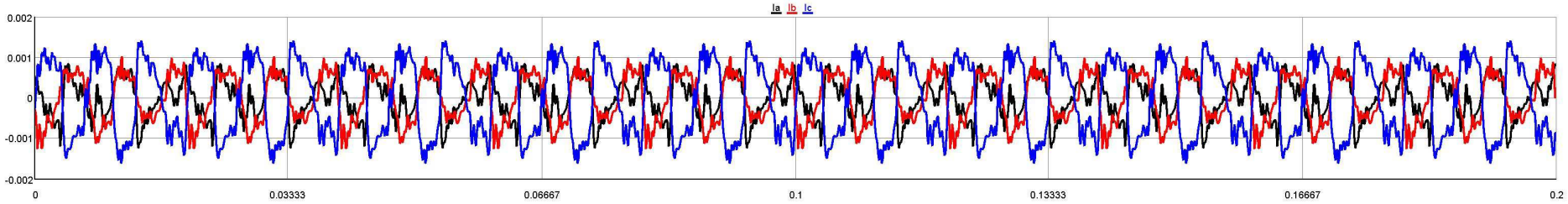

Figure 125 Harmonic current – case 18

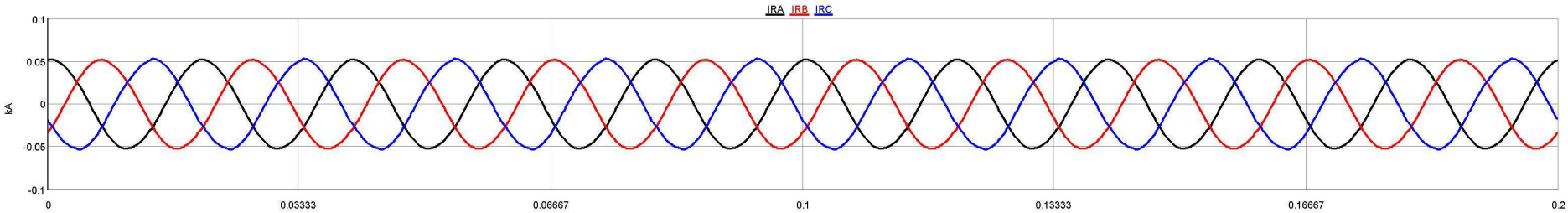

Figure 126 Current – case 18

	Voltage at the beginning of the line [V]			Voltage in the middle of line [V]			Voltage at the end of the line [V]		
Case	Line a	Line b	Line c	Line a	Line b	Line c	Line a	Line b	Line c
18	230,3	230,5	230,6	226,9	228	228,6	225,9	226,8	227,6

Table 33 Voltage values – case 18

8.1.19 Case 19 – Power at 50 kW – At the beginning of the line –03:00

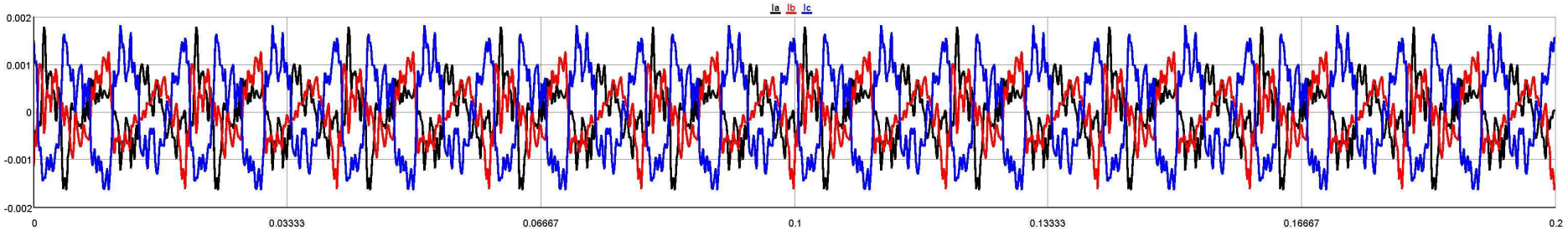

Figure 127 Harmonic current – case 19

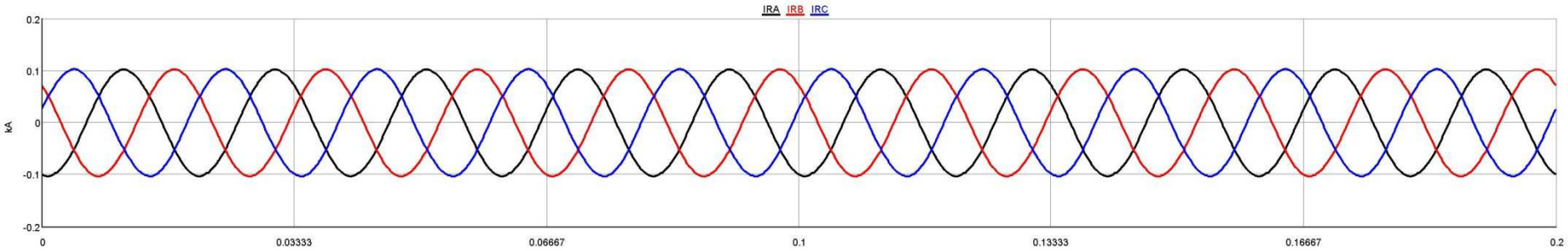

Figure 128 Current – case 19

	Voltage at the beginning of the line [V]			Voltage in the middle of line [V]			Voltage at the end of the line [V]		
Case	Line a	Line b	Line c	Line a	Line b	Line c	Line a	Line b	Line c
19	230,2	230,5	230,5	228,7	229,1	229,4	228,3	228,7	229

Table 34 Voltage values – case 19

8.1.20 Case 20 – Power at 50 kW – At the beginning of the line –13:00

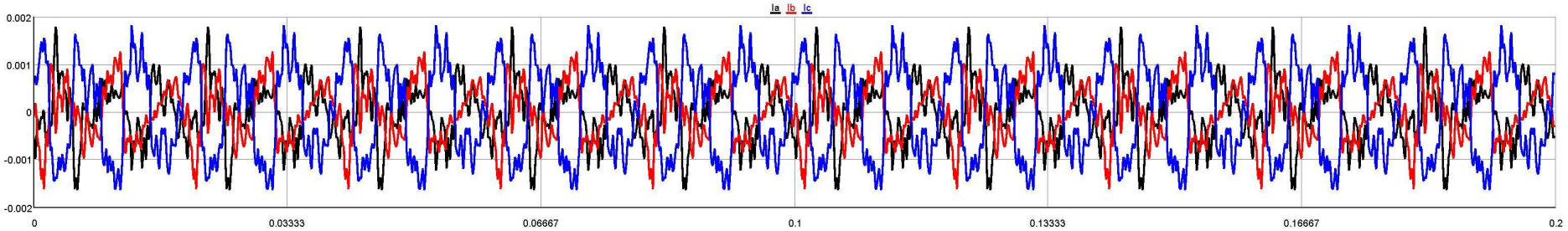

Figure 129 Harmonic current – case 20

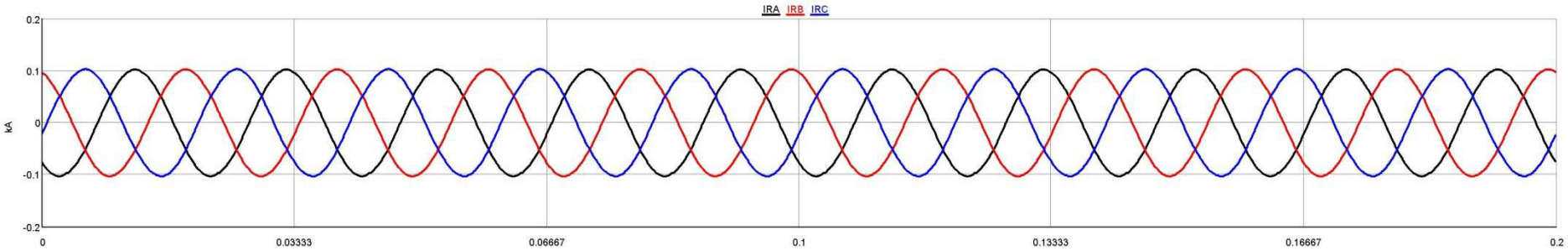

Figure 130 Current – case 20

	Voltage at the beginning of the line [V]			Voltage in the middle of line [V]			Voltage at the end of the line [V]		
Case	Line a	Line b	Line c	Line a	Line b	Line c	Line a	Line b	Line c
20	230,4	230,3	230,6	229,1	229,2	230	228,8	288,9	229,7

Table 35 Voltage values – case 20

8.1.21 Case 21 – Power at 50 kW – At the beginning of the line –20:00

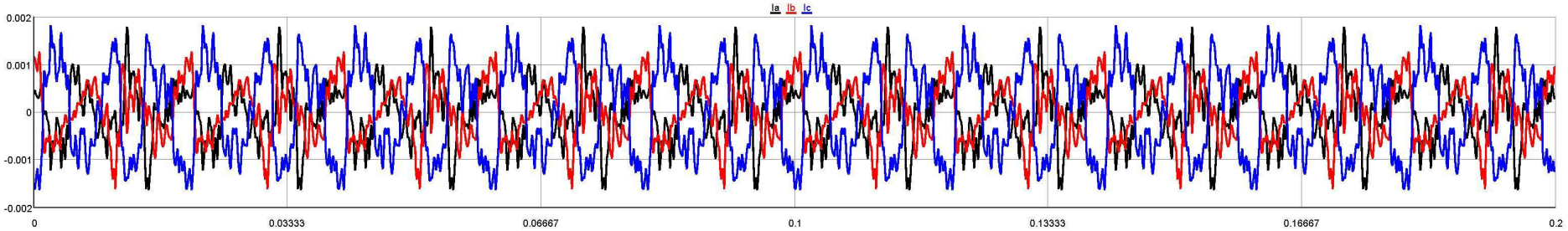

Figure 131 Harmonic current – case 21

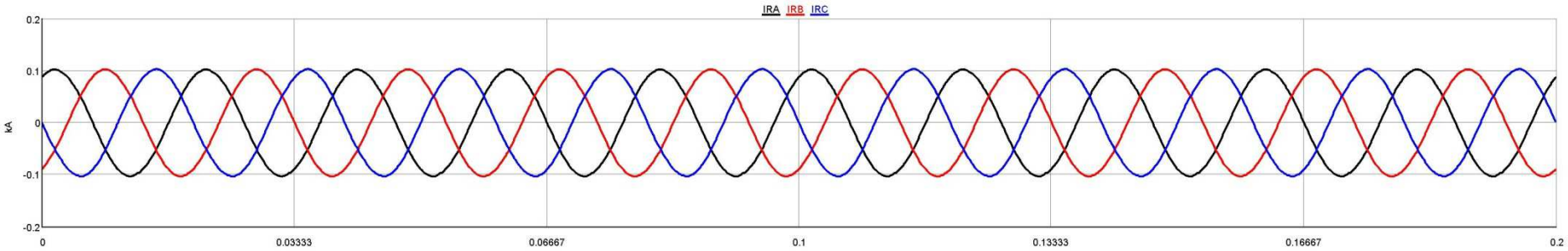

Figure 132 Current – case 21

	Voltage at the beginning of the line [V]			Voltage in the middle of line [V]			Voltage at the end of the line [V]		
Case	Line a	Line b	Line c	Line a	Line b	Line c	Line a	Line b	Line c
21	230,2	230,5	230,5	227,8	229	229,5	227,4	228,4	229,1

Table 36 Voltage values – case 21

8.1.22 Case 22 – Power at 50 kW – In the middle of the line –03:00

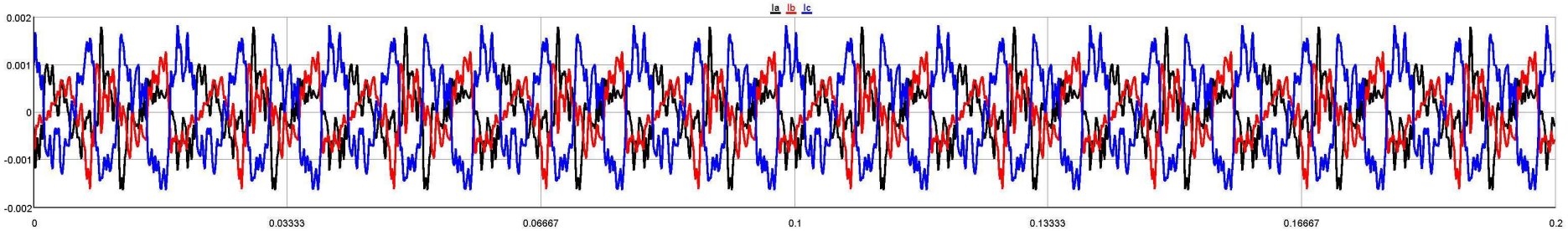

Figure 133 Harmonic current – case 22

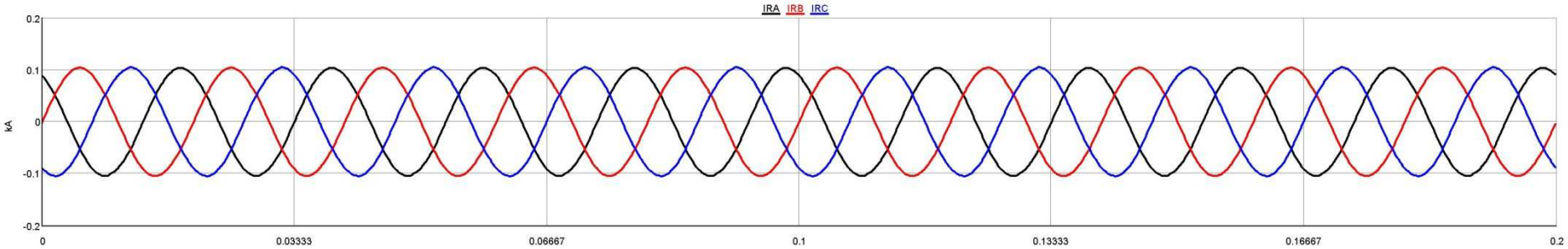

Figure 134 Current – case 22

	Voltage at the beginning of the line [V]			Voltage in the middle of line [V]			Voltage at the end of the line [V]		
Case	Line a	Line b	Line c	Line a	Line b	Line c	Line a	Line b	Line c
22	230,4	230,5	230,3	226,8	227,2	227,2	226,4	226,7	226,8

Table 37 Voltage values – case 22

8.1.23 Case 23 – Power at 50 kW – In the middle of the line –13:00

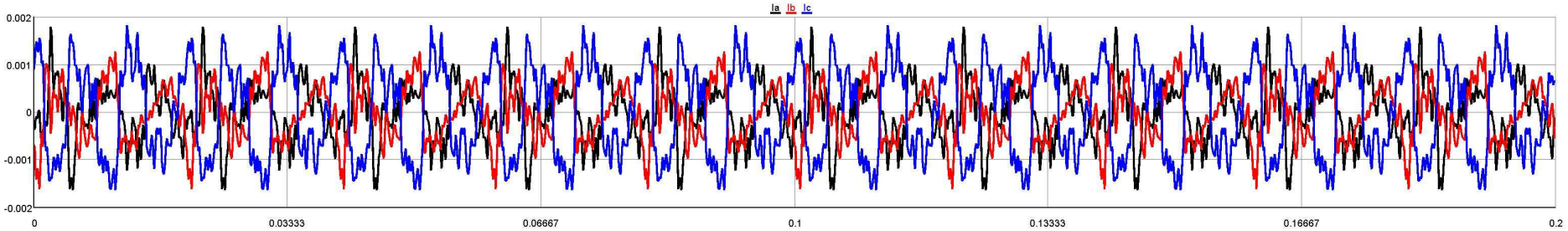

Figure 135 Harmonic current – case 23

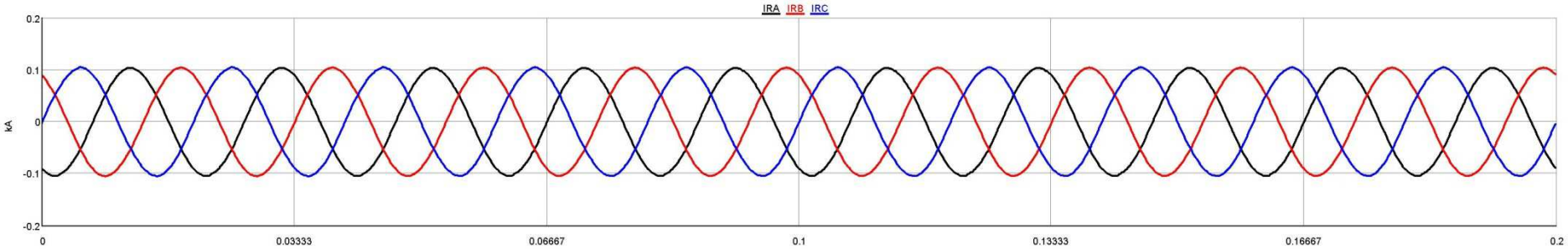

Figure 136 Current – case 23

	Voltage at the beginning of the line [V]			Voltage in the middle of line [V]			Voltage at the end of the line [V]		
Case	Line a	Line b	Line c	Line a	Line b	Line c	Line a	Line b	Line c
23	230,4	230,6	230,3	227,1	227,4	227,7	226,8	227,1	227,5

Table 38 Voltage values – case 23

8.1.24 Case 24 – Power at 50 kW – In the middle of the line –20:00

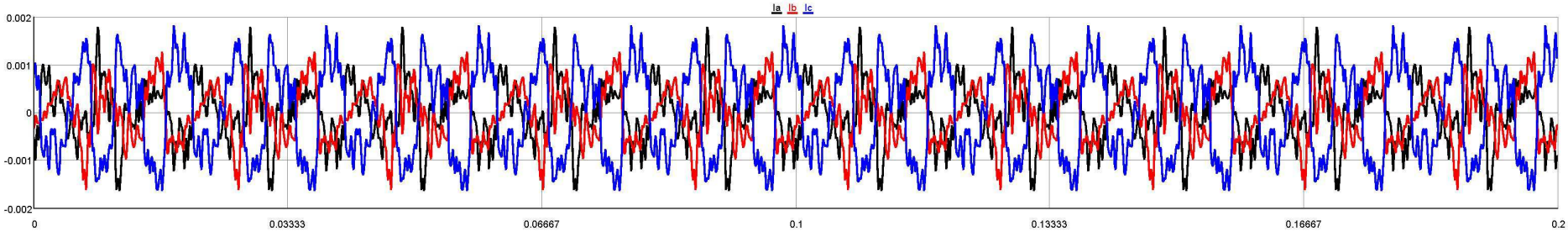

Figure 137 Harmonic current – case 24

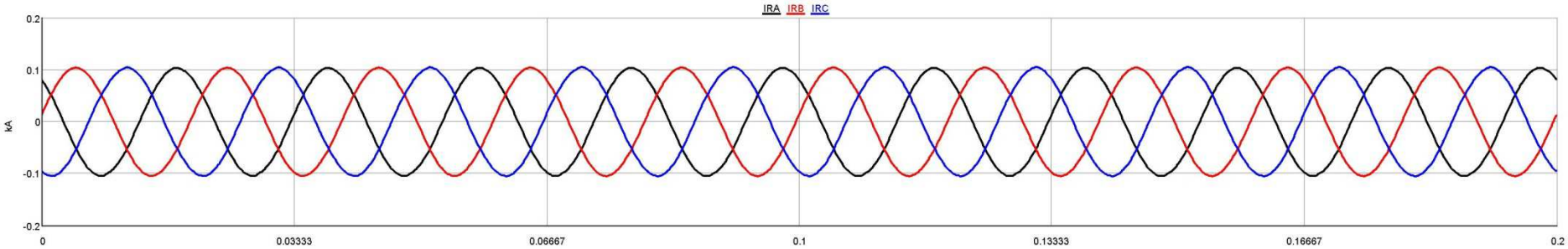

Figure 138 Current – case 24

	Voltage at the beginning of the line [V]			Voltage in the middle of line [V]			Voltage at the end of the line [V]		
Case	Line a	Line b	Line c	Line a	Line b	Line c	Line a	Line b	Line c
24	230,3	230,2	230,5	226	226,7	227,6	225,6	226,2	227,2

Table 39 Voltage values – case 24

8.1.25 Case 25 – Power at 50 kW – At the end of the line –03:00

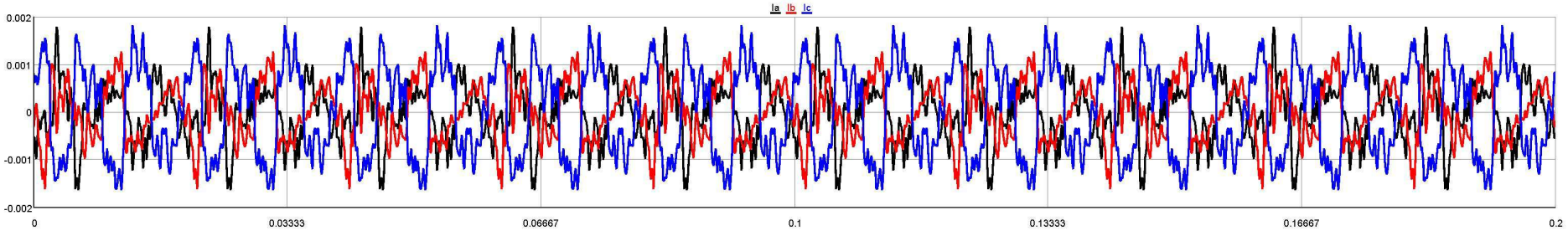

Figure 139 Harmonic current – case 25

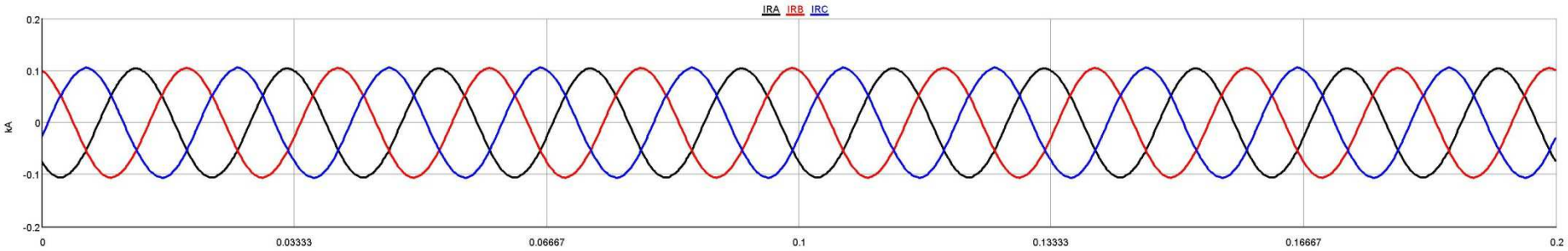

Figure 140 Current – case 25

	Voltage at the beginning of the line [V]			Voltage in the middle of line [V]			Voltage at the end of the line [V]		
Case	Line a	Line b	Line c	Line a	Line b	Line c	Line a	Line b	Line c
25	230,4	230,3	230,5	226,8	226,9	227,4	225,1	225,1	225,6

Table 40 Voltage values – case 25

8.1.26 Case 26 – Power at 50 kW – At the end of the line –13:00

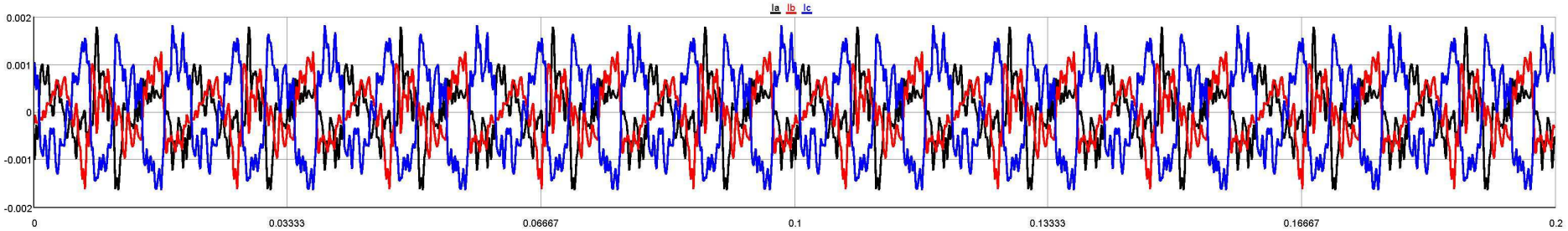

Figure 141 Harmonic current – case 26

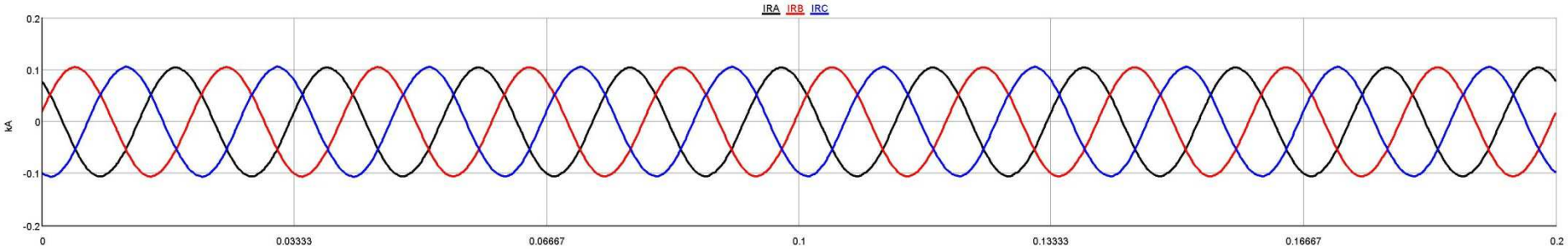

Figure 142 Current – case 26

	Voltage at the beginning of the line [V]			Voltage in the middle of line [V]			Voltage at the end of the line [V]		
Case	Line a	Line b	Line c	Line a	Line b	Line c	Line a	Line b	Line c
26	230,5	230,4	230,3	227,2	227,3	227,7	225,6	225,6	226,1

Table 41 Voltage values – case 26

8.1.27 Case 27 – Power at 50 kW – At the end of the line –20:00

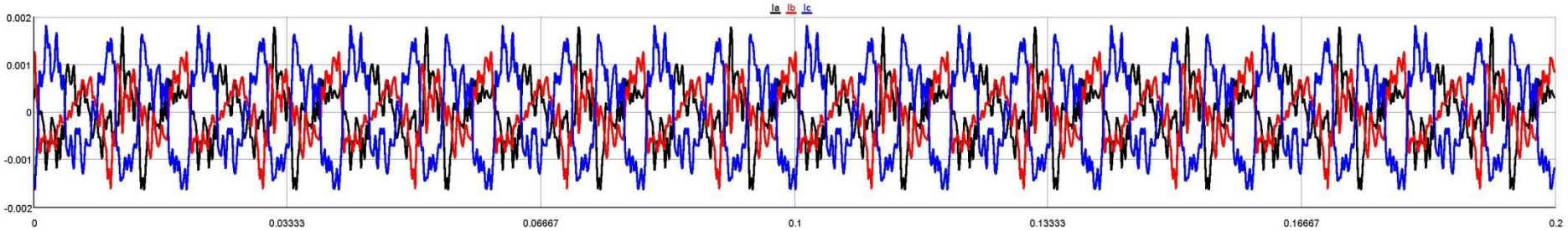

Figure 143 Harmonic current – case 27

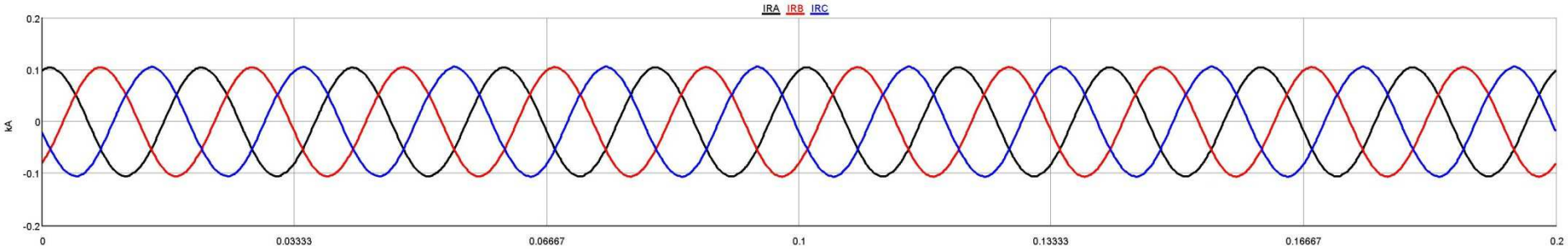

Figure 144 Current – case 27

	Voltage at the beginning of the line [V]			Voltage in the middle of line [V]			Voltage at the end of the line [V]		
Case	Line a	Line b	Line c	Line a	Line b	Line c	Line a	Line b	Line c
27	230,3	230,5	230,3	225,9	227	227,3	224,2	225,1	225,6

Table 42 Voltage values – case 27

8.2 Analysis of the results

Table 45 reports all values of the voltage measured for each phase in the line for each case.

	Voltage at the beginning of the line [V]			Voltage in the middle of line [V]			Voltage at the end of the line [V]		
Case	Line a	Line b	Line c	Line a	Line b	Line c	Line a	Line b	Line c
1	230,4	230,5	230,7	228,8	229,2	229,6	228,4	228,7	229,2
2	230,6	230,6	230,4	229,3	229,5	229,8	229	229,2	229,6
3	230,5	230,6	230,4	228,1	229,1	229,5	227,7	228,6	229,1
4	230,5	230,7	230,4	228,4	228,7	228,8	228	228,3	228,3
5	230,6	230,4	230,6	228,7	228,7	229,4	228,5	228,4	229,2
6	230,6	230,5	230,4	227,6	228,4	228,9	227,2	227,9	228,5
7	230,4	230,6	230,7	228,2	228,6	290	227,4	227,8	228,2
8	230,6	230,6	230,5	228,8	228,8	229,3	228,1	228,1	228,6
9	230,3	230,6	230,5	227,4	228,6	229	226,6	227,6	228,2
10	230,5	230,4	230,6	229	229	229,5	228,6	228,6	229,1
11	230,6	230,4	230,5	229,3	229,3	229,9	229	229	229,7
12	230,4	230,5	230,7	227,8	228,1	228,6	227,4	227,7	228,2
13	230,4	230,7	230,5	227,8	228,3	228,4	227,4	227,9	228
14	230,6	230,5	230,5	228,3	228,3	228,9	228,1	228	228,6
15	230,4	230,6	230,4	227	228,1	228,5	226,6	227,6	228,1
16	230,3	230,6	230,6	227,8	228,3	228,5	226,7	227,1	227,4
17	230,6	230,5	230,4	228,3	228,4	228,8	227,4	227,4	227,9
18	230,3	230,5	230,6	226,9	228	228,6	225,9	226,8	227,6
19	230,2	230,5	230,5	228,7	229,1	229,4	228,3	228,7	229
20	230,4	230,3	230,6	229,1	229,2	230	228,8	288,9	229,7
21	230,2	230,5	230,5	227,8	229	229,5	227,4	228,4	229,1
22	230,4	230,5	230,3	226,8	227,2	227,2	226,4	226,7	226,8
23	230,4	230,6	230,3	227,1	227,4	227,7	226,8	227,1	227,5
24	230,3	230,2	230,5	226	226,7	227,6	225,6	226,2	227,2
25	230,4	230,3	230,5	226,8	226,9	227,4	225,1	225,1	225,6
26	230,5	230,4	230,3	227,2	227,3	227,7	225,6	225,6	226,1
27	230,3	230,5	230,3	225,9	227	227,3	224,2	225,1	225,6

Table 43 Voltage values recorded for each case

The results show how the last case, id 27, is the worst for the voltage drop due to longer distance from the transformer and for the biggest power level set at 50 kW. Anyway the value of voltage are in perfect line with the requirements of the IEC 50160, which fixes the range in ±10% U_n (207 V – 253 V).

Moreover using the DFT the THD values of the voltage calculated at the end of the line confirm the fully compliant to the limits as for IEC 50160, lower than 8%.

Case	THD a	THD b	THD c
1	0,026533	0,028722	0,029817
2	0,027064	0,029099	0,030186
3	0,025878	0,028399	0,02994
4	0,054333	0,058662	0,061025
5	0,055498	0,059389	0,061674
6	0,052948	0,057904	0,061125
7	0,07296	0,078562	0,081832
8	0,074406	0,07964	0,083397
9	0,072718	0,078361	0,081952
10	0,026989	0,027509	0,035026
11	0,029039	0,028358	0,03644
12	0,026244	0,027198	0,035105
13	0,054727	0,055724	0,071456
14	0,056325	0,056415	0,07236
15	0,053455	0,056989	0,071945
16	0,072966	0,074127	0,095505
17	0,074577	0,07577	0,098199
18	0,07111	0,073187	0,095326
19	0,036564	0,032812	0,040362
20	0,037489	0,033233	0,040614
21	0,040411	0,033249	0,040996
22	0,071486	0,064248	0,079845
23	0,072712	0,06497	0,081001
24	0,070102	0,064178	0,079229
25	0,093146	0,083664	0,10464
26	0,094692	0,085443	0,107615
27	0,094802	0,083964	0,105759

Table 44 THD voltage for each case

9 Reference list

[1] ICNIRP GUIDELINES FOR LIMITING EXPOSURE TO TIME-VARYING ELECTRIC, MAGNETIC AND ELECTROMAGNETIC FIELDS (UP TO 300 GHZ). HEALTH PHYSICS 74 (4):494-522; 1998

[2] IEC 50160 “Voltage characteristics of electricity supplied by public distribution networks”

[3] IEC 61000-3-12 “Limits for harmonic currents produced by equipment connected to public low-voltage systems with input current > 16 A and inferior or equal 75 A per phase”